Unregulated toxic emissions from automotive diesel engines operating with potential neutral carbon diesel fuel substitutes

Silvana Arias Arias

Thesis submitted for the degree of Doctor of Philosophy in Environmental Engineering

Directors

John Ramiro Agudelo, Doctor (PhD) in Thermal Sciences
Francisco José Molina, Doctor (PhD) in Chemical and Environmental Engineering

Universidad de Antioquia
Facultad de Ingeniería
Doctorado en Ingenieria Ambiental
Medellín, Antioquia, Colombia
2023

Acknowledgements

I would like to thank the University of Antioquia, my Alma Mater, for giving me the opportunity to achieve many of my greatest dreams.

I would like to express my deepest gratitude to my supervisors Prof. Dr. John Ramiro Agudelo and Prof. Dr. Francisco José Molina, for their invaluable advice, continuous support, assistance at every stage of the research project and belief in me. Thank you for giving me the opportunity to continue growing as a researcher.

I would like to acknowledge to all members of the GIMEL and GAIA research groups for their help, feedback sessions, and moral support. Special thanks to Yina F. Jimenez and Dr. Maria L. Botero for their insightful comments and suggestions.

I am very grateful to the Fuels and Engines Group of the University of Castilla-La Mancha. It is their kind help and support that has made my PhD internship in Spain a wonderful time. I am especially grateful to Prof. Dr. Magín Lapuerta, his immense knowledge and plentiful experience have enriched me in my academic research. Thanks to him and his wife, Mariaje, for opening the doors of their home to me and my daughter and filling us with the best memories.

Thanks to the CAMBIO program (contract N° 175-2021- Minciencias) for providing the financial support for the last two years of my thesis. Thanks to Ecopetrol, Neste (NesteMY), Selabtec and ChemCom Industries B.V for donating the fuel and biofuels to develop part of my thesis.

I must express my very profound gratitude to my family. Mommy, infinite thanks for always loving me, taking care of me and supporting me. Didier, my love, you were always there, wherever and whenever that was. Thank you for your unconditional love and encouragement.

I owe my deepest gratitude to Stefanía, who is my life. I am forever thankful for the unconditional love, support, but above all, your time throughout the entire thesis process and every day. I could not have undertaken this journey without you. Finally, thank God for everything.

To Stefanía, for always inspiring me.

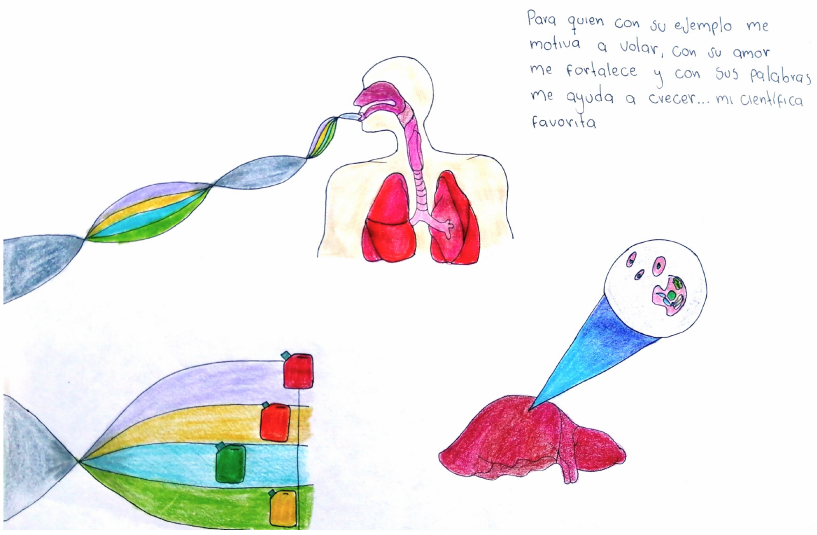

Abstract

The global transportation sector is dominated by energy from fossil fuel sources, however, in the context of climatic change there is a growing need to shift towards renewable energy sources. In addition, this sector plays a leading role for the deteriorating air quality in urban areas which is a major risk to human health, and it is expected to be the highest source of air pollution in the foreseeable future. Climate change, energy security, containment of regulated emissions and environmental concerns are considered as the main driving forces behind alternative fuels research. Potential low and neutral carbon fuels produced from renewable resources seem to be a preferable class of fuels for internal combustion engines. Although it is recognized that the combustion of low and neutral carbon fuels still generates pollution, the levels of regulated emissions and the carbon footprint decreases compared to the use of fossil fuels.

The best-known family of low and neutral carbon fuels are biodiesel, ethers, renewable diesel, bioalcohols, which have proved advantages as they are aromatic-free, sulfur-free and some of them can provide extra oxygen content. They have emerged as cleaner alternatives to mineral diesel and they can significantly reduce regulated emissions without compromising engine performance. However, several harmful volatile organic species which pose significant hazards to human health can be affected by using these low and neutral carbon fuels. This thesis studied the impact of a broad group of conventional and non-conventional biofuels on the formation of two groups of unregulated toxic emissions and in the induced biological risk in terms of cytotoxicity (cell death), genotoxicity (DNA damage), apoptosis (induced cell death) and ecotoxicity. Different methods were used to characterise the exhaust gases, both particles and gas phase, and a sampling system for unregulated toxic pollutants was designed and built.

In the first part, unregulated emissions of carbonyl compounds and polycyclic aromatic hydrocarbons in solid particle and gaseous phase, the contribution to ozone formation potential and the biological response of soluble organic fraction and water-soluble fraction extracted from particulate matter were investigated. Tests were conducted in an automotive diesel engine fueled with butanol, pentanol and hydrotreated vegetable oil blended with diesel, operating under two stationary modes, representative of urban driving conditions from the worldwide light duty test cycle (WLTC). Results showed that independently of the engine operating mode, alcohols exhibited the highest carbonyl compound emissions and thus the highest ozone formation potential. Independently of the fuel and engine operating mode, most of the PAH were present in the gas-phase. It was observed that some local combustion conditions might increase the emissions of PAH for renewable fuels. Regarding the biological response, all PM samples exhibited genotoxic effects. However, none of them showed cytotoxicity nor ecotoxicity effects.

Following the same sampling methodology, the second part investigated the unregulated emis-

sions in both, gas and particle phases, from a Euro 6b diesel engine, operated with four unconventional and advanced biofuels blended with diesel fuel and hydrotreated vegetable oil as base biofuel. The engine was operated following the WLTC driving cycle, starting from cold-engine conditions. Gas phase samples were collected and analyzed at each one of the four phases of the driving cycle. In addition, the apoptotic index induced by gas and particle emissions was determined. Results showed that the total gaseous PAH and carbonyl emission factors were higher at the low-speed phase for all fuels. Gas-phase PAH emission factors exceeded particle-bound PAH. Carbonyl emission factors markedly exceeded gaseous PAH emissions. Although particle-bound PAH comprises only a small fraction of total PAH emissions, both phases (gas and particles) contributed approximately equal to the toxicity associated with carcinogenic PAH. The apoptotic cells percentage increased in a dose-dependent manner and it was significantly higher in cells exposed to gas phase-derived samples in comparison with particle phase.

Finally, special care on unregulated emissions and biological risk is highly recommended when promoting low or zero carbon footprint fuels for internal combustion engines. Although the net carbon emissions could be drastically decreased, several harmful PAH and carbonyl compounds can be significantly increased and thus the risk to human health.

Preface

This dissertation is my own work. The work was performed at the University of Antioquia between August 2019 and October 2022. No part of this thesis has been submitted for a degree to this or any other university.

This dissertation contains approximately 31000 words and 77 figures and tables.

The work in this dissertation has been published as follows:

- **Silvana Arias**, Francisco Molina, Rubén Palacio, Diana López and John R. Agudelo. Assessment of carbonyl and PAH emissions in an automotive diesel engine fueled with butanol and renewable diesel fuel blends. ***Fuel***, 316, 2022. doi.org/10.1016/j.fuel.2022.123290

- **Silvana Arias**, Maria L. Botero, Francisco Molina and John R. Agudelo. Pentanol/diesel fuel blends: Assessment of inhalation cancer risk and ozone formation potential from carbonyl emissions emitted by an automotive diesel engine. ***Fuel***, 321, 2022. doi.org/10.1016/j.fuel.2022.124054

- **Silvana Arias**, Verónica Estrada, Isabel C. Ortiz, Francisco Molina and John R. Agudelo. Biological toxicity risk assessment of two potential neutral carbon diesel fuel substitutes. ***Environmental Pollution***, 308, 2022. doi.org/10.101–16/j.envpol.2022.119677

- **Silvana Arias**, John R. Agudelo, Ángel Ramos and Magín Lapuerta. Emissions from a Euro 6 engine using polyoxymethylene 2 dimethyl ethers: chemical effects vs. mapping strategy. ***Fuel***, 335, 2023. doi.org/10.1016/j.fuel.202–2.127017

- **Silvana Arias**, John R. Agudelo, Francisco J. Molina, Emilio Llanos, Francisco J. Alcaín, Rosario Ballesteros and Magín Lapuerta. Environmental and health risk implications of unregulated emissions from advanced biofuels in a Euro 6 engine. ***Chemosphere***, 313, 2023. doi.org/10.1016/j.chemosphere.202–2.137462

- **Silvana Arias**, Francisco Molina and John R. Agudelo. Cancer risk assessment induced by PAH and aldehydes from an automotive diesel engine fueled with renewable fuel blends. **IEEE *Xplore***, 1–4, 2021. doi:10.1109/CASAP54–985.2021.9703427

Some of the work presented in this dissertation has also contributed, to a lesser degree to the following publication:

- Maria L. Botero, Carolina Medoza, **Silvana Arias**, Oscar D. Hincapié, John R. Agudelo, Isabel C. Ortiz. In vitro evaluation of the cytotoxicity, mutagenicity and DNA damage induced by particle matter and gaseous emissions from a medium-duty diesel vehicle under real driving conditions using palm oil biodiesel blends. ***Environmental Pollution***, 265, 2020. doi.org/10.1016/j.env–pol.2020.115034.

- Yina F. Jiménez, **Silvana Arias**, Rubén Palacio, Diana López, Juan C. Casas and John R. Agudelo. Experimental comparison of carbonyl compounds from a diesel engine fueled with pentanol in blended and fumigation modes. **IEEE *Xplore***, 1–4, 2021. doi:10.1109/CASAP54985.2021.9703399

Contents

List of Figures

List of Tables

Chapter 1

Introduction

1.1 Motivation

Energy demand has been rising remarkably due to increasing population and urbanization. Global economy and society are significantly dependent on energy availability because it touches every facet of human life and activities. However, the world community are at a turning point in world energy history, the concept of “carbon neutrality" by 2050 has become the primary objective in energy transition policies [1, 2], but ¿how to achieve it? It is not entirely clear. Achieving this goal will require multidisciplinary research, breakthroughs and innovations.

Currently, this transition seeks to prioritize sustainable mobility with the massive introduction of low-to-zero carbon footprint biofuels [3], the use of hybrid and electric vehicles, and energy efficiency policies. Therefore, the gradual reduction and future disappearance of fossil fuels and decarbonization of the transportation sector is a reality. However, internal combustion engines (ICE) will not necessarily disappear, not in the near future [4, 5].

To date, electric vehicles equipped with batteries have not overcome barriers such as high costs, weight, as well as the limitations of the exploitation and transformation of precious and rare metals involved in the electrical system. Topics such as the low vehicle range (km/kWh) of electric vehicles due to the reduced energy storage capacity of current batteries compared to fossil fuels, and the inherent difficulty in supplying electricity from renewable energy (mainly hydro, wind and solar) are still a challenge.

Despite this situation, diesel engines continue to be a key factor in current economic development, since there are still no real alternatives that can compete with the

ICE in the full range of applications it covers. It is estimated that they will retain still a leading role since they are the most efficient thermal machines for people transportation and cargo. Therefore, scientists have been searching for alternative fuels that can provide an equal exchange for the huge demands of conventional diesel fuel usage and that can also mitigate the associated effects of fossil fuels [6].

In a realistic scenario, ICE will continue to be present due to their high efficiency; and second generation biofuels (renewable, electro-fuels -e-fuels- and/or synthetic) with neutral carbon footprint, are one of the necessary and crucial trends to guarantee a solid path in the global transition towards renewable and sustainable energies and towards neutral CO_2 mobility by 2050 [4, 7, 8]. These alternative liquid fuels coupled with highly efficient emission control systems offer the potential for future carbon neutrality .

In terms of regulated pollutants, thanks to advanced combustion modes and innovative post-treatment systems, some renewable fuels are close to achieving the goal of zero environmental impacts. However, regarding unregulated pollutants, the results are not yet clear. Unregulated pollutants directly affect human health. They are emitted in low concentrations, but their health implications are acute. In addition, some of them are precursors of tropospheric ozone and secondary aerosols, which affect the radiative balance of the planet.

In this context, it is necessary to evaluate the emissions of unregulated pollutants from low-to-zero carbon footprint biofuels (second-generation renewable fuels and e-fuels) with demonstrated potential in ICE. This allows to comprehensively verify the wide spectrum of potential effects (negative and positive) of biofuels, considering that, although net carbon emissions are reduced with the use of renewable fuels and e-fuels, several unregulated pollutants might increase.

According to the above, the main motivation of this thesis was to gain fundamental understanding on the influence of different conventional and unconventional alternative biofuels on unregulated pollutant emissions with a high potential for affecting human health. These biofuels were tested in representative driving conditions and in a homologation driving cycle. Some of these fuels have not been previously evaluated in terms of unregulated emissions. In addition, this work sought to understand the biological effects of gaseous and particle emissions from potential carbon-neutral diesel fuel substitutes, in order to broaden the understanding of the possible effects on human health.

1.2 Contributions of this thesis

In the main body of this thesis, new data, and analysis for understanding the impact of different alternative fuels on unregulated emissions and biological activity are pre-

sented. Following that, the combustion characteristics and engine performance are analyzed in terms of the fuel properties. Novel contributions of this thesis are:

- Provide useful and cutting-edge information about the comparative evaluation of unregulated pollutants with a high toxic potential to humans, in both, gas and particle phases, for a broad group of possible substitutes for diesel fuel (long-chain alcohols, paraffins, e-fuels, hydrogenated waste-derived). For the first time, the extremely dangerous dibenzo[a,l]pyrene compound is reported as specific emission [g/kWh] for these fuels.

- *In-vivo* and *in-vitro* biological effects of diesel exhaust particle matter were assessed. For the first time, the assessment of the oxidative DNA damage of diesel particulate matter through FPG and Endo III enzymes is presented. In addition, the assessment of the ecotoxicity of the water-soluble fraction of PM through *D. Pulex* is also a novelty.

- New insight into the influence of the fuel chemical characteristics and engine mapping strategy on the regulated and unregulated emissions in a modern Euro 6b engine following the current WLTC driving cycle.

- Novel information on the biological toxicity risk impact through the measurement of the apoptotic index of the gas phase and particles of six biofuels used in a modern engine under transient conditions.

- Development of a sampling system and sampling methodology for unregulated pollutants in diesel engine exhaust which can be adapted to a pre-dilution system, if desired).

- This is the first study reported about the use of 20% OME (higher contents are unpractical due to sealing and immiscibility problems) blended with ULSD, following the current WLTC driving cycle and analyzing instantaneous emissions.

1.3 Structure of this thesis

This thesis has been divided into six chapters.

Chapter 2 provides a review of the current understanding of advanced biofuels and unregulated emissions that have been studied and the most representative results. In addition to the unregulated emissions review, the main properties of alternative biofuels and their combustion characteristics were presented. In this chapter, studies of biological activity induced by engine emissions were included.

Technical details of the sampling systems, the test plan and each of the biofuels are discussed in Chapter 3. Analytical techniques and conditions for chemical and biological analysis are also presented in this Chapter.

Results from this thesis are divided in Chapter 4 and Chapter 5.

Steady state engine test results of unregulated emissions (carbonyl compounds and PAH) in solid particles and gaseous phase from 3 biofuels and different blends with diesel are discussed in Chapter 4, The contribution to ozone formation potential and the biological response through a wide spectrum of tests (cytotoxicity, genotoxicity, oxidative damage and ecotoxicity) are also presented in this Chapter.

In Chapter 5, the unregulated emissions results obtained from a Euro 6b diesel engine operating in a transient state following the WLTC driving cycle and fueled with six selected biofuels blended with diesel and HVO are discussed. The effects of OME addition on engine performance, pollutant emissions (CO, NO_2, NO, THC, PN), and particle size distribution are also presented.

The findings of the thesis are summarised and suggestions for future work are presented in Chapter 6.

Bibliography

[1] COP26: Together for our planet | United Nations.

[2] Colombia Ministerio de Minas y Energía and BID Banco interamericano de Desarrollo. Transición energética: un legado para el presente y el futuro de Colombia. page 128, 2021.

[3] Vijayashree and V. Ganesan. A Comprehensive Review on Oxygenated Fuel Additive Options for Unregulated Emission Reduction from Diesel Engines. *Energy, Environment, and Sustainability*, pages 141–165, 2020.

[4] N.D.S.A. Santos, V.R. Roso, A.C.T. Malaquias, and J.G.C. Baêta. Internal combustion engines and biofuels: Examining why this robust combination should not be ignored for future sustainable transportation. *Renew Sustain Energy Rev*, 148, 2021.

[5] Alberto Boretti. The Future of the Internal Combustion Engine after "diesel-Gate". *SAE Technical Papers*, 2017-July(July), 2017.

[6] H.-J. Liu, R.-H. Chen, and W.-C. Wang. The non-regulated emissions from a turbo-charged diesel engine under steady-state operation with hydro-processed renewable diesel (hrd). *Fuel*, 263, 2020.

[7] Avinash Kumar Agarwal and Hardikk Valera. *Introduction of Potential and Challenges of Low Carbon Fuels for Sustainable Transport*, pages 3–6. Springer Singapore, Singapore, 2022.

[8] Selçuk Sarıkoç. *Some of the Bio-fuels for Internal Combustion Engines: Alcohols and Biodiesel*, pages 9–31. Springer Singapore, Singapore, 2022.

Chapter 2

Background

This chapter reviews the context in which the present work has taken place. It provides a theoretical background on unregulated emissions from diesel engines, as well as the toxicity of those emissions. Conventional and unconventional biofuels are introduced in this chapter, together with their most relevant properties and characteristics as substitutes for diesel. Finally, a literature review on unregulated emissions, following the PRISMA framework is given for each biofuel.

2.1 Introduction

Signatories of the Climate Change Conference in Glasgow (COP26) agreed on moving away from fossil fuels. This was, perhaps, the most contested decision in Glasgow. Countries ultimately agreed to a provision calling for a phase-down of coal power and a phase-out of "inefficient" fossil fuel subsidies – two key issues that had never been explicitly mentioned in decisions of United Nations (UN) climate talks before, despite coal, oil, and gas being the main drivers of global warming [1]. Therefore, in addition to zero-emission vehicles and improvements in fuel economy, biofuels, especially advanced and electrofuels are currently being promoted, and will be further boosted in the Fit-for-55 legislative package in order to align current laws with the 2030 and 2050 mandates.

The most studied alternative fuels include on the one side, oxygenated fuels such as biodiesel, bio-alcohols and ethers including dimethyl ether (DME), and on the other side, non-oxygenated ones such as hydrotreated vegetable oils (HVO) and Fischer–Tropsch fuels. Other less studied waste-derived renewable fuels have demonstrated to be also suitable for diesel applications, such as terpene-based fuels, i.e., hydrogenated turpentine (HT) and hydrogenated orange oil (HO), and glycerol-derived

biofuel [2, 3]. In the last years, polyoxymethylene dimethyl ethers (OME, mainly 3-5) are becoming promising non-biological renewable fuels [4, 5, 6]. Their high oxygen content, the lack of aromatic rings, and their high hydrogen-to-carbon ratio are some of the characteristics that have been shown to reduce soot formation and different regulated emissions [7, 8].

Some of the mentioned renewable fuels have been considered as a prospective drop-in alternative fuels for compression ignition engine applications in recent past, since they have shown a reduction in several harmful regulated emissions by offering diesel-like or even better thermal efficiency [9, 10, 11, 12, 13, 14]. However, the formation of highly toxic and carcinogenic pollutants such as polycyclic aromatic hydrocarbons (PAH) and aldehydes, which are not regulated yet, have been little reported in literature, or some of them have shown contradictory effects. In addition, there are several pollutants for which toxicological knowledge is too limited, as are long-term bioassay observations and epidemiological studies.

It is important to assess potential harmful impacts of these new alternative biofuels before they can be widely adopted as diesel fuel substitutes. This chapter presents the context around the research on unregulated emissions from the target renewable fuels and introduces the relevance of the thesis in the global context. The reason behind the selected fuels, as well as their impact on the diesel engines performance based on their properties, are also described. In addition, a literature review on unregulated emissions and toxicity from the conventional and non-conventional biofuels evaluated in this thesis is presented.

2.2 Unregulated emissions with toxic health effects

Air pollution has become the largest environment and health challenge to society. Combustion processes involving fossil fuels are largely responsible for air pollution and climate change, both of which have a direct negative effect on human health [15].

Combustion processes in diesel engines produce a complex mixture of gaseous and particulate emissions. The highest proportion of emitted compounds are generally carbon dioxide-CO_2, carbon monoxide-CO, nitrogen oxides-NOx, and unburned hydrocarbons-HC. Among these pollutants, the standards that regulate vehicle emissions have included: NOx, CO, HC and particulate matter-PM (by mass and/or by number).

With the exception of those pollutants in the previous paragraph, a large number of compounds, some of them volatile and semivolatile, are not regulated, and although they are emitted in small concentrations, some have a high potential for affecting human health and the environment. Volatile and semivolatile organic compounds are mainly lower (C1–C4) paraffin, olefins, aldehydes (e.g., formaldehyde),

ketones (e.g., acetone), monoaromatics (e.g., benzene, toluene, benzaldehyde, phenol) and PAH.

These toxic compounds enter the human body mainly through the respiratory system, although they can also be ingested or absorbed through the pores of skin. Part of the inhaled pollutants can be exhaled, but most reach the lungs, with some penetrating through the lungs and entering the circulation system. These contaminants can be then transported all over the body, with some chemical reactions forming new chemicals [15].

2.2.1 Polycyclic aromatic hydrocarbons (PAH)

The most important category of aromatic compounds from diesel combustion are PAH, which are found both in the gaseous phase and adsorbed on PM. They are considered to be suspected of being carcinogenic, teratogenic and genotoxic [16, 17, 18].

PAH are a group of organic compounds formed by multiple aromatic rings and are among the most widespread pollutants in the environment [19]. In internal combustion engines, they can originate in various processes, such as fuel fragmentation that leads to pyrolysis, pyrosynthesis of aromatic compounds and lubricating oil that remains unburned [20]. However, their formation depends on many factors, such as engine type, fuel type, engine speed and load, etc.[21]. PAH are classified according to their molecular weights into three classes, low molecular weight (LMW) compounds (2–3 rings), medium molecular weight (MMW) compounds (4 rings), and high molecular weight (HMW) compounds (5 rings–6+ rings) [22]. The American Environmental Protection Agency (U.S.EPA) has defined 16 PAH structures as substances for priority evaluation due to the potential harmful risk they would have on living beings **Figure** 2.1.

PAH can enter the body through ingestion, inhalation, and dermal absorption. As a consequence of their low solubility in water and high solubility in substances of a lipid nature, they accumulate in organisms and in the organic matter of particles and sediments, being able to remain for long periods of time, which guarantees their bioavailability [19, 21, 22]. Benzo(a)pyrene (BaP) is one of the PAH that has the ability to develop carcinogenic, genotoxic and/or mutagenic effects; and this compound can remain for long periods in the environment (half-life in the soil of 162 days). Therefore, BaP is considered as the reference compound in different environmental studies by U.S. EPA.

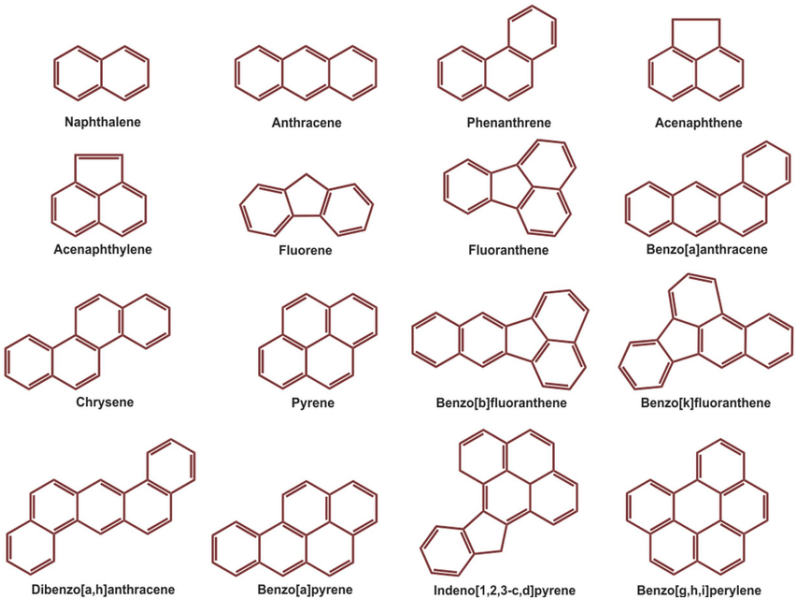

Figure 2.1: Structures of the 16 PAH on the U.S.EPA priority pollutant list [23]

.

In recent years, attention has been directed also to both, PAH, and their nitrated and oxygenated derivatives emitted by combustion sources, and mainly as products of both gaseous and heterogeneous photo-oxidation reactions of PAH with atmospheric oxidants (OH, NO_3, O_3), photolysis and thermal conversions [24].

2.2.2 Carbonyl compounds

Other atmospheric pollutants emitted during vehicle combustion are carbonyl compounds. They are a category of organic compounds that contain the functional group C=O in their structure (**Figure** 2.2).The simplest carbonyl groups are aldehydes and ketones. They fall into the category of toxic pollutants and are responsible for the formation of smog. They are also found in the atmosphere as part of the ozone cycle. Since they are the most abundant of the easily photolyzed compounds in the atmosphere (except for NO_2) they are an essential source of free radicals for tropospheric photochemistry, and even the most important source in moderate to strong polluted atmospheres [25]. Carbonyl compounds can react with the hydroxyl radical (·OH) to generate HO_2 and RO_2 radicals, which can oxidize NO to NO_2 and further promote the formation of O_3 in the troposphere [26]. In addition, they are also important intermediates in the formation of secondary aerosols. The oxidation of carbonyl compounds could produce formic acid, acetic acid, and other acidic substances, which may enhance atmospheric acidity and intensify the formation of acid rain [26].

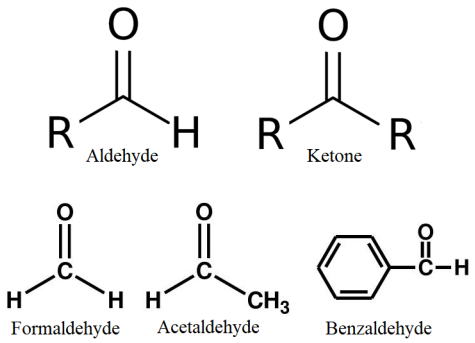

Figure 2.2: Carbonyl group and some example compounds

These compounds not only degrade the environment [27], most carbonyl compounds are highly irritating and dangerous for human health, as they can induce nasal diseases and cause headaches and irritation of the skin, eyes and mucous membranes of the respiratory system [17, 28]. In particular, formaldehyde poses serious risks to the human eyes, skin, and respiratory system, and has been confirmed as a first-class human carcinogen by the IARC [29], which can cause nasopharyngeal cancer and may also be related to leukemia [30]. Acetaldehyde is also considered as a carcinogenic compound [28].

2.2.3 Other unregulated pollutants

Trace level metals, which are emitted from the engine, might be non-carcinogenic or carcinogenic. Ni, Cd and Cr are considered carcinogenic metallic elements [31]. Trace metals in PM can penetrate deep into the respiratory tract of the human body and can even enter the cells of the human body. These trace metals increase the activity of reactive oxygen species (ROS) in cellular structures [32], resulting in elevated oxidative stress [33].

2.2.4 Toxicity of pollutant emissions

The overall impact of engine emissions on human health has been studied for a long time, diesel exhaust particles were classified as carcinogens [16] and epidemiological data indicate that exposure to diesel exhaust particles from traffic emissions is associated with a higher risk of morbidity and mortality related to cardiovascular and pulmonary diseases. However, beyond mortality, non-cardiopulmonary adverse outcomes through systemic effects such as inflammation, oxidative stress, immune modulation and epigenetic alterations are also induced by both particulate matter and gaseous contaminants. This situation has gained prominence as a global public health concern [34].

From a toxicological perspective, part of the mass of PM consists of biologically

inert material: ammonium sulfates and nitrates, etc., while the content of heavy metals and organic compounds have relatively small masses but contribute significantly to the reported health effects in the literature [35, 36]. The smallest PM (<100nm) can penetrate and deposit deep into the small airways and alveoli, where they can accumulate and trigger inflammation and oxidative stress resulting in acute or chronic lung injuries [37]. Absorbed organic compounds consisting of highly mutagenic chemicals that have been shown to cause lung tumors, induce mutations in bacterial and mammalian cells, sister chromatid exchanges, and chromosomal aberrations in cultured mammalian cells. There is also consensus on the ability of inhaled PM to cause oxidative stress at the air-lung interface that may cause or contribute to many acute and chronic diseases [38, 39].

The toxicological potential of the diesel exhaust emissions have been assessed through a wide spectrum of tests (cytotoxicity, genotoxicity, oxidative stress), in order to identify substances that can cause genetic alterations in somatic or germ cells, and this information is used in making regulatory decisions. National and international regulatory agencies historically have used genotoxicity information as part of a weight-of-evidence approach to evaluate potential human carcinogenicity and its corresponding mode of action [40]. On the other hand, information on mutagenicity is also valuable in assessing the risk of other adverse effects, particularly developmental effects occurring through mutation of germ cells or genotoxicity occurring in somatic cells during embryogenesis and fetal development [40]. **Table** 2.1 shows the biological categories to assess risks associated with diesel exhaust emissions.

Genotoxicity is an important step in the development of lung cancer by exposure to outdoor air pollution and diesel exhaust [16]. DNA adducts can be produced when PAH bind to DNA, whereas oxidative damage to DNA is caused by ROS that are generated by particulate matter, transition, and certain organic compounds in the combustion gas exhaust, or by inflammatory cells in the body. ROS can cause both DNA strand breaks and oxidation of DNA nucleobases [41].

Table 2.1: Biological categories to assess risks associated with diesel exhaust emissions

Biological category	**Description**
Mutagenicity	The term "mutation" refers to permanent changes in the structure or amount of the genetic material of an organism that can lead to heritable changes in its function; these changes include gene mutations as well as structural and numerical chromosomal alterations. The term "mutagen" refers to a chemical that induces heritable genetic changes, most commonly through interaction with DNA, and "mutagenicity" refers to the process of inducing a mutation [40].
Genotoxicity	The broader terms "genotoxicity" or "genetic toxicity", include mutagenicity, but also include DNA damage, which may be reversed by DNA repair processes or other known cellular mechanisms or result in cell death and may not result in permanent alterations in the structure or information content of the surviving cell or its progeny [40].
Cytotoxicity	Cell death by endogenous and/or exogenous effects is called cytotoxicity and the effect that leads to cell death is called the cytotoxic effect. The basic pathway of cytotoxicity is determined by the pattern by which the cell dies. Accordingly, the cell either attempts to die in a multi-step manner in the presence of a genetically controlled mechanism, which is called **apoptosis** (programmed cell death), or dies by a necrosis-like mechanism (without genetic control) that suddenly occurs for unpredictable reasons leading to inflammation. Although not genetically controlled, some exogenous effects may also trigger apoptosis by reprogramming the genetic control of the cell-killing mechanism [42].
Oxidative stress	Oxidative stress refers to the excessive production of ROS in the cells and tissues and antioxidant system cannot be able to neutralize them. Imbalance in this protective mechanism can lead to the damage of cellular molecules such as DNA, proteins, and lipids. Oxidative stress can activate a variety of transcription factors, which lead to the differential expression of some genes involved in inflammatory pathways [43].

Although there is consensus that the use of biofuels can reduce regulated emissions, several investigations have shown that the toxicity of emissions of biodiesel increases, since their particles are more reactive than fossil fuels counterpart, and induce high cytotoxicity, mutagenicity and oxidative stress [44, 34, 45]. Regardless of the biofuel feedstock, its raw material and production process, the combustion of biofuel/diesel blends produce a complex mixture of exhaust gases containing PM , metals, organic compounds (e.g. volatile compounds and PAH) and elemental carbon, that can exacerbate the biological response, making these emissions potentially more dangerous to health than diesel fuel alone.

2.2.5 Literature review on unregulated emissions

A literature review on unregulated emissions of the alternative biofuels evaluated in this thesis was carried out. For some of them any report on unregulated emissions was found. The search strategy was focused through Scopus database with the following inputs for title, abstract and keywords.

Table 2.2: Database inputs to complete search

Input 1	Input 2	Input 3	Input 4	Input 5
Biofuel name	"unregulated emissions" OR "non regulated emissions"	"PAH" OR "polycyclic aromatic hydrocarbons"	"carbonyls"	"engine"

The literature searches recovered 159 unique results from which 32 were included in this literature review following the PRISMA framework [46] as shown in **Figure** 2.3.

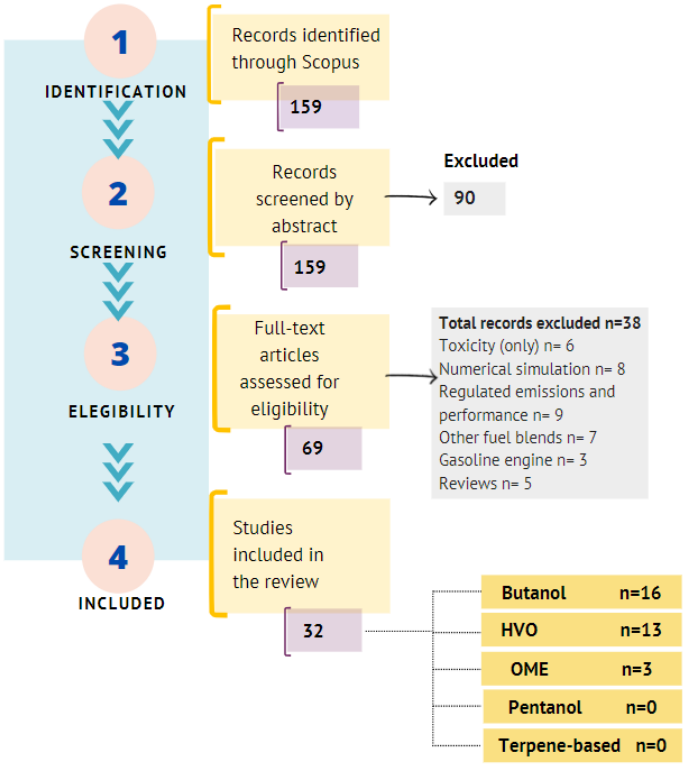

Figure 2.3: Flowchart of the literature review following the PRISMA framework [46]

The summary of the search results is shown in **Figure** 2.4. For pentanol and terpene-based fuels no results were found. The details of each search are shown and

discussed in **sections** 2.3.1, 2.3.2, and 2.3.4 (**Tables** 2.3, 2.4 and 2.6). The search returned results for unregulated emissions and biological activity (Bio.Act.) and this last one was included as long as they were reported together with any unregulated emission.

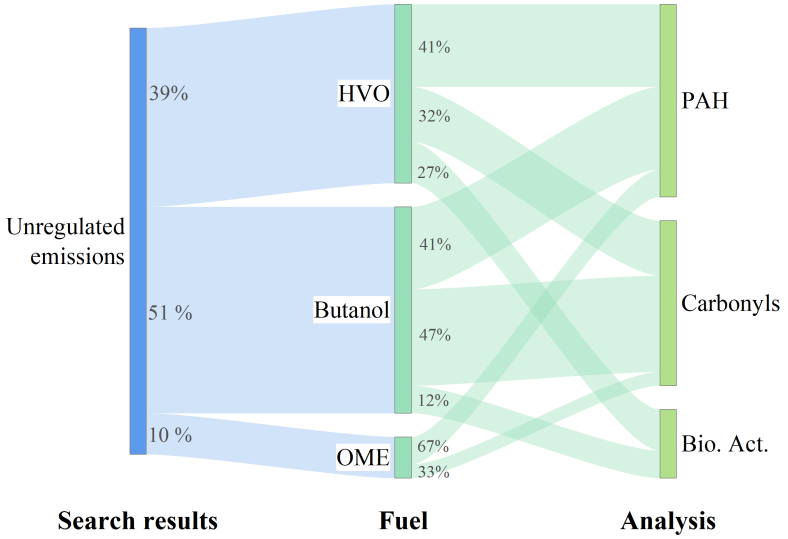

Figure 2.4: Summary of findings on unregulated emissions

2.3 Conventional and non-conventional alternative biofuels

2.3.1 Hydrotreated vegetable oil -HVO

Hydrotreated vegetable oil is a mixture of straight chain and branched paraffins – the simplest type of hydrocarbon molecules from combustion point of view –. Typical carbon numbers are C15...C18. Paraffins exist also in fossil diesel fuels, which additionally contain significant amounts of aromatics and naphthenes. Its properties are quite similar to Gas-to-Liquid (GTL) and BTL fuels made by Fischer Tropsch synthesis from natural gas and gasified biomass, respectively [9].

HVO produced from triglycerides through hydro-deoxygenation reactions has been considered as a prospective drop-in alternative fuel for CI engine applications in recent past [9]. HVO is a non-fossil hydrocarbon fuel characterised by the same chemical structure as conventional diesel fuel that (1) can be blended with conventional diesel fuel, (2) can use the same fuel supply infrastructure, and (3) does not require adaptation of the vehicle powertrain or engines [47]. The high cetane number (CN) is appropriate for lower compression ratio engines resulting in better NOx-PM trade-offs, and the absence of sulphur reduces the ageing and deterioration of after-treatment devices and engine components. HVO is characterized by a higher Lower Heating Value (LHV) and density than standard diesel fuel, related to high paraffin

content, with a dropping trend of mass-based fuel consumption [48].

HVO fuel can potentially be carbon neutral in a sense that the carbon produced by its combustion can be offset by the carbon absorbed during the feedstock growth. Therefore, HVO fuels hold great potential for reducing greenhouse gases [49]. HVO has higher energy content and superior thermal and storage stabilities than biodiesel and alcohols. It also has excellent combustion quality and good low-temperature properties [50].

HVO is increasingly being produced from waste and residue fat fractions coming from non-food grade vegetable oil fractions, as well as from the food industry. The HVO production is a mature commercial technology. Companies such as Neste with Neste MY Renewable Diesel, Honeywell UOP/ENI with Green Diesel, and Haldor Topsoe with UPM BioVerno have developed stand-alone HVO production processes and products [51]. Moreover, in South America, HVO has already been co-processed with fossil diesel in a pilot plant in Brazil, and large scale production is expected to start in Paraguay and Bolivia in the next years. Uruguay recently adapted national regulations to open pathways for producing HVO locally, and case studies indicated the viability of similar projects in Colombia where the Colombian oil company (Ecopetrol) already has a patent -Biocetano [52].

HVO production

Catalytic hydroprocessing is designed to convert vegetable oils to high quality diesel, which can be used in existing diesel engines. Catalytic hydroprocessing is a common refinery process aiming to increase hydrogen to carbon ratio, decrease the concentration of heteroatoms and metals, and reduce the boiling point of petroleum fractions. Catalytic hydroprocessing of vegetable oils is focused on producing a high quality biofuel product that is compatible with existing diesel fuel infrastructure without by-products, while during Fatty Acid Methyl Ester (FAME or biodiesel) transesterification, glycerin is produced [53, 9, 51].

The HVO production process starts with fatty oils (triglyceride). In the first step, the triglyceride is hydrotreated involving hydrogenation of the C double bond C bonds of the vegetable oils resulting in diglycerides, monoglycerides and acids. The following step converts the intermediates into straight-chain alkanes ranging from C15 to C18 (at 350–450°C in the presence of H_2 at 50–150 bar) by three different pathways: decarboxylation, decarbonylation and hydrogenation, and finally, one catalytic isomerization step which will lead to a mixture of n- and iso-paraffins [53, 9, 51]

The **decarboxylation** pathway involves converting a carboxylic acid into a methyl group and CO_2 as shown in **Equation 2.1**. No hydrogen is required to convert a carboxylic acid group to an alkane by the decarboxylation pathway [53].

$$R - CH_2 - COOH \rightarrow R - CH_3 + CO_2 \tag{2.1}$$

The **decarbonylation** pathway involves the reaction between carboxylic group with hydrogen to produce a methyl group, CO and water as shown by **Equation 2.2** [53].

$$R - CH_2 - COOH + H_2 \rightarrow R - CH_3 + CO + H_2O \tag{2.2}$$

The **hydrodeoxygenation** pathway involves converting the carboxylic acid with hydrogen to produce an alkane and water as shown by **Equation 2.3** [53].

$$R - CH_2 - COOH + 3H_2 \rightarrow R - CH_2 - CH_3 + 2H_2O \tag{2.3}$$

HVO combustion characteristics

The effects of HVO on engine performance and regulated emissions have been widely reported in literature, since it is a reference biofuel under commercial use in some countries. HVO has potential advantages with respect to both diesel and biodiesel in terms of production costs, exhaust emissions and adaptability to current engine designs. Most studies have shown that use of HVO reduce emissions of regulated compounds (NOx, PM, HC and CO), as well as fuel consumption without any changes to the engine or its control in heavy-duty engines [54, 55, 56, 57, 58, 59, 60, 61].

HVO fueled engine results in lower in-cylinder peak pressure than diesel owing to its higher CN which ultimately leads to shorter ignition delay [61], resulting in more rapid development and advance of combustion, particularly at low speed and loads, where the combustion rates are limited by chemical processes. Examination of diesel particle filter (DPF) regeneration revealed, comparable or lower particle loading for HVO, and higher rate of penetration of fuel into lubricating oil for HVO compared to diesel [8].

In conclusion, HVO is a promising fuel for compression ignition engines which possesses superior physico-chemical properties such as higher CN, heating value, negligible unsaturation level, oxygen, sulphur and aromatic content as compared to diesel which results in better performance and emissions characteristics and it can be developed into a sustainable alternative to diesel [61].

Regarding unregulated emissions, the results of the literature review are presented in **Table** 2.3.

Table 2.3: Summary of unregulated pollutans (biological activity included) reported for HVO-diesel blends tested in diesel engines

Diesel-HVO blends							
Ref (Country)	**Fuel**	**Engine**	**Mode**	**Phase**	**PAH**	**Carbonyls**	**Bio. Act**
[62] (2022, U.S.)	Diesel(Ref) HVO HVO50B50	2009 John Deere single cylinder, 4.5L off-road	nonroad cycle and the 5-mode D2 ISO 8718	Gas + PM	↑ (HVO) ↓ (HVO50B50)	–	↑ (HVO) ↓ (HVO50B50)
[63] (2020, Denmark)	Diesel(Ref) HVO13	N.A.	N.A.	PM	↑	–	≈
[64] (2020, Sweden)	Diesel(Ref) HVO	6-cylinder 13-L, modified to a single cylinder	6 bar BMEP 1200 r/min	PM	↑	–	≈ (ROS)
[65] (2020, Taiwan)	Diesel(Ref) HVO20	Hyundai Tucson 1.9 L CRDI, Euro 6	At different engine loads	Gas	–	≈ (HCHO)	–
[66] (2018, Poland)	HVO13B7	Euro 5 Fiat Panda-2014 1.3 JTD	45%- 43.75 km/h 50% load- 20 km/h.	Gas + PM	↓	–	↑
[67] (2017, Poland)	B7(Ref) HVO13B7	Euro 5 Fiat Panda-2014 1.3 JTD	45%- 43.75 km/h 50% load- 20 km/h.	Gas	–	≈	–
[68] (2017, Czech R.)	Diesel(Ref) HVO30 HVO	6-cylinder turbocharged 2001 model year 5.9 L Iveco Tector	WHTC	PM	↓ (HVO) ↑ (HVO30)	–	–
[8] (2019, Czech R.)	Diesel(Ref)	Euro 6, 4-cylinder 1.59 L	NEDC, WLTP CADC	Gas	–	↓ (HCHO)	–
[69] (2015, Germany)	Diesel(Ref) HVO	OM 906 LA 6.3 L, 6-cylinder, Euro III	ESC test	Gas + PM	↓↓	↑	↑ (Mutag.)
[70] (2015, Poland)	Diesel(Ref) HVO30	Midsize passenger car, 1.92 L, CRDI, Euro 4	UDC, EUDC, NEDC	Gas (Carbonyl) PM (PAH)	↑	↓↓	–
[71] (2013, Germany)	Diesel(Ref) HVO	Mercedes-Benz OM 906 LA, Euro III	ESC	PM	↓	≈	↓↓

Diesel-HVO blends (cont.)							
Ref (Country)	**Fuel**	**Engine**	**Mode**	**Phase**	**PAH**	**Carbonyls**	**Bio. Act**
		6.37 L, 6-cylinder					(Mutag.)
[72]	Diesel(Ref)	2000 Freightliner	City and high	Gas	–	↓	–
(2012, U.S.)	HVO50	Truck 2000 with a	speed cruise				
	HVO	Caterpillar C-15	drive cycles				
[73]	Diesel(Ref)	Small engine	ISO standard	PM	↓↓	–	≈
(2010, Finland)	HVO	Kubota D1105-T	cycle				

↑:Increase with respect to the reference fuel (Ref) ↑↑: Sharp increase ↓:Decrease ↓↓:Sharp decrease ≈: Remain constant –:not presented
HVO*X*: *X*% by volume of HVO blended with diesel
HVO*X*B*Y*: *X*% by volume of HVO blended with *Y*% by volumen of biodiesel and and 100–*X*–*Y* of diesel

From the literature review, 12 investigations on unregulated emissions with HVO were found, which have been carried out in both, gas phase and particles, and some of them include biological activity tests (see summary in **Figure** 2.5). All the gas phase studies correspond to carbonyl compounds, which, according to the reported results, remain constant (43%) or decrease (43%) compared to diesel, only 14% reported an increase. Most of the studies have been carried out in steady state with blends from 13% to pure HVO. For PAH emissions there were no consensus, 48% of the studies reported an increase, while the rest a decrease. These reductions in PAH emissions have been attributed to the absence of aromatics. However, the increase emissions would originate from pyrosynthesis pathways of lower molecular weight hydrocarbons in the fuel. Finally, from the biological activity studies, only mutagenicity and ROS were reported, and 44% reported an increase in biological activity with respect to diesel fuel.

It could be concluded that the use of HVO blends tends to reduce total carbonyl emissions, but could increase the biological response. However, the disparity of findings (mainly with PAH emissions) corroborates the substantial dependence of unregulated emissions on factors such as the engine type, and operation modes.

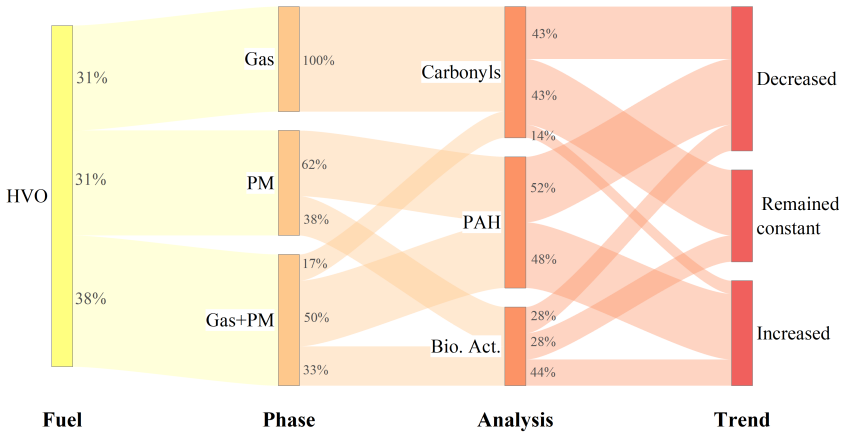

Figure 2.5: Summary of findings on unregulated emissions and biological activity with HVO

2.3.2 Butanol

Butanol is a biomass-based renewable fuel with four-carbon structure and is considered a high-chain alcohol ($CH_3(CH_2)_3OH$). Butanol is of particular interest as a renewable biofuel as it is less hydrophilic, and possesses higher energy content, higher cetane number, higher viscosity, lower vapor pressure, higher flash point and higher miscibility than ethanol, making it more preferable than methanol and ethanol for blending with diesel fuel [74].

Despite butanol is more promising as a renewable blending component for diesel fuels (their physicochemical properties are closer to diesel fuel) than ethanol, butanol can not directly replace diesel fuel. Lapuerta et.al. [75] reported that the maximum butanol content is limited by engine starting difficulties at very low ambient temperatures. Therefore, butanol should be introduced up to 13% at any ambient conditions and under any certification procedure.

Some other points that make butanol suitable for blending with diesel are: stoichiometric air/fuel ratio of butanol is similar to diesel fuel, the high flash point ensures safe transportation and handling.

Butanol shows lower heating value than diesel, therefore, more amount is required to produce the same power output in the engine. Comparing ethanol, methanol and butanol, the latter has more energy density in volume than ethanol, reducing the fuel consumption needed to keep an specific load in diesel engines [76, 74, 77, 78]. The presence of butanol affects the fuel-air mixing process and the injection spray development. The lower density, lower kinematic viscosity and higher volatility of n-butanol with respect to diesel fuel lead to a better atomization for butanol-diesel blends, which is helpful to form homogeneous fuel-air mixtures, thus decreasing the soot emissions when the blend is tested [76, 74, 77, 78]. Blending and fumigation techniques are the most preferred methods for using butanol in diesel engines [79, 80].

Butanol production

Butanol can be produced through biological or chemical routes (**Figure** 2.6). Among the biological routes, ABE fermentation, in which sugar, glycerol, or lignocellulose feedstocks are fermented by microorganisms to produce acetone, ethanol and n-butanol, is the most widely used. However, to achieve a better economic competitiveness of ABE fermentation, research efforts are focused on the high cost of substrates, the low butanol concentration in the fermentation broth and the excessive cost from downstream processing. Other biological pathways for n-butanol production are IBE fermentation in which also ethanol and isopropanol are obtained, and syngas fermentation. In this process, before fermentation, the biomass or waste feedstock is previously thermochemically converted to carbon monoxide (CO), and hydrogen (H_2) synthesis gas (syngas). Among the chemical options, n-butanol can be produced from oxo synthesis, Reppe synthesis or crotonaldehyde hydrogenation [76].

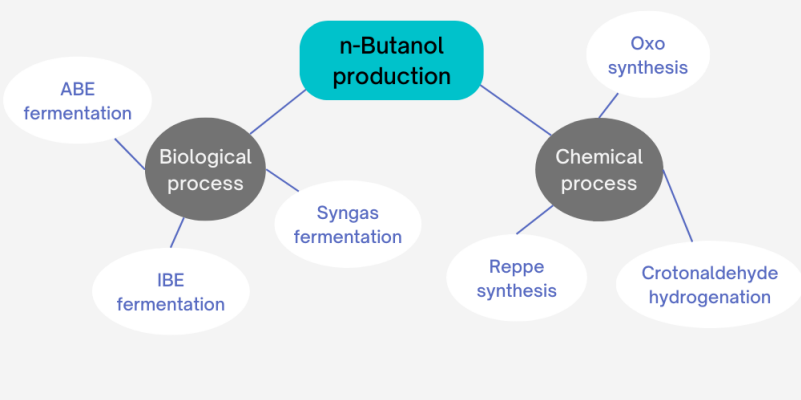

Figure 2.6: Sumary of n-butanol production processes [76]

Butanol combustion characteristics

To date, most studies on butanol-diesel blends have focused on performance and regulated emissions from diesel engines. Kumar and Saravanan [78] and Vinod Babu et al. [77] have summarized the effects of n-butanol on combustion based on more than 50 scientific publications, in the following points:

- Increased butanol content resulted in a lower CN of the blends, which in turn increases the ignition delay. This enhances the premixed combustion phase due to which peak heat release rate and peak in-cylinder pressure increases slightly [77].

- Increased butanol quantity in the blends results in improvement of break thermal efficiency (BTE) due to higher burning velocity and deterioration of brake-specific fuel consumption (BSFC) owing to inferior calorific value of butanol [77].

- The enhanced oxygen content of butanol improves the combustion process, particularly during the diffusion combustion phase. Higher burning velocities lead to higher efficiency [78].

- The heating value of butanol is approximately 21% lower than diesel and hence the engine requires more amount of fuel to produce the same output torque [78].

- NOx emissions generally decrease with increasing butanol content in the blends. This is due to the engine running overall leaner and the temperature lowering effect of butanol (due to its lower calorific value and higher heat of evaporation) dominating the possibly higher temperatures during the premixed combustion

phase as a result of longer ignition delay (due to its lower cetane number) [78].

- The presence of fuel-bound oxygen in the blends especially in locally rich zones improved the combustion process resulting in less smoke emissions [78].

- HC emissions increased with increasing butanol content in the blends. The slower evaporation and poorer air–fuel mixing due to the higher latent heat of evaporation of butanol blends and fuel impingement on the walls due to increased spray penetration are the major causes for unburned hydrocarbons [78].

- The combustion temperature is lowered owing to higher LHV and heat of evaporation of butanol and also by using more EGR fraction which in turn decreases the NOx emissions besides prolonging ignition delay period [77].

- Also, ignition delay can be extended by EGR and retarded injection timing which provide ample time for better mixing of air and fuel. This results in lowering the overall combustion temperature which in turn results in suppressing the smoke and NOx formation [77].

In conclusion, in terms of regulated emissions and engine performance, butanol can be considered as an promising option to be blended with diesel fuel. Regarding unregulated emissions, the results of the literature review are presented in **Table** 2.4.

Table 2.4: Summary of unregulated pollutans (biological activity included) reported for butanol-diesel blends tested in diesel engines

Diesel-butanol blends							
Ref (Country)	**Fuel**	**Engine**	**Mode**	**Phase**	**PAH**	**Carbonyls**	**Bio. Act**
[81] (2022,U.S.)	Diesel(Ref) B90Bu10	Indirect-injected, 4-cylinder Onan DJC	Idle	Gas+PM	↓	–	–
[82] (2020, India)	Diesel(Ref) Bu10	Tata; Safari DICOR 3 L 4-cylinder in-line, 4-stroke, CRDI	At different BMEP	Gas	–	↓ (HCHO)	–
[83] (2019, China)	Biodiesel(Ref) B90Bu10, B80Bu20 B70Bu30	Water-cooled 4-cylinder 4-stroke direct injection compression ignition	At different BMEP	Gas	–	↑ (CH3CHO)	–
[84] (2014, Singapore)	Diesel(Ref) B20Bu5 B20Bu10 B20Bu15	L70AE, Yanmar Corp Power generator single cylinder, four-stroke	At different engine loads	PM	↓	–	↑ (Citotoxicity)
[85] (2019, Korea)	Diesel(Ref) Bu10W2 Bu10W5	Single cylinder CRDI	900 and 1900 r/min	Gas	–	↑	–
[86] (2019, India)	Diesel(Ref) Bu10 Bu20	Single cylinder, Kirloskar, 4-strokes, DI.	At different Equivalence ratios with fumigation	Gas	–	↑	–
[87] (2019, France)	Diesel(Ref) Bu10	4-cylinder 4-stroke CRDI	0.75 MPa-1500 r/min	Gas	–	↑↑	–
[68] (2019, Czech R.)	Diesel(Ref) Bu30HVO70	6-cylinder turbocharged 2001 model year 5.9 L Iveco Tector	WHTC	PM	↓↓	–	–
[88] (2016, U.S.)	Biodiesel(Ref) B90Bu10,	Indirect-injected, 4-cylinder Onan DJC	Idle	Gas+PM	> in gas ↓	–	–

Diesel-butanol blends (cont.)							
Ref (Country)	**Fuel**	**Engine**	**Mode**	**Phase**	**PAH**	**Carbonyls**	**Bio. Act**
	B80Bu20 B60Bu40				≈ (B60Bu40)		
[89] (2015, Taiwan)	Diesel(Ref) B20Bu10 - B20Bu50	4-stroke, water-cooled, single cylinder diesel-engine generator	3 kW load	Gas+PM	↑	–	–
[90] (2015, Taiwan)	Diesel(Ref) B10Bu10 - B40Bu10	Robin SDG 2200- Subaru single cylinder, 0.23L	2.8 kW 3000 r/min	Gas	–	↑	–
[91] (2015, Korea)	Diesel(Ref) Bu5 Bu10 Bu20	Hyundai D4CB 2.5 L, Common rail 4-cylinder	At different engine loads	Gas	–	↑ (HCHO) (at low loads)	–
[92] (2015, Taiwan)	Bu5(Ref) Bu10 Bu15	Mitsubishi 4M40-2AT1 4-cylinders DI	2200 r/min 50 Nm	Gas + PM	↓↓	–	–
[93] (2014, Singapore)	Diesel(Ref) Bu2 Bu4	L70AE, Yanmar Corp Power generator single cylinder, 4-stroke	3000 r/min and at 50% related power	PM	↓ (Bu2) ↑ (Bu4)	–	↓ (Bu4) (Citotoxicity)
[94] (2014, Taiwan)	B2(Ref) Bu10 Bu20	6-cylinder, 6 L, DI heavy-duty engine Hino W06E	At different engine loads	Gas+PM	↓	–	–
[95] (2012, Spain)	Diesel(Ref) Bu16	Nissan Euro 5 M1D-Bk	Urban mode and extra-urban mode	Gas	–	↑	–

↑:Increase with respect to the reference fuel (Ref) ↑↑: Sharp increase ↓:Decrease ↓↓:Sharp decrease ≈: Remain constant –:not presented

Bu*X*: *X*% by volume of butanol blended with diesel

B*Y*Bu*X*, *X*% by volume of butanol blended with *Y*% by volumen of biodiesel and and 100–*X*–*Y* of diesel

The increase in carbonyl emissions is well known for oxygenated fuels. Particularly for alcohol fuels, carbonyls are direct intermediates in dehydrogenation reactions and indirect intermediates in dehydration reactions [96], and the type of carbonyl species emitted are strongly influenced by the alcohol molecular structure [82]. Therefore, most studies of unregulated emissions with butanol have focused on carbonyl compounds (see summary in **Figure** 2.7), many of them with biodiesel-butanol blends. Carbonyl emissions increased in almost 100% of the studies, while for PAH, most studies (67%) reported a decrease. Only two studies have evaluated biological response, and they have focused on cytotoxicity. Therefore, more in-depth studies are required to evaluate the biological response from a comprehensive perspective, including genotoxicity and oxidation potential.

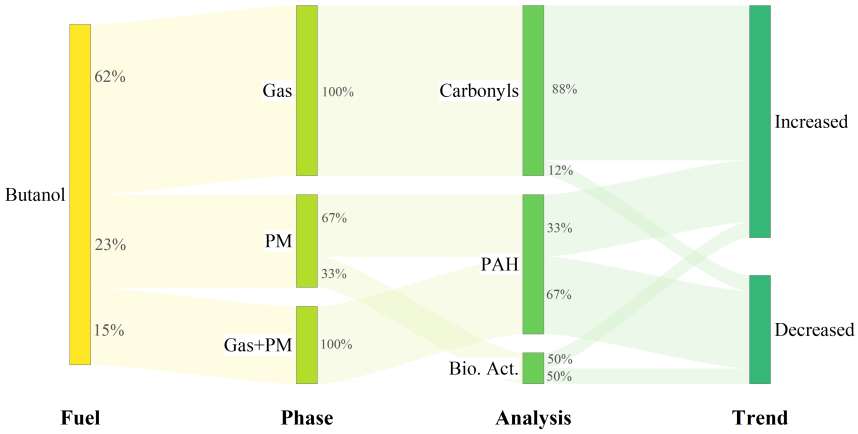

Figure 2.7: Summary of findings on unregulated emissions and biological activity with butanol

2.3.3 Pentanol

In the last years, pentanol has been explored as an alternative fuel in diesel engines for automotive applications because of its advantages over other alcohols. Pentanol is a five-carbon straight-chain alcohol ($CH_3(CH_2)_4OH$) that has greater potential as a blending component with diesel fuel owing to its higher energy density and cetane number, that leads to a better combustion efficiency and consequently improved thermal efficiency and specific fuel consumption in comparison to other low carbon alcohols. Furthermore, pentanol has better blend stability and less hygroscopic nature when compared to other widely studied alcohols. Some properties of pentanol such as density, viscosity, latent heat of vaporization, and lower heating value are closer to diesel [49].

Pentanol production

Pentanol, as a second-generation biofuel, has been explored as a liquid alternative fuel in diesel engines for automotive applications.

Pentanol microbial synthesis from cellulose or glucose fermentation technology for its production is under continuous development [97, 98]. Pentanol can be produced from biological pathways like natural microbial fermentation using engineered micro-organisms and bio-synthesis from glucose using *Escherichia coli*, though many of the key enzymes utilized are derived from other important and useful organisms such as yeast strains and *lactobacilli*. These microbes along with others can potentially offer advantages to make them better hosts for pentanol production [98]. Pentanol being a longer-chain alcohol requires less energy for its production when compared to other lower alcohols.

There are also some chemical methods for the pentanol production such as fractional distillation of mixed alcohols resulting from the chlorination and alkaline hydrolysis of pentane and fractional distillation of fusel oil [99].

Pentanol combustion characteristics

Although there is much more research for butanol and short-chain alcohols than for pentanol in ICE applications, some research has investigated regulated emissions and performance of diesel engines fueled with pentanol blends. Briefly, Liang et al. [100] used seven different EGR rates with two ternary blends of biodiesel-pentanol-diesel (B10P20 and B20P10) fuels to investigate the effects on combustion and emission characteristics. They found a decrease in HC at high EGR rates and there was no significant difference in NOx emissions, in addition, these ternary blends not only reduced soot emissions but also reduced CO under different EGR rates compared with diesel. Zhao W et al.[101] investigated the effects of different intake pressures on the performance and emission characteristics of an engine fueled with 20% and 40% pentanol blends. Results showed that pentanol helped to extend the operating range of diesel engines when the intake pressure was low, for example operating at high altitude. They also reported similar thermal efficiency, higher NOx emissions, and lower soot and HC emissions compared to diesel. On the contrary, Pinzi et al. [102] reported an increase of HC and a decrease of NOx, and PM and particle number concentration (PN). A similar result was found by Santhosh et al. [103], showing that the diesel engine can run with blends up to 30% of pentanol without any engine modification. Campos-Fernández et al. [104] studied the engine performance using three pentanol/diesel blends. The results showed that the BTE of the blend was higher than that of diesel fuel alone, and that blends with up to 25% pentanol could be used as a fuel for diesel engines without a significant power loss.

The combustion, performance and emission characteristics of diesel engines using this alcohol have been summarized by [77, 78] as follows:

- The lower cetane number of pentanol resulted in a prolonged ignition delay,which in turn helped in overcoming the trade-off between NOx and PM.

- Pentanol/diesel blends showed higher peak cylinder pressure and higher premixed heat release rate compared to diesel.

- Pentanol/diesel fueled diesel engines generally offered diesel-like or better thermal efficiency. This was due to the lower viscosity and more oxygen quantity of the blends result in improved atomization and combustion.

- The low LHV of pentanol/diesel blends resulted in higher BSFC.

- High NOx emissions were prevalent at high engine loads when using pentanol/diesel blends which can be mitigated by using EGR.

- Pentanol blends decreased soot emissions as a result of its increasing oxygenated nature.

- Some researchers have reported a drop in CO and HC emissions with pentanol content up to 20%.

Although there is an overall agreement that adding pentanol to diesel fuel decreases particulate matter while maintaining thermal efficiency, there is still a lack of knowledge on their unregulated emissions, particularly of carbonyl compounds, which are of major concern when blending alcohols with fossil fuels. No studies were found on unregulated emissions with pentanol-diesel blends.

2.3.4 Polyoxymethylene dimethyl ether -OME

Electrofuels (or e-fuels) are gaseous or liquid fuels which can be used in ICE. They are produced from hydrogen and captured carbon dioxide using renewable electricity as the power source [105]. New oxygenated e-fuels are being developed for use in ICE and may contribute to the decarbonization of transport. Polyoxymethylene dimethyl ethers (abbreviated as PODEn, DMMn, OMEn, POMDMEn, and OMDMEn) are promising e-fuels for diesel engines because they contain nearly 50% oxygen and have high cetane number. They are characterized by a CH_3-O-$(CH_2$-$O)_n$-CH_3 general structure, with n as the number of oxymethylene groups. Long chain OME (n>3) have proven to be suitable for diesel engine applications due to their physical properties and eco-friendly based on life-cycle assessments [106]. The viscosity, lubricity, vapor pressure and flash point are significantly improved with n ranging between 3-5 [107], and are miscible with diesel at any ratio without changing the structure of the diesel engine (drop-in fuel) [106]. Currently, $OME_{3\text{-}5}$ is manufactured in China at a scale of > 240,000 t/y. In the Netherlands there is a pilot project

for the production of OME in a company that currently produces formaldehyde and methanol [108].

Among the most outstanding characteristics of the OMEn, is its ability to reduce soot during the combustion in diesel engines. The presence of activated methylene groups next bound to oxygen atoms (–O–CH_2–) in the chemical structure of the OMEs leads to the formation of hydroperoxides in an early stage of the combustion. These hydroperoxides decompose into OH-radicals which subsequently degrade soot precursors by oxidative processes [106].

OME production

All common production pathways for OMEn proceed via methanol as an intermediate. Methanol in turn can be produced from hydrogen (H_2), which can be obtained from water electrolysis and carbon dioxide (CO_2). Thus, OMEn are potential e-fuels [7]. That kind of fuel production concept, using only water (H_2O), carbon dioxide (CO_2) and electrical energy as feedstock (**Figure** 2.8), is generally known under the term Power-to-Fuel (PtF).

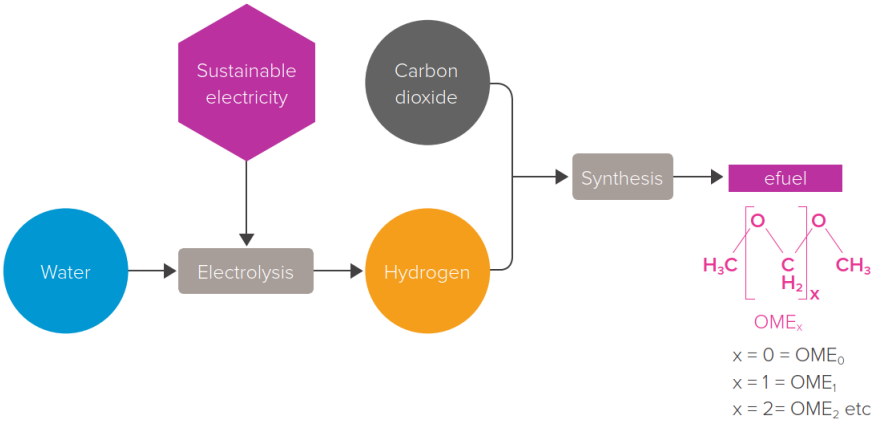

Figure 2.8: Production of e-fuels [109]

There are several routes for the OMEn production via different intermediate steps. All technologically viable routes currently start from methanol as a platform chemical and involve a formaldehyde (HCHO) unit to supply the OME monomer units, the oxymethylene groups (CH_2O). Among the most studied routes for the synthesis of OME are the synthesis of OME directly from methanol and formaldehyde and the synthesis of OME through the two intermediates methylal and trioxane (**Figure** 2.9) [110, 111].

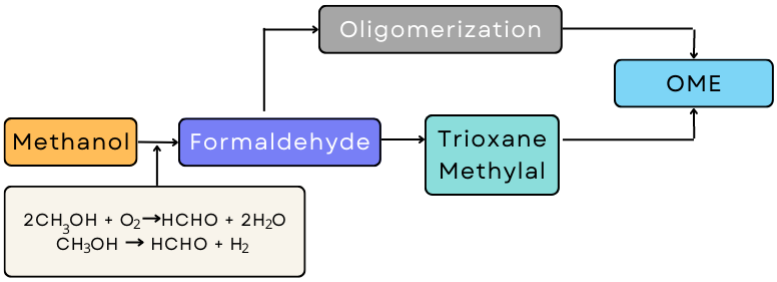

Figure 2.9: OME synthesis pathways [110, 111]

The OME production costs are strongly dominated by the raw material costs. The economy of the process chain in OME production was assessed by Schmitz et al. [112], analyzing the influence of the price of methanol and the investment costs. Over a wide range of the price of methanol and the investment costs, they concluded that the production of OME is competitive or even cheaper than conventional diesel fuel production.

OME combustion characteristics

The research on OMEn, particularly that focusing on their use in CI engines, has progressed significantly over the past eight years. Recent studies investigating the effect of OME blending ratio on the performance and regulated emissions of diesel engines and are summarized in **Table** 2.5. Nevertheless, factors such as polymerization degree, blend ratio, and combustion mode have varied by study as can be seen in **Table** 2.5. Researchers revealed meaningful reductions in soot emissions in the raw exhaust gas, due to the oxygen content and to the absence of C-C bonds. In some articles a reduction of NOx emissions was observed [113, 114], while in others an increase was reported [115, 116]. Most published studies have been performed at steady state engine condition. Instead, transient operation is more likely to provide realistic results since the main impact on emissions is observed during accelerations, considering that engine load and speed change frequently during driving cycles. Few studies have been published following cycles for heavy-duty diesel engines and according to the literature, only a few investigations were found reporting the effect on particle size distributions [4, 113].

Table 2.5: Summary of regulated pollutans and BTE reported for OME-diesel blends tested in diesel engines.

Ref	Engine	Blends	Mode	PM	CO	NOx	THC	BTE
[113] (2017)	4-cylinder turbocharged intercooled CRDI. 4.09L	0, 10%, 20% and 30% of OME_{3-8} - diesel	25%, 50%, 75% and 100% of engine load	↓ (27.6%, 41.5% and 47.6%)	↓	↑	↓	↑
[114] (2015)	Single-cylinder research engine retrofitted from a 4-cylinder	0, 10%, 20% of OME_{3-4} - diesel	At 2, 4 and 6 bar IMEP	↓ (Smoke opacity)	↓	↑	↓	↑
[5] (2017)	Single-cylinder research engine retrofitted from a 4-cylinder	20% of OME_{3-4} -	ESC test cycle	↓ (Smoke opacity)	↓	↑	↓	↑
[117] (2017)	Single-cylinder research engine retrofitted from a 4-cylinder	Diesel Biodiesel 15% of OME_{3-4} - biodiesel	1600 r/min 0.4, 0.6, 0.8, 0.9. 1 Mpa	↓	↑ (at low load) ↓ (at high load)	↓ (at low load) ↑ (at high load)	↑	↑
[118] (2017)	Single cylinder based on a MTU 396 CRDI	5% and 10%, of OME_{2-7} - diesel	1600 r/min 100% engine load	↓ (Smoke opacity)	↓	↑	N.A.	
[4] (2019)	Single cylinder engine. 0.39L	35% OME_{3-5} - diesel	At 5 different loads	↓	↓	N.A.	↓	
[119] (2020)	4-cylinder, turbocharged, CR 2.7 L	0, 10%, 20% of OME_{3-8} - diesel	1600 r/min 100% engine load	↓	↓	↑	↓	N.A.
[116] (2021)	L12 small agricultural diesel engine	25% of OME_{3-5} - diesel	1800 r/min 1-5 kW	↓ (Smoke opacity)	↓	↓ (NO)	N.A.	N.A.
[6] (2021)	4-cylinder, four-stroke, turbocharge, intercooled, CR 4.2 L	0, 10%, 20% and 30% of OME_{3-6} - diesel 2%, 4%	2400 r/min 0%,25%, 50%, 75% and 100% of engine load	↓ (Smoke opacity) (PN)	N.A.	N.A.	N.A.	N.A.
[120] (2021)	Single cylinder CR engine	6%, 8% 10% of OME_3 - diesel	1200 r/min 30%, 40%, 50%, 60% of engine load		N.A.	↑	↑	N.A.
[115] (2022)	6-cylinder Weichai WP12.460 HD 11.59 L	0, 10%, 20% and 30% of OME_{3-6} - diesel	1900 r/min 25%, 50%, 75% and 100% of engine load	↓ ↓ (PN)	↓	↓	↓	↑
[121] (2016)	6-cylinder, 24-valve, CRDI HD	0, 15%, and 25% of OME_{3-6} - diesel	WHSC test cycle	↓	↓	↓	↓	↓

↑:Increase with respect to lower OME blend or diesel fuel ↓:Decrease ≈: Remain constant N.A.:not available

As revealed by the research summary above, the impacts of OMEn on engine regulated emissions are favorable, primarily in terms of PM reductions. However, few studies have focused on unregulated emissions (**Table** 2.6), and none of them in

biological activity induced by OME blends.

Table 2.6: Summary of unregulated pollutans reported for OME-diesel blends tested in diesel engines.

Diesel-OME blends						
Ref (Country)	**Fuel**	**Engine**	**Mode**	**Phase**	**PAH**	**Carbonyls**
[116] (2021, China)	Diesel(Ref) OME25	L12 small agricultural	At different engine loads	Gas + PM	↓↓	–
[122] (2014, U.S.)	Diesel(Ref) OME7.5	Euro 3, 4-cylinders CR diesel engine	50 and 120 km/h	Gas + PM	↑	–
[4] (2019, Germany)	Diesel(Ref) OME35	Single cylinder 0.39L	At different engine loads	Gas	–	↑ (HCHO)
↑:Increase ↑ ↑: Sharp increase ↓:Decrease ↓ ↓:Sharp decrease ≈: Remain constant –:not presented OME*X*: *X*% by volume of OME blended with diesel						

Two of the studies have evaluated PAH emissions and reported contradictory results, only one study evaluated formaldehyde and reported an increase, which is common in other oxygenated fuels (see summary in **Figure** 2.10). In addition, all studies have been performed at steady state engine conditions. Although OMEn fuels have received attention in recent years, more research is still needed regarding the impact of their use on unregulated emissions under representative operating conditions.

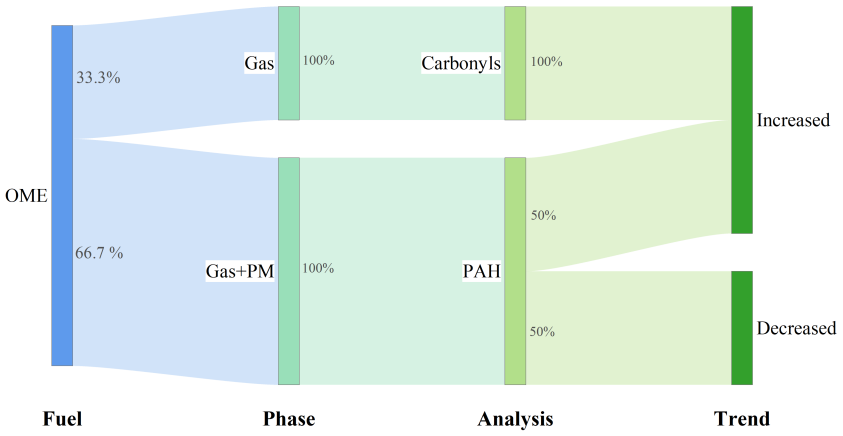

Figure 2.10: Summary of findings on unregulated emissions and biological activity with OME

2.3.5 Terpene-based fuels

Terpene-based fuels can be obtained from different processes, for example turpentine, a mixture of terpenes, is mainly obtained from the process of kraft softwood pulping as a by-product of the paper industry (in this case called crude sulfate turpentine) and by vacuum or steam distillation of oleoresin as a secondary product of resin industry

(in this case called gum turpentine) [3]. However, terpene mixtures have been mainly used as a component of additives and as a new type of cold flow improver [123], and to a lesser extent, as component of gasoline and diesel fuels [3].

The most used terpene-based fuel is turpentine. Turpentine oil extracted from pine trees is composed of terpenoids and terpenes ($C_{10}H_{16}$), which is its main constituent. It can readily be obtained from resins, oleoresins etc. [124]. There are various methods of obtaining resins from pine trees which are known as resin tapping methods. This oil is an important potential alternative fuel as it readily mixes with biodiesel and can be used as replacement of diesel fuel [124].

Some researchers have reported performance and regulated emissions using diesel/ biodiesel blends with turpentine in diesel engines (**Table** 2.7). The use of this terpene-based fuel have shown a reduction in several harmful emissions. Turpentine oil shows properties close to diesel, but the most interesting feature is that it mixes almost completely with any other fuels which in turn leads to lower amount of HC, CO and smoke emissions [124].

Table 2.7: Studies of performance and emissions for turpentine-diesel/biodiesel blends tested in diesel engines.

Diesel/biodiesel-turpentine blends								
Ref	**Fuel**	**engine**	**CO**	**HC**	**NOx**	**PM**	**BTE**	**BSFC**
[125] (2017)	B90T10 - B50T50	TAF1 model single cylinder	≈	↑	↑	↓	↓	↑
[126] (2020)	T20	Euro 6 Nissan, K9K (1.5 dCi).	↑	↑	↓	↓	↓	↑
[127, 128] (2017)	B50T50, B70T30 B90T10	Single cylinder four stroke	↓	↓	↓	↓	↓	↑
[129] (2017)	B90T10 - B50T50 (mineral turpentine)	TAF1 model single cylinder	↓	↓	↑	↓	↓	↑
[130] (2010)	T30 T40 T50	TAF1 model single cylinder	↓	↓	↓	↓	↓	↑
↑:Increase with increasing turpentine content ↓:Decrease with increasing turpentine content T*X*: *X*% by volume of turpentine blended with diesel B*Y*T*X*, *X*% by volume of turpentine blended with *Y*% by volumen of biodiesel								

Some chemical transformations have been proposed for turpentine to improve its properties as fuel, such as hydrogenation. Hydrogenated turpentine has shown convincing effects on the properties of the fuels obtained. For example, hydrogenated turpentine has great advantages as a fuel, such as high energy density and excellent cold flow properties [3].

Finally, although there is consensus in the literature regarding the potential of

some of the most studied biofuels in reducing regulated emissions such as CO, HC and PM, the same does not occur with unregulated pollutant emissions and biological response from a perspective beyond cytotoxicity. Faced with a panorama of increasing substitution of diesel by biofuels, the need for detailed research is evident to assess the suitability of using mixtures of potential interest in terms of the emission of pollutants with a high potential for affecting human health and the environment.

Bibliography

[1] COP26: Together for our planet | United Nations.

[2] David Donoso, David Bolonio, Rosario Ballesteros, Magín Lapuerta, and Laureano Canoira. Hydrogenated orange oil: A waste derived drop-in biojet fuel. *Renewable Energy*, 188:1049–1058, 2022.

[3] David Donoso, Rosario Ballesteros, David Bolonio, María-Jesús García-Martínez, Magín Lapuerta, and Laureano Canoira. Hydrogenated turpentine: A biobased component for jet fuel. *Energy & Fuels*, 35(2):1465–1475, 2021.

[4] Ahmad Omari, Benedikt Heuser, Stefan Pischinger, and Christoph Rüdinger. Potential of long-chain oxymethylene ether and oxymethylene ether-diesel blends for ultra-low emission engines. *Applied Energy*, 239:1242–1249, 2019.

[5] Haoye Liu, Zhi Wang, Jun Zhang, Jianxin Wang, and Shijin Shuai. Study on combustion and emission characteristics of Polyoxymethylene Dimethyl Ethers/diesel blends in light-duty and heavy-duty diesel engines. *Applied Energy*, 185:1393–1402, 2017.

[6] Junheng Liu, Zengguang Liu, Lejian Wang, Pan Wang, Ping Sun, Hongjie Ma, and Pengcheng Wu. Effects of PODE/diesel blends on particulate matter emission and particle oxidation characteristics of a common-rail diesel engine. *Fuel Processing Technology*, 212, 2021.

[7] Omar I. Awad, Xiao Ma, Mohammed Kamil, Obed M. Ali, Yue Ma, and Shijin Shuai. Overview of polyoxymethylene dimethyl ether additive as an eco-friendly fuel for an internal combustion engine: Current application and environmental impacts. *Science of the Total Environment*, 715, 2020.

[8] Martin Pechout, Martin Kotek, Petr Jindra, David Macoun, Jan Hart, and Michal Vojtisek-Lom. Comparison of hydrogenated vegetable oil and biodiesel effects on combustion, unregulated and regulated gaseous pollutants and DPF regeneration procedure in a Euro6 car. *Science of the Total Environment*, 696:133748, 2019.

[9] Ashraf Amin. Review of diesel production from renewable resources: Catalysis, process kinetics and technologies. *Ain Shams Engineering Journal*, 10(4):821–839, 2019.

[10] H. Suhaimi, A. Adam, A.G. Mrwan, Z. Abdullah, M.F. Othman, M.K. Kamaruzzaman, and F.Y. Hagos. Analysis of combustion characteristics, engine performances and emissions of long-chain alcohol-diesel fuel blends. *Fuel*, 220:682–691, 2018.

[11] A. Atmanli and N. Yilmaz. A comparative analysis of n-butanol/diesel and 1-pentanol/diesel blends in a compression ignition engine. *Fuel*, 234:161–169, 2018.

[12] A. Álvarez, M. Lapuerta, and J.R. Agudelo. Prediction of flash-point temperature of alcohol/biodiesel/diesel fuel blends. *Industrial and Engineering Chemistry Research*, 58(16):6860–6869, 2019.

[13] J.R. Agudelo, M. Lapuerta, O. Moyer, and A.L. Boehman. Autoignition of alcohol/c7-esters/n-heptane blends in a motored engine under hcci conditions. *Energy and Fuels*, 31(3):2985–2995, 2017.

[14] J.P. Hernández, M. Lapuerta, R. García-Contreras, and J.R. Agudelo. Modelling of evaporative losses in n-alcohol/diesel fuel blends. *Applied Thermal Engineering*, 102:302–310, 2016.

[15] Zhongchao Tan. *Air Pollution and Greenhouse Gases*. 2014.

[16] IARC. Diesel engine exhaust carcinogenic. *Journal of the National Cancer Institute*, 104(11):855–868, 2012.

[17] IARC. List of Classifications by cancer sites with sufficient or limited evidence in humans Volumes 1 to 114, 2014.

[18] Hussein I. Abdel-Shafy and Mona S.M. Mansour. A review on polycyclic aromatic hydrocarbons: Source, environmental impact, effect on human health and remediation. *Egyptian Journal of Petroleum*, 25(1):107–123, 2016.

[19] Nguyen-Duy Duy Dat and Moo Been Chang. Review on characteristics of PAHs in atmosphere, anthropogenic sources and control technologies, dec 2017.

[20] H. Richter and J.B B. Howard. Formation of polycyclic aromatic hydrocarbons and their growth to soot-a review of chemical reaction pathways. *Progress in Energy and Combustion Science*, 26(4):565–608, aug 2000.

[21] Esther Borrás, Luis A. Tortajada-Genaro, Monica Vázquez, and Barbara Zielinska. Polycyclic aromatic hydrocarbon exhaust emissions from different reformulated diesel fuels and engine operating conditions. *Atmospheric Environment*, 43(37):5944–5952, 2009.

[22] Christine Achten and Jan T. Andersson. Overview of Polycyclic Aromatic Compounds (PAC). *Polycyclic Aromatic Compounds*, 35(2-4):177–186, mar 2015.

[23] Pankaj Kumar Arora, Matthias E Kaestner, Eric D Van Hullebusch, Tapan K Dutta, Youngho Ahn, Debajyoti Ghosal, and Shreya Ghosh. Current State of Knowledge in Microbial Degradation of Polycyclic Aromatic Hydrocarbons (PAHs): A Review. 2016.

[24] Benjamin A.Musa Bandowe and Hannah Meusel. Nitrated polycyclic aromatic hydrocarbons (nitro-PAHs) in the environment – A review. *Science of the Total Environment*, 581-582:237–257, 2017.

[25] P. Carlier, H. Hannachi, and G. Mouvier. The chemistry of carbonyl compounds in the atmosphere-A review. *Atmospheric Environment (1967)*, 20(11):2079–2099, 1986.

[26] Jinhe Wang, Shan Chen, Xiaoguo Qiu, Wenya Niu, Ouyang Li, Chao Zhu, Xi Zhang, Xue Yang, and Guiqin Zhang. Pollution Characteristics of Atmospheric Carbonyl Compounds in a Large City of Northern China. *Journal of Chemistry*, 2022, 2022.

[27] Roger L. Tanner, Antonio H. Miguel, Jallson B. De Andrade, Jeffrey S. Gaffney, and Gerald E. Strelt. Atmospheric Chemistry of Aldehydes: Enhanced Peroxyacetyl Nitrate Formation from Ethanol-Fueled Vehicular Emissions. *Environmental Science and Technology*, 22(9):1026–1034, 1988.

[28] IARC. Agents classified by the iarc monographs. *IARC Monographs on the Evaluation of Carcinogenic Risks to Humans*, 1, 2016.

[29] IARC. Formaldehyde. IARC Monographs on the evaluation of carcinogenic risks to humans, volume 100F. *IARC Monographs*, 100F:401–435, 2012.

[30] Luoping Zhang, Craig Steinmaus, David A. Eastmond, Xianjun K. Xin, and Martyn T. Smith. Formaldehyde exposure and leukemia: A new meta-analysis and potential mechanisms. *Mutation Research - Reviews in Mutation Research*, 681(2-3):150–168, 2009.

[31] Richard B. Hayes. The carcinogenicity of metals in humans. *Cancer Causes and Control*, 8(3):371–385, 1997.

[32] Ken Donaldson, Lang Tran, Luis Albert Jimenez, Rodger Duffin, David E. Newby, Nicholas Mills, William MacNee, and Vicki Stone. Combustion-derived nanoparticles: A review of their toxicology following inhalation exposure. *Particle and Fibre Toxicology*, 2, 2005.

[33] Augustin Baulig, Michèle Garlatti, Véronique Bonvallot, Alexandre Marchand, Robert Barouki, Francelyne Marano, and Armelle Baeza-Squiban. Involvement of reactive oxygen species in the metabolic pathways triggered by

diesel exhaust particles in human airway epithelial cells. *American Journal of Physiology - Lung Cellular and Molecular Physiology*, 285(3 29-3), 2003.

[34] Daniel Southern, Paul Hellier, Midhat Talibi, Martin O. Leonard, and Nicos Ladommatos. Re-assessing the toxicity of particles from biodiesel combustion: A quantitative analysis of in vitro studies. *Atmospheric Environment*, 261(March):118570, 2021.

[35] Elias Sanidas, Dimitris P. Papadopoulos, Harris Grassos, Maria Velliou, Kostas Tsioufis, John Barbetseas, and Vasilios Papademetriou. Air pollution and arterial hypertension. A new risk factor is in the air. *Journal of the American Society of Hypertension*, 11(11):709–715, nov 2017.

[36] G. Grimmer, H. Brune, R. Deutsch-Wenzel, G. Dettbarn, J. Jacob, K. W. Naujack, U. Mohr, and H. Ernst. Contribution of polycyclic aromatic hydrocarbons and nitro-derivatives to the carcinogenic impact of diesel engine exhaust condensate evaluated by implantation into the lungs of rats. *Cancer Letters*, 37(2):173–180, 1987.

[37] Mahyar Aghapour, Niki D. Ubags, Dunja Bruder, Pieter S. Hiemstra, Venkataramana Sidhaye, Fariba Rezaee, and Irene H. Heijink. Role of air pollutants in airway epithelial barrier dysfunction in asthma and COPD. *European Respiratory Review*, 31(163), 2022.

[38] J. Song and S. H. Ye. Study on the mutagenicity of diesel exhaust particles. *Biomedical and environmental sciences : BES*, 8(3):240–245, 1995.

[39] Li Ning, Sioutas Constantinos, Cho Arthur, Schmitz Debra, Misra Chandan, Sempf Joan, Wang Meiying, Oberley Terry, Froines John, and Nel Andre. Ultrafine particulate pollutants induce oxidative stress and mitochondrial damage. *Environmental Health Perspectives*, 111(4):455–460, apr 2003.

[40] Dr Virunya Bhat, Emeritus Professor Alan R. Boobis(co-lead author), Dr Riccardo Crebelli, Dr Nathalie Delrue, ProfessorDavid Eastmond(co-lead author), Dr Susan Page Felter, Dr Rainer Guertler, Professor Andrea Hartwig, Dr Frank Le Curieux, Professor Angelo Moretto, Professor Pasquale Mosesso, Dr Utz Mueller, Dr Takehiko Nohmi, Dr Grace Patlewicz, Professor David H. Phillips, Dr Andrea Richarz, Dr Raymond R. Tice, Dr Paul A. White, and Dr Kristine L. Witt. Genotoxicity Second edition. 2020.

[41] R.H. Scholten, Y.J. Essig, M. Roursgaard, A. Jensen, A.M. Krais, L. Gren, K. Dierschke, A. Gudmundsson, A. Wierzbicka, and P. Møller. Inhalation of hydrogenated vegetable oil combustion exhaust and genotoxicity responses in humans. *Archives of Toxicology*, 95(10):3407–3416, 2021.

[42] Hasan Basri Ila, Erman Salih Istifli. *Cytotoxicity - Definition, Identification, and Cytotoxic Compounds*. 2019.

[43] Durackova Z. Some current insights into oxidative stress. *Physiological Research*, 59(4):459–469, 2010.

[44] Maria L. Botero, Carolina Mendoza, Silvana Arias, Oscar D. Hincapié, John R. Agudelo, and Isabel C. Ortiz. In vitro evaluation of the cytotoxicity, mutagenicity and DNA damage induced by particle matter and gaseous emissions from a medium-duty diesel vehicle under real driving conditions using palm oil biodiesel blends. *Environmental Pollution*, 265, 2020.

[45] S. Arias, F. Molina, and J.R. Agudelo. Palm oil biodiesel: An assessment of pah emissions, oxidative potential and ecotoxicity of particulate matter. *Journal of Environmental Sciences (China)*, 101:326–338, 2021.

[46] David Moher, Alessandro Liberati, Jennifer Tetzlaff, and Douglas G. Altman. Preferred reporting items for systematic reviews and meta-analyses: The PRISMA statement. *BMJ (Online)*, 339(7716):332–336, 2009.

[47] Magín Lapuerta, José Rodríguez-Fernández, John R. Agudelo, and André L. Boehman. Blending scenarios for soybean oil derived biofuels with conventional diesel. *Biomass and Bioenergy*, 49:74–85, feb 2013.

[48] Gabriele Di Blasio, Roberto Ianniello, and Carlo Beatrice. Hydrotreated vegetable oil as enabler for high-efficient and ultra-low emission vehicles in the view of 2030 targets. *Fuel*, 310(PB):122206, 2022.

[49] Soo Young No. Paraffinic Biofuels: HVO, BTL Diesel, and Farnesane. In *Application of Liquid Biofuels to Internal Combustion Engines*, pages 147–172. Springer, 2019.

[50] Ricardo Suarez-Bertoa, Marina Kousoulidou, Michael Clairotte, Barouch Giechaskiel, Jukka Nuottimäki, Teemu Sarjovaara, and Laura Lonza. Impact of HVO blends on modern diesel passenger cars emissions during real world operation. *Fuel*, 235(March 2018):1427–1435, 2019.

[51] Neste Corporation. Neste Renewable Diesel Handbook. *Neste*, pages 1–33, 2015.

[52] T. A.Z. de Souza, G. M. Pinto, A. A.V. Julio, C. J.R. Coronado, R. Perez-Herrera, B. O.P.S. Siqueira, R. B.R. da Costa, J. J. Roberts, and J. C.E. Palacio. Biodiesel in South American countries: A review on policies, stages of development and imminent competition with hydrotreated vegetable oil. *Renewable and Sustainable Energy Reviews*, 153, 2022.

[53] George W. Huber, Paul O'Connor, and Avelino Corma. Processing biomass in conventional oil refineries: Production of high quality diesel by hydrotreating vegetable oils in heavy vacuum oil mixtures. *Applied Catalysis A: General*, 329:120–129, 2007.

[54] Soo Young No. Application of hydrotreated vegetable oil from triglyceride based biomass to CI engines - A review. *Fuel*, 115:88–96, 2014.

[55] M. Kuronen, S. Mikkonen, P. Aakko, and T. Murtonen. Hydrotreated vegetable oil as fuel for heavy duty diesel engines. *SAE Technical Papers*, 2007.

[56] H. Aatola, M. Larmi, T. Sarjovaara, and S. Mikkonen. Hydrotreated vegetable oil (hvo) as a renewable diesel fuel: Trade-off between nox, particulate emission, and fuel consumption of a heavy duty engine. *SAE International Journal of Engines*, 1(1):1251–1262, 2009.

[57] T. Murtonen, P. Aakko-Saksa, M. Kuronen, S. Mikkonen, and K. Lehtoranta. Emissions with heavy-duty diesel engines and vehicles using fame, hvo and gtl fuels with and without doc+poc aftertreatment. *SAE International Journal of Fuels and Lubricants*, 2(2):147–166, 2010.

[58] L. Rantanen, R. Linnaila, P. Aakko, and T. Harju. Nexbtl - biodiesel fuel of the second generation. *SAE Technical Papers*, 2005.

[59] O. Armas, R. García-Contreras, Á. Ramos, and A.F. López. Impact of animal fat biodiesel, gtl, and hvo fuels on combustion, performance, and pollutant emissions of a light-duty diesel vehicle tested under the nedc. *Journal of Energy Engineering*, 141(2), 2015.

[60] M. Kousoulidou, A. Dimaratos, A. Karvountzis-Kontakiotis, and Z. Samaras. Combustion and emissions of a common-rail diesel engine fueled with hwco. *Journal of Energy Engineering*, 140(3), 2014.

[61] D. Singh, K.A. Subramanian, and M.O. Garg. Comprehensive review of combustion, performance and emissions characteristics of a compression ignition engine fueled with hydroprocessed renewable diesel. *Renewable and Sustainable Energy Reviews*, 81:2947–2954, 2018.

[62] C. McCaffery, H. Zhu, C.M. Sabbir Ahmed, A. Canchola, J.Y. Chen, C. Li, K.C. Johnson, T.D. Durbin, Y.-H. Lin, and G. Karavalakis. Effects of hydrogenated vegetable oil (hvo) and hvo/biodiesel blends on the physicochemical and toxicological properties of emissions from an off-road heavy-duty diesel engine. *Fuel*, 323, 2022.

[63] K.M. Bendtsen, L. Gren, V.B. Malmborg, P.C. Shukla, M. Tunér, Y.J. Essig, A.M. Krais, P.A. Clausen, T. Berthing, K. Loeschner, N.R. Jacobsen, H. Wolff, J. Pagels, and U.B. Vogel. Particle characterization and toxicity in c57bl/6 mice following instillation of five different diesel exhaust particles designed to differ in physicochemical properties. *Particle and Fibre Toxicology*, 17(1), 2020.

[64] L. Gren, V.B. Malmborg, N.R. Jacobsen, P.C. Shukla, K.M. Bendtsen, A.C. Eriksson, Y.J. Essig, A.M. Krais, K. Loeschner, S. Shamun, B. Strandberg,

M. Tunér, U. Vogel, and J. Pagels. Effect of renewable fuels and intake o2 concentration on diesel engine emission characteristics and reactive oxygen species (ros) formation. *Atmosphere*, 11(6), 2020.

[65] H.-J. Liu, R.-H. Chen, and W.-C. Wang. The non-regulated emissions from a turbo-charged diesel engine under steady-state operation with hydro-processed renewable diesel (hrd). *Fuel*, 263, 2020.

[66] K. Dziendzikowska, M. Gajewska, J. Wilczak, R. Mruk, M. Oczkowski, E. Żyła, T. Królikowski, M. Stachoń, J. Øvrevik, O. Myhre, M. Kruszewski, M. Wojewódzka, A. Lankoff, and J. Gromadzka-Ostrowska. The effects of 1st and 2nd generation biodiesel exhaust exposure on hematological and biochemical blood indices of fisher344 male rats – the fuelhealth project. *Environmental Toxicology and Pharmacology*, 63:34–47, 2018.

[67] M. Odziemkowska, J. Czarnocka, A. Frankiewicz, M. Szewczyńska, A. Lankoff, J. Gromadzka-Ostrowska, and R. Mruk. Chemical characterization of exhaust gases from compression ignition engine fuelled with various biofuels. *Polish Journal of Environmental Studies*, 26(3):1183–1190, 2017.

[68] M. Vojtisek-Lom, V. Beránek, P. Mikuška, K. Křůmal, P. Coufalík, J. Sikorová, and J. Topinka. Blends of butanol and hydrotreated vegetable oils as drop-in replacement for diesel engines: Effects on combustion and emissions. *Fuel*, 197:407–421, 2017.

[69] A. Singer, O. Schröder, C. Pabst, A. Munack, J. Bünger, W. Ruck, and J. Krahl. Aging studies of biodiesel and hvo and their testing as neat fuel and blends for exhaust emissions in heavy-duty engines and passenger cars. *Fuel*, 153:595–603, 2015.

[70] A. Prokopowicz, M. Zaciera, A. Sobczak, P. Bielaczyc, and J. Woodburn. The effects of neat biodiesel and biodiesel and hvo blends in diesel fuel on exhaust emissions from a light duty vehicle with a diesel engine. *Environmental Science and Technology*, 49(12):7473–7482, 2015.

[71] G.A. Westphal, J. Krahl, A. Munack, N. Rosenkranz, O. Schröder, J. Schaak, C. Pabst, T. Brüning, and J. Bünger. Combustion of hydrotreated vegetable oil and jatropha methyl ester in a heavy duty engine: Emissions and bacterial mutagenicity. *Environmental Science and Technology*, 47(11):6038–6046, 2013.

[72] T.M. Cahill and R.A. Okamoto. Emissions of acrolein and other aldehydes from biodiesel-fueled heavy-duty vehicles. *Environmental Science and Technology*, 46(15):8382–8388, 2012.

[73] P.I. Jalava, M. Tapanainen, K. Kuuspalo, A. Markkanen, P. Hakulinen, M.S. Happo, A.S. Pennanen, M. Ihalainen, P. Yli-Pirilä, U. Makkonen, K. Teinilä,

J. Mäki-Paakkanen, R.O. Salonen, J. Jokiniemi, and M.-R. Hirvonen. Toxicological effects of emission particles from fossil- and biodiesel-fueled diesel engine with and without doc/poc catalytic converter. *Inhalation Toxicology*, 22(SUPPL. 2):48–58, 2010.

[74] Evangelos G. Giakoumis, Constantine D. Rakopoulos, Athanasios M. Dimaratos, and Dimitrios C. Rakopoulos. Exhaust emissions with ethanol or n-butanol diesel fuel blends during transient operation: A review. *Renewable and Sustainable Energy Reviews*, 17:170–190, 2013.

[75] M. Lapuerta, Á. Ramos, J. Barba, and D. Fernández-Rodríguez. Cold- and warm-temperature emissions assessment of n-butanol blends in a euro 6 vehicle. *Applied Energy*, 218:173–183, 2018.

[76] David Fernández Rodríguez. *Evaluation of N-Butanol As Blending Component for Diesel Engines With Euro 6 Aftertreatment System*. PhD thesis, Universidad de Castilla -La Mancha, 2019.

[77] V. B.M. Vinod Babu, M. M.K. Madhu Murthy, and G. Amba Prasad Rao. Butanol and pentanol: The promising biofuels for CI engines – A review. *Renewable and Sustainable Energy Reviews*, 78:1068–1088, 2017.

[78] B. Rajesh Kumar and S. Saravanan. Use of higher alcohol biofuels in diesel engines: A review. *Renewable and Sustainable Energy Reviews*, 60:84–115, 2016.

[79] A.F. López, M. Cadrazco, A.F. Agudelo, L.A. Corredor, J.A. Vélez, and J.R. Agudelo. Impact of n-butanol and hydrous ethanol fumigation on the performance and pollutant emissions of an automotive diesel engine. *Fuel*, 153:483–491, 2015.

[80] Frank A. Ruiz, Marlon Cadrazco, Andrés F. López, Jesús Sanchez-Valdepeñas, John R. Agudelo, Jesús Valdepeñas, and John R. Agudelo. Impact of dual-fuel combustion with n-butanol or hydrous ethanol on the oxidation reactivity and nanostructure of diesel particulate matter. *Fuel*, 161:18–25, dec 2015.

[81] N. Yilmaz and S.M. Davis. Formation of polycyclic aromatic hydrocarbons and regulated emissions from biodiesel and n-butanol blends containing water. *Journal of Hazardous Materials*, 437, 2022.

[82] V. Kumar, A.P. Singh, and A.K. Agarwal. Gaseous emissions (regulated and unregulated) and particulate characteristics of a medium-duty crdi transportation diesel engine fueled with diesel-alcohol blends. *Fuel*, 278, 2020.

[83] H. Xiao, F. Guo, S. Li, R. Wang, and X. Yang. Combustion performance and emission characteristics of a diesel engine burning biodiesel blended with n-butanol. *Fuel*, 258, 2019.

[84] Zhi Hui Zhang and Rajasekhar Balasubramanian. Influence of butanol addition to diesel-biodiesel blend on engine performance and particulate emissions of a stationary diesel engine. *Applied Energy*, 119:530–536, 2014.

[85] K.H. Kim, B. Choi, S. Park, E. Kim, and D. Chiaramonti. Emission characteristics of compression ignition (ci) engine using diesel blended with hydrated butanol. *Fuel*, 257, 2019.

[86] M. Gowtham, C.G. Mohan, and R. Prakash. Effect of n-butanol fumigation on the regulated and unregulated emission characteristics of a diesel engine. *Fuel*, 242:84–95, 2019.

[87] P. Dagaut, Y. Bedjanian, G. Dayma, F. Foucher, B. Grosselin, M. Romanias, and R. Shahla. Emission of carbonyl and polyaromatic hydrocarbon pollutants from the combustion of liquid fuels: Impact of biofuel blending. *Journal of Engineering for Gas Turbines and Power*, 141(3), 2019.

[88] N. Yilmaz and S.M. Davis. Polycyclic aromatic hydrocarbon (pah) formation in a diesel engine fueled with diesel, biodiesel and biodiesel/n-butanol blends. *Fuel*, 181:729–740, 2016.

[89] J.-H. Tsai, S.-J. Chen, K.-L. Huang, W.-Y. Lin, C.-C. Lin, J.-Y. Ding, C.-H. Yang, J.-Y. Chiu, and C.-H. Chiu. Characteristics of exhaust emissions of a diesel generator fueled with water-containing butanol and waste-edible-oil-biodiesel blends. *Aerosol and Air Quality Research*, 15(5):2129–2139, 2015.

[90] P.-M. Yang, Y.-C. Lin, K.C. Lin, S.-R. Jhang, S.-C. Chen, C.-C. Wang, and Y.-C. Lin. Comparison of carbonyl compound emissions from a diesel engine generator fueled with blends of n-butanol, biodiesel and diesel. *Energy*, 90:266–273, 2015.

[91] B. Choi and X. Jiang. Individual hydrocarbons and particulate matter emission from a turbocharged crdi diesel engine fueled with n-butanol/diesel blends. *Fuel*, 154:188–195, 2015.

[92] J.K. Mwangi, W.-J. Lee, J.-H. Tsai, and T.S. Wu. Emission reductions of nitrogen oxides, particulate matter and polycyclic aromatic hydrocarbons by using microalgae biodiesel, butanol and water in diesel engine. *Aerosol and Air Quality Research*, 15(3):901–914, 2015.

[93] Z.-H. Zhang and R. Balasubramanian. Effect of oxygenated fuels on physicochemical and toxicological characteristics of diesel particulate emissions. *Environmental Science and Technology*, 48(24):14805–14813, 2014.

[94] Y.-C. Chang, W.-J. Lee, H.-H. Yang, L.-C. Wang, J.-H. Lu, Y.I. Tsai, M.-T. Cheng, L.-H. Young, and C.-J. Chiang. Reducing emissions of persistent organic pollutants from a diesel engine by fueling with water-containing butanol diesel blends. *Environmental Science and Technology*, 48(10):6010–6018, 2014.

[95] R. Ballesteros, J.J. Hernández, and J. Guillén-Flores. Carbonyls speciation in a typical european automotive diesel engine using bioethanol/butanol-diesel blends. *Fuel*, 95:136–145, 2012.

[96] T.S. Norton and F.L. Dryer. The flow reactor oxidation of c1-c4 alcohols and mtbe. *Symposium (International) on Combustion*, 23(1):179–185, 1991.

[97] Yongjun Liu, Xuan Deng, Peide Han, and Wei Huang. Higher alcohols synthesis from syngas over P-promoted non-noble metal Cu-based catalyst. *Fuel*, 208:423–429, 2017.

[98] Anthony F. Cann and James C. Liao. Pentanol isomer synthesis in engineered microorganisms. *Applied Microbiology and Biotechnology*, 85(4):893–899, 2010.

[99] 1-Pentanol | C5H12O - PubChem.

[100] J. Liang, Q. Zhang, Z. Chen, and Z. Zheng. The effects of EGR rates and ternary blends of biodiesel/n-pentanol/diesel on the combustion and emission characteristics of a CRDI diesel engine. *Fuel*, 286, 2021.

[101] W. Zhao, J. Yan, S. Gao, T.H. Lee, and X. Li. The combustion and emission characteristics of a common-rail diesel engine fueled with diesel, propanol, and pentanol blends under low intake pressures. *Fuel*, 307, 2022.

[102] S. Pinzi, M.D. Redel-Macías, M. Carmona-Cabello, A. Cubero, J.M. Herreros, and M.P. Dorado. Influence of 1-butanol and 1-pentanol addition to diesel fuel on exhaust and noise emissions under stationary and transient conditions. *Fuel*, 301, 2021.

[103] K. Santhosh, G.N. Kumar, Radheshyam, and P.V. Sanjay. Experimental analysis of performance and emission characteristics of crdi diesel engine fueled with 1-pentanol/diesel blends with egr technique. *Fuel*, 267, 2020.

[104] J. Campos-Fernandez, J.M. Arnal, J. Gomez, N. Lacalle, and M.P. Dorado. Performance tests of a diesel engine fueled with pentanol/diesel fuel blends. *Fuel*, 107:866–872, 2013.

[105] Transport and Environment. Electrofuels what role in EU transport decarbonisation? *European Federation for Transport and Environment AISBL*, (November):1–7, 2017.

[106] Jakob Burger, Markus Siegert, Eckhard Ströfer, Michael Nilles, and Hans Hasse. Poly(oxymethylene) dimethyl ethers as components of tailored diesel fuel - properties, synthesis and purification concepts. *11AIChE - 2011 AIChE Annual Meeting, Conference Proceedings*, 2011.

[107] Martin Härtl, Philipp Seidenspinner, Eberhard Jacob, and Georg Wachtmeister. Oxygenate screening on a heavy-duty diesel engine and emission characteristics of highly oxygenated oxymethylene ether fuel OME1. *Fuel*, 153:328–335, 2015.

[108] ChemCom staat voor "Chemical Competence".

[109] The Royal Society. *Sustainable synthetic carbon based fuels for transport*. 2019.

[110] Dan Wang, Gangli Zhu, Zhen Li, Machen Xue, and Chungu Xia. Conceptual design of production of eco-friendly polyoxymethylene dimethyl ethers catalyzed by acid functionalized ionic liquids. *Chemical Engineering Science*, 206:10–21, 2019.

[111] Maximilian Held, Yannic Tönges, Dominik Pélerin, Martin Härtl, Georg Wachtmeister, and Jakob Burger. On the energetic efficiency of producing polyoxymethylene dimethyl ethers from CO2 using electrical energy. *Energy and Environmental Science*, 12(3):1019–1034, 2019.

[112] Niklas Schmitz, Jakob Burger, Eckhard Ströfer, and Hans Hasse. From methanol to the oxygenated diesel fuel poly(oxymethylene) dimethyl ether: An assessment of the production costs. *Fuel*, 185:67–72, dec 2016.

[113] Junheng Liu, Ping Sun, He Huang, Jian Meng, and Xiaohua Yao. Experimental investigation on performance, combustion and emission characteristics of a common-rail diesel engine fueled with polyoxymethylene dimethyl ethers-diesel blends. *Applied Energy*, 202:527–536, 2017.

[114] Haoye Liu, Zhi Wang, Jianxin Wang, Xin He, Yanyan Zheng, Qiang Tang, and Jinfu Wang. Performance, combustion and emission characteristics of a diesel engine fueled with polyoxymethylene dimethyl ethers (PODE3-4)/ diesel blends. *Energy*, 88:793–800, 2015.

[115] Yanju Wei, Yajie Zhang, Zengqiang Zhu, Xiaodong Zhu, Haoming Gu, and Shenghua Liu. Effect of PODE on Emission Characteristics of a China VI Heavy-Duty Diesel Engine. *Applied Sciences (Switzerland)*, 12(3), 2022.

[116] Shiliang Wu, Jiajing Bao, Ziwei Wang, Huiyan Zhang, and Rui Xiao. The regulated emissions and PAH emissions of bio-based long-chain ethers in a diesel engine. *Fuel Processing Technology*, 214, 2021.

[117] Haoye Liu, Xiao Ma, Bowen Li, Longfei Chen, Zhi Wang, and Jianxin Wang. Combustion and emission characteristics of a direct injection diesel engine fueled with biodiesel and PODE/biodiesel fuel blends. *Fuel*, 209:62–68, 2017.

[118] Stefano Emanuele Iannuzzi, Christophe Barro, Konstantinos Boulouchos, and Jakob Burger. POMDME-diesel blends: Evaluation of performance and exhaust emissions in a single cylinder heavy-duty diesel engine. *Fuel*, 203:57–67, 2017.

[119] Tianting Wang, Junheng Liu, Ping Sun, Qian Ji, Wanying Gao, and Chen Yang. Influence of injection parameters on combustion, gaseous emissions and particle size distribution of a CRDI diesel engine operating with PODE/diesel blends. *Fuel*, 281, 2020.

[120] Qiren Zhu, Yichen Zong, Wenbin Yu, Wenming Yang, and Markus Kraft. Understanding the blending effect of polyoxymethylene dimethyl ethers as additive in a common-rail diesel engine. *Applied Energy*, 300, 2021.

[121] Jialin Liu, Hu Wang, Ying Li, Zunqing Zheng, Zhenzhen Xue, Hongyan Shang, and Mingfa Yao. Effects of diesel/PODE (polyoxymethylene dimethyl ethers) blends on combustion and emission characteristics in a heavy duty diesel engine. *Fuel*, 177:206–216, 2016.

[122] L. Pellegrini, R. Patrini, and M. Marchionna. Effect of pomdme blend on pah emissions and particulate size distribution from an in-use light-duty diesel engine. *SAE Technical Papers*, 1, 2014.

[123] Xiaokang Zhang, Nana Li, Sheng Han, Zhong Wei, and Bin Dai. Terpene resin prepared from renewable turpentine oil as a new type of cold flow improver for soybean biodiesel-diesel blends. *Fuel*, 320, 2022.

[124] Anil Singh Yadav, Padam Singh, Rahul Sahu, P. Thangamuthu, Renuka Shyam Narain, Y. Anupam Rao, Azmeera Balu, Bishnu Prasad Panda, and Abhishek Sharma. Potential utilization of turpentine oil as an alternative fuel. *Materials Today: Proceedings*, 63:A1–A8, jan 2022.

[125] Karikalan Loganathan and Chandrasekaran Manoharan. Evaluation of performance and emission features of jatropha biodiesel-turpentine blend as green fuel. *Thermal Science*, 21:615–625, 2017.

[126] Duban García, Ángel Ramos, José Rodríguez-Fernández, Felipe Bustamante, Edwin Alarcón, and Magín Lapuerta. Impact of oxyfunctionalized turpentine on emissions from a Euro 6 diesel engine. *Energy*, 201, 2020.

[127] Pankaj Dubey and Rajesh Gupta. Effects of dual bio-fuel (Jatropha biodiesel and turpentine oil) on a single cylinder naturally aspirated diesel engine without EGR. *Applied Thermal Engineering*, 115:1137–1147, 2017.

[128] Pankaj Dubey and Rajesh Gupta. Influences of dual bio-fuel (Jatropha biodiesel and turpentine oil) on single cylinder variable compression ratio diesel engine. *Renewable Energy*, 115:1294–1302, 2018.

[129] L. Karikalan and M. Chandrasekaran. Performance and pollutants analysis on diesel engine using blends of Jatropha Biodiesel and Mineral Turpentine as fuel. *International Journal of Environmental Science and Technology*, 14(2):323–330, 2017.

[130] B. Prem Anand, C. G. Saravanan, and C. Ananda Srinivasan. Performance and exhaust emission of turpentine oil powered direct injection diesel engine. *Renewable Energy*, 35(6):1179–1184, 2010.

Chapter 3

Experimental Methods

With the broad range of experimental methodologies available for sampling and measuring environmental pollutants, our first concern was to develop a methodology for unregulated pollutants sampling applicable to engine exhaust gases, in addition to chemical and biological characterization techniques. A sampling system and methodology to capture gases and particles from exhaust gases, as well as analytical techniques for PAH and carbonyls were developed. Furthermore, in vivo and in vitro tests were selected to assess the biological activity of the emissions samples.

3.1 Introduction

Taking into account environmental considerations as well as concern for the health and life, it is important to asses the effect of potential alternative biofuels on unregultated toxic emissions, and their induced biological response. For this purpose, it was necessary to develop and implement accurate and reliable methodologies, adapted from environmental sampling to on-site sampling for engine emissions.

This thesis assessed the effect of a group of conventional and unconventional biofuels on unregulated emissions in both particles and gaseous phases, gathered from the exhaust gas stream of an automotive diesel engine operating under steady and transient states. The chemical characterization methods included green chemistry techniques and chromatography, both liquid and gas. In addition, the biological effects of soluble organic fraction (SOF) and water-soluble fraction (WSF) of PM were assessed. Cytotoxicity, genotoxicity, apoptosis and oxidative DNA damage were evaluated on SOF using *in vitro* approach with a Human Hepatocarcinoma epithelial cell line, while acute eco-toxicity of WSF was evaluated *in vivo* using *Daphnia*

Pulex. The standard comet assay has been used for the evaluation of direct genotoxic damage, and its modified version with the enzymes Formamidopyrimidine DNA glycosylase (FPG) and Endonuclease III (Endo III) to recognize the bases of the genetic material that has been oxidized, thus evaluating the oxidation process of the puric and pyrimidine bases, respectively.

To achieve these objectives, an experimental test plan was designed which included: a) design and construction of a sampling system for gases and particles from engines and vehicles, b) development of a methodology for PAH (PM and gaseous phase) and carbonyls (gaseous phase) analysis, and c) biological analysis through a wide spectrum of tests (cytotoxicity, genotoxicity, apoptosis, oxidative damage). Some of the above methodologies were validated and all of them were verified.

3.2 Test plan and fuels

The experimental part of this doctoral thesis was divided according to the type of test: steady and transient states.

3.2.1 Tested fuels

Seven fuels were selected for the steady-state experiments, which were carried out in two stages. In the first one, four fuels were assessed: Ultra-low Sulfur Diesel (ULSD) supplied by the Colombian Oil Company (Ecopetrol) which was used as reference fuel, two blends of renewable diesel (HVO) produced from a wide variety of renewable fats and oils (NExBTL, Neste Oil) with ULSD (HVO13 and HVO20˜the number indicates the volume fraction of HVO in the fuel blend), and a blend of n-butanol with ULSD (Bu13). It has been reported that butanol can be introduced up to 13% at any ambient conditions and under any certification procedure, since the maximum butanol content is limited by starting difficulties at very low ambient temperatures [1]. For this reason, 13% was selected to compare with the HVO13 blend at the same aromatic content in both fuels. In general, these blends were chosen as highly representative since they have shown to provide good balance between cold weather operability, performance, and emission benefits.

After analyzing the results of carbonyl emissions obtained for Bu13 blend, the second stage was carried out with a higher alcohol than butanol blended with ULSD. In this stage four fuels were tested: neat USLD as reference fuel, and three pentanol (Sigma-Aldrich) -ULSD blends: 13%(Pe13), 15.5% (Pe15) and 20% (Pe20) by volume, providing 2.3%, 2.7% and 3.5 %wt. of oxygen to the fuel blend, respectively. These blends were chosen in order to compare them by aromatic content and oxygen concentration with Bu13, HVO13 and HVO20. **Table 3.1** shows the most relevant characteristics of the tested fuels.

For the transient state tests, six different conventional and advanced biofuels

were selected. Among them, a fossil diesel supplied by Repsol (Spain) was used as reference fuel. Pure HVO provided by Neste (NExBTL) was used as base biofuel. Four unconventional advanced biofuels blended at 20% by volume with diesel were tested. Hydrogenated turpentine and hydrogenated orange oil each blended at 20% by volume with diesel (HT20 and HO20, respectively). Details about extraction and hydrogenation of turpentine and orange oil were previously published by [2, 3]. OME was blended at 20% by volume with diesel (OME20), with OME fuel being supplied by ChemCom Industries B.V- Netherlands. Finally, 20% of a glycerol-derived biofuel consisting of a blend of FAME (70% v/v), fatty acid glycerol esters (FAGE, 27% v/v) and acetals (3% v/v) were blended with HVO. This blend was provided by Selabtec with the commercial name of SLB100. The physical and chemical properties of the test fuels are shown in **Table 3.1**

For the steady state tests, it was decided to test fuels with potential for production and use in Colombia, such as HVO and long-chain alcohols due to their higher calorific value and cetane number. On the other hand, for the transient state tests, unconventional and advanced fuels with potential for production and use in the world were selected.

Table 3.1: Physicochemical properties of the tested fuels

Tested fuels in steady state								
Property	**Method**	**ULSD**	**HVO**	**Butanol**	**Pentanol**	**HVO13**	**HVO20**	**Bu13**
Density at 15 °C (kg/m^3)	ASTM D4052-11	861	780.6	814	809.5	851.45	845.61	837.9
Kinematic viscosity at 40 °C (mm^2/s)	ASTM D445-12	4.36	2.92	2.23	2.89	4.09	3.96	2.62
Lower heating value (MJ/kg)	ASTM D240-09	42.43	44	33.1	35.06	42.60	42.69	41.58
Derived cetane number	ASTM D7668-14	51.36	79.5	17	20	58.10	61.87	45.92
Aromatics (% v/v)	-	31.5	0	0	0	27.41	25.20	27.41
Naphthenes (% v/v)	-	35.95	0	0	0	31.28	28.76	31.28
Paraffins (% v/v)	-	32.55	100	0	0	41.32	46.04	0
Sulphur content (mg/kg)	ASTM D2622-16	12	<5	0	0	< 5	<5	< 5
C (% w/w)	ASTM D5291-16	86.91	84.86	64.78	68.10	86.64	86.50	83.98
H (% w/w)	ASTM D5291-16	13.09	15.14	13.63	18.15	13.36	13.50	13.29
O (% w/w)	ASTM D5291-16	0	0	21.59	13.61	0	0	2.71
Heat of evaporation (kJ/kg)	-	270	-	585	308	-	-	-

Tested fuels in transient state							
Property	**Method**	**Diesel**	**HVO**	**HT20**	**HO20**	**OME20**	**SLB100**
Density (kg/m^3)	EN 3675	826.6	779.3	833.1	825.6	872.8	808.7
Viscosity (cSt)	EN 3104	2.59	2.77	2.19	1.99	2.2	3.76
Lubricity (μm)	EN 12156-1	428.9	-	358	320	330.9	-
Lower heating value (LHV)(MJ/kg)	ASTM D240	42.9	44.03	42.8	42.8	38.14	42.37
C content (%wt)	-	86.23	84.7	86.54	86.44	76.29	82.32
H content (%wt)	-	13.77	15.3	13.39	13.50	12.62	13.15
O content (%wt)	-	-	-	0.07	0.06	11.07	4.53
Molecular weight (kg/kmol)	-	203.09	221.6	-	-	187.55	231.5
Stoichiometric air/fuel ratio	-	1/14.49	1/14.88	1/14.43	1/14.46	1/12.71	1/13.74
Derived cetane number	EN 16715	52.56	72.72	45.5	43.9	54.65	69.07

3.2.2 Test plan

Figure 3.1 summarizes the test plan and the physicochemical and biological analyzes carried out in this thesis. The different fuel blends were prepared to compare them based on the aromatic content, and in the case of alcohols (butanol and pentanol), they were also compared in terms of oxygen percentage, **Table 3.2** shows the comparison matrix.

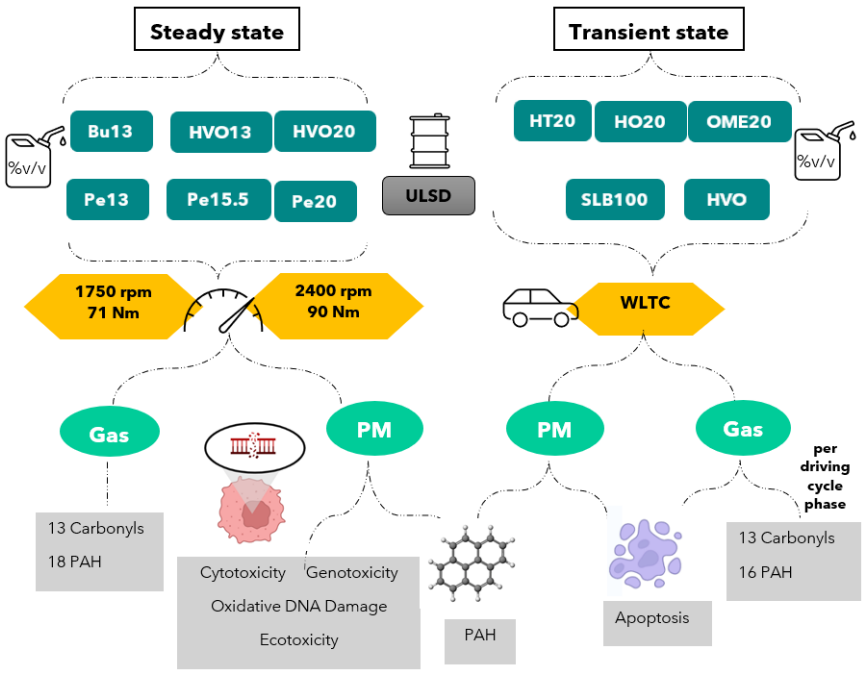

Figure 3.1: Test plan summary

Table 3.2: Test matrix for fuel comparison

	Fuel $(\%v/v)$	**13**	**15.5**	**20**	**100**
Steady state	Diesel	-	-	-	✓
	Butanol	✓*	-	-	-
	HVO	✓	-	-	
	Pentanol	✓	✓*	✓	
Transient state	Diesel	-	-	-	✓
	Hydroturpentine	-	-	✓	-
	Orange hydro-oil	-	-	✓	-
	OME	-	-	✓	-
	HVO	-	-	-	✓
	SLB100**	-	-	✓	-

*Same oxygen content.
**20% of a glycerol-derived biofuel blended with HVO.

3.3 Steady State Tests

3.3.1 Engine test bench

The experiments were carried out in an automotive, common rail, turbocharged and intercooled Cummins ISF 2.8 L diesel engine (Euro 4 emissions standard)(**Figure 3.2**). This high pressure, split injection, engine was equipped with an oxidation catalyst (DOC) and with a cooled EGR system. This engine is very common in the Colombian fleet, particularly in last mile parcel delivery vehicles.

The torque output of the engine was regulated by a controlled eddy current dynamometer brake (W230, Schenck, Germany) and tested under two steady-state operating modes.

Figure 3.2: Cummins ISF 2.8 L diesel engine

The main characteristics of the engine are listed in **Table 3.3** and the engine operating modes are shown in **Table 3.4**.

Table 3.3: Engine specifications

Type and Configuration	Cummins ISF 2.8, 4 stroke, common rail, split and direct injection, 4 cylinders in line, turbocharged, intercooler, diesel oxidation catalyst (DOC) and cooled EGR
Compression ratio	17.5:1
Displacement (L)	2.8
Bore/Stroke (mm)	94/100
Power (kW at r/min)	120 at 3600
Maximum Torque (Nm at r/min)	360 at 1800
Emission standard	Euro 4

Combustion diagnosis

For the thermodynamic combustion diagnosis, in-cylinder pressure was measured with a piezoelectric pressure transducer (6056A, Kistler, Germany) coupled to a charge amplifier (5011B, Kistler, Germany). Crankshaft rotational speed and instantaneous piston position were determined with an angle enconder providing 1024 pulses/rev (ROD 426, Heidenhain, Germany). A total of 100 pressure curves, and 3 repetitions were registered at each operating mode to guarantee reliability in combustion diagnosis results.

For the combustion diagnosis, the starting point was the instantaneous pressure signal in the cylinder and by means of a thermodynamic diagnosis model of an area, the way in which the energy of the fuel was released was determined. The analysis of the combustion allowed to obtain the parameters of the combustion process such as the rate of heat release, the duration of the combustion and the pressure gradient, among others [4].

3.3.2 Operation modes

The operating modes were selected as the most representative of urban driving conditions in a frequency approach by means of longitudinal dynamics analysis and the Vehicular Specific Power (VSP) methodology of the pickup truck simulated with the WLTC. These operating modes correspond to the low and medium speed phase in the WLTC (**Figure 3.3**), which is representative of the urban driving phases.

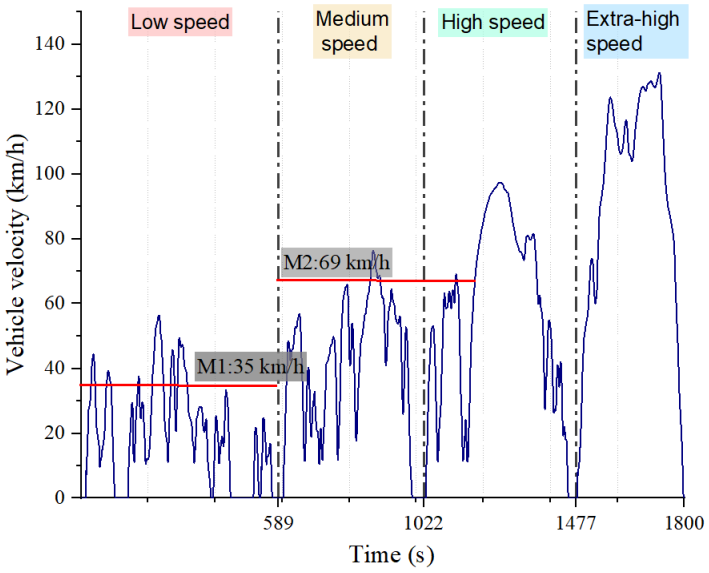

Figure 3.3: Selected operating points

Table 3.4: Engine operating modes representative of urban driving conditions

Mode	**Rotational speed** (r/min)	**Torque** (Nm)	**Vehicle speed** km/h
M1	1750	71	35
M2	2400	90	69

Although with a small engine speed variation range of only 650 r/min, both M1 and M2, were stable and repeatable during operation with markedly different vehicle speed.

3.3.3 Unregulated pollutants sampling

Gaseous and particulate samples were collected in a homemade sampling system adapted to the exhaust pipe, downstream of the DOC, as shown in **Figure** 3.4.

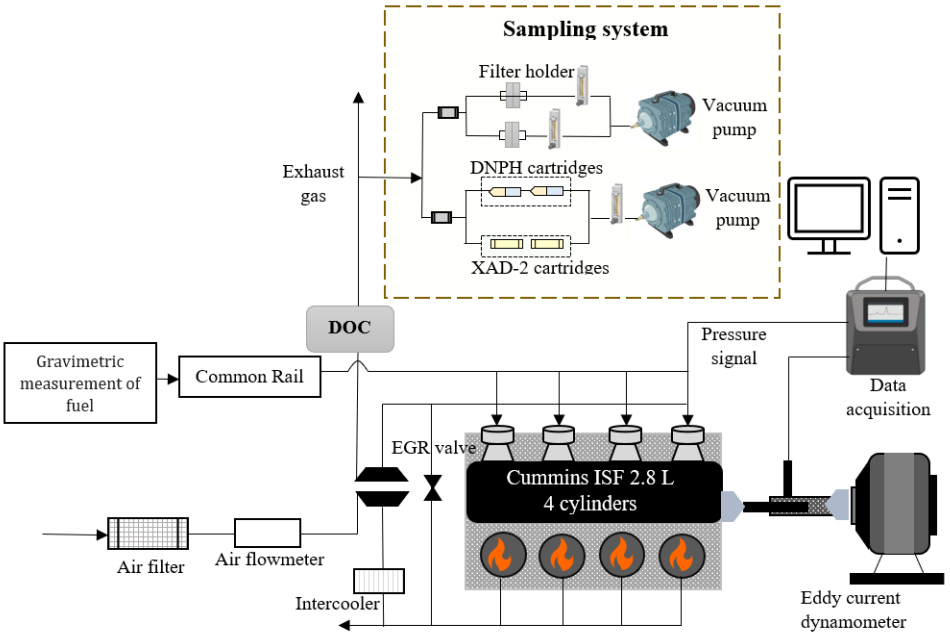

Figure 3.4: Engine configuration and sampling system

Gaseous pollutant sampling system

For gaseous sampling, the line was kept at 80°C (covered with an insulator) to avoid condensation in the sampling line [5]. A fraction of undiluted exhaust gases was carried out through a stainless-steel buffer lung which also acted as humidity trap. The flow was induced by a vacuum pump located downstream of the sampling system. The exhaust gas passed through a glass fiber filter in order to retain particles and

was divided into two parallel lines: 1) carbonyl compounds and 2) PAH sampling (**Figure 3.5**). At the sampling point (location of the cartridges) the temperature was not sensed. However, it had to be slightly close to 80°C (temperature of the heat line).

In the first line, a volumetric flow of 0.7 L/min for ULSD and HVO and 0.5 L/min for Bu13 controlled with a rotameter, passed through 2 cartridges in series containing 130 mg of 1,2-bis (2-pyridyl) ethylene (BPE) coated silica, and 270 mg of 2,4-dinitrophenylhydrazine (DNPH) coated silica (Sigma-Aldrich, Germany) for 10 minutes of sampling. The second cartridge was used to quantify leaks. Sampling was repeated by triplicate.

In the second line, two stainless steel cartridges of 30 cm^3 in series filled with 3 g of Amberlite® XAD®-2 resin previously washed with dichloromethane were used (Sigma-Aldrich, Germany). Sampling was performed for 5 min at a constant volumetric flow of 10 L/min controlled with a rotameter. Sampling was repeated by triplicate. A sample blank was exposed during the sampling time.

Particle sampling system

For particulate sampling, quartz filters (Whatman, 47mm diameter) were used. The filters were preconditioned before the sampling campaign, washed with dichloromethane (DCM) and extracted by solvent accelerated extraction (ASE, Dionex®,Thermo Scientific) at 1500 psi and 120 °C. The filters were additionally baked in a furnace at 400 °C for 5 h and then stored in clean containers covered from light. Sampled flow was divided into two parallel and identical sampling lines, followed by two stainless-steel filter holders (**Figure 3.5**), the flow was set to 20 L/min and the sampling time maintained during 10 min. Three samples were collected under each condition. The specific particulate matter emissions were obtained by weighting (before and after sample collection) three times, the conditioned (controlled humidity and temperature) quartz filters. The filters and cartridges were covered with aluminum foil to avoid exposure to light and stored under refrigeration conditions 4 °C ±1, until analysis. These PM samples were used for PAH and biological analyses.

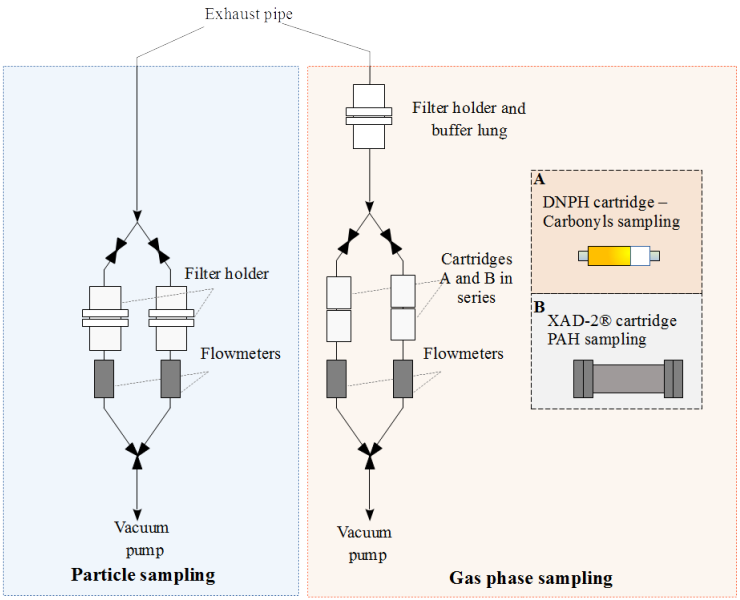

Figure 3.5: Gas phase and particle sampling systems -steady state tests

3.3.4 Chemical characterization of unregulated emissions

PAH analysis

Eighteen PAH were analyzed (**Table 3.5**). Prior to extraction, the collected PAH samples, particles and gas phase adsorbed on Amberlite® XAD®-2) were spiked with an internal recovery standard consisting of several deuterated species (naphthalene-d8, acenaphthene-d10, phenanthrene-d10, chrysene-d12, perylene-d12) followed by Pressurized Hot Water Extraction (PHWE) with water and methanol (3:1), in a 66 mL stainless steel vessel using an ASE 300 system (Dionex® Thermo Scientific, PA, USA). Extraction temperature was 200 °C and 5 min of static times at a high-pressure of 10,000 kPa. Extracting solution (50 mL) was used in the Vortex-assisted dispersive liquid–liquid microextraction (VADLLE) with 1000 μL of hexane as an extractor solvent in a sterile centrifuge tube and completely sealed. The cloudy solution formed was vortexed for 180 sec to distribute extractor solvent through the solution. Then, centrifugation at 3500 r/min for 240 sec was applied to separate organic phase from aqueous solution. The top phase was injected into the GC/MS system.

Table 3.5: PAH compounds analyzed

Compound	**Formula**	**Molecular weight** (g/mol)	**TEF***
Naphthalene (NAP)	$C_{10}H_8$	128	0.001
Acenaphthylene (Acy)	$C_{12}H_8$	152	0.001
Acenaphthene (Ace)	$C_{12}H_{10}$	154	0.001
Anthracene (Ant)	$C_{14}H_{10}$	178	0.01
Phenanthrene $(Phen)$	$C_{14}H_{10}$	178	0.001
Fluorene (Flu)	$C_{13}H_{10}$	166	0.001
Fluoranthene (Flt)	$C_{16}H_{10}$	202	0.001
Pyrene (Pyr)	$C_{16}H_{10}$	202	0.001
Benz[a]anthracene $(B[a]A)$	$C_{18}H_{12}$	228	0.1
Chrysene (Cry)	$C_{18}H_{12}$	228	0.01
Benzo[a]pyrene $(B[a]P)$	$C_{20}H_{12}$	252	1
Benzo[e]pyrene $(B[e]P)$	$C_{20}H_{12}$	252	0.1
Benzo[b]fluoranthene $(B[b]F)$	$C_{20}H_{12}$	252	0.1
Benzo[k]fluoranthene $(B[k]F)$	$C_{20}H_{12}$	252	0.1
Benzo[ghi]perylene $(B[g,h,iP)$	$C_{22}H_{12}$	276	0.01
Dibenzo[a,h]anthracene $(DB[a,h]A)$	$C_{22}H_{14}$	278	1
Indeno[1,2,3cd]pyrene (IP)	$C_{22}H_{12}$	276	0.1
Dibenzo[a,l]pyrene $(DB[a,l]P)$	$C_{24}H_{14}$	302.3	10*

*Toxicity Equivalent Factor (TEF – dimensionles). TEF was assigned using values provided by Office of Environmental Health Hazard Assessment (OEHHA) [6]

A Thermo Scientific GC/MS instrument (TRACE GC Ultra/ ISQ, Thermo Scientific, USA) was used to analyze PAH samples. Analytical conditions for GC/MS were as follows: Chromatographic separation was performed on an Agilent J'I&' W Select PAH column (CP 7462), 30 m × 0.25 mm x 0.15 μm. The oven temperature was programmed as follows: 70 °C for 0.8 min, ramping 60 °C/min to 180 °C, 5 °C/min to 300 °C and finally ramping 1°C/min to 320 °C for 2 min. Total run time was 48.63 min. Injection temperature was 280 °C, the ion source was electron impact (EI) mode, source temperature 275 °C, and mass selective detector (MSD) transfer line 300 °C. This chromatographic method was developed and validated in the laboratory.

For calibration, PAH standard solution with 18 PAH was diluted with hexane (Unisolv®, Merck, USA) to 5, 10, 25, 50, 150, 250 and 500 μg/mL. The calibration conditions were controlled before each analysis introducing a standard sample and an analytical blank. For more detail refer to **Appendix A**

The PAH emission factors were calculated from the concentrations obtained in

the GC/MS multiplied by the extraction volume (1 mL) and the total volumetric flow of exhaust gases (m^3/h) and divided by the engine power (13 kW and 22.6 kW).

A blank cartridge was exposed to environment in the engine room during the sampling time. Three sample replicates were taken for each fuel blend and operating mode. One of the replicates was made with two cartridges in series to quantify possible sample breakthrough. All data reported here were corrected for the sample breakthrough.

Carbonyl compound analysis

The DNPH cartridges were eluted individually with 4 mL of acetonitrile. The carbonyls were subsequently quantified using HPLC (Agilent® 1200) with ultraviolet–visible detector ($\lambda = 360nm$). For quantification, a calibration curve was performed with a standard solution (Chem Service Inc) at five different concentrations, containing the 13 hydrazones analyzed during the experiments. The concentrations were 1, 5, 10, 20, and 40 μg/mL for formaldehyde-DNPH and 0.5, 2.5, 5, 10, and 20 μg/mL for the other twelve compounds. A column ZORBAX Eclipse XDB-C18 (ID 5 μm, 4.6 x150mm) (Agilent Technologies, USA) was used for the separation of the carbonyl compounds. Acetonitrile and water with a 5% (v/v) of methanol were used as a mobile phase with gradient elution 40:60. The flow rate was maintained at 0.4 mL/min and the injection volume was 10 μL. Formaldehyde, acetaldehyde, benzaldehyde, butyraldehyde, acetone, propionaldehyde, acrolein, crotonaldehyde, hexaldehyde, valeraldehyde, p-tolualdehyde, methacrolein, 2-butanone with DNPH derivative were identified and quantified in the exhaust.This chromatographic method was developed and validated in the laboratory. For more detail refer to **Appendix A**.

The carbonyl emission factors were calculated from the concentrations obtained in the HPLC multiplied by the extraction volume (4 mL) and the total volumetric flow of exhaust gases (m^3/h) and divided by the engine power (13 kW and 22.6 kW).

As for PAH, a blank cartridge was exposed to environment in the engine room during the sampling time. Three sample replicates were taken for each fuel blend and operating mode. One of the replicates was made with two cartridges in series to quantify possible sample breakthrough. All data reported here were corrected for the sample breakthrough.

Ozone formation potential

Diesel engine exhaust gas can be a crucial source for the formation of photochemical ozone by the emission of highly chemically reactive Volatile Organic Compounds (VOCs), and ozone is known to have adverse effects on human health and on the environment. For carbonyl compounds, which are highly reactive intermediates during the photo-oxidation of hydrocarbons, the ozone formation potential (OFP) or ozone

equivalent production was calculated using the method reported by [7].This method is based on a model scenario in which VOCs produce maximum ozone formation, represented by maximum incremental reactivity (MIR). MIR values were updated by [8] and they are shown in (**Table 3.6**).

Table 3.6: MIR for each carbonyl compound [8]

Carbonyls	**MIR**
Formaldehyde	9.46
Acetaldehyde	6.54
Acrolein	7.45
Acetone	0.36
Propionaldehyde	7.08
Crotonaldehyde	9.39
Methacrolein	6.01
Butiraldehyde	5.97
Methyl ethyl ketone	1.48
Benzaldehyde	0.67
Valeraldehyde	5.08
o,m,p-Tolualdehyde	0.59
Hexaldehyde	4.35

The OFP was estimated as the sum of the product of each individual compound emission factor (Ci) in mg/kWh and its corresponding MIR value (**Table 3.6**), as shown in **Equation 3.1**.

$$OFP = \sum C_i \times MIR \tag{3.1}$$

PAH equivalence toxicity

The PAH equivalence toxicity was expressed as benzo(a)pyrene total toxicity equivalent (BaP-TEQ) and calculated as the sum of the product of each of the EPA16 priority PAH emission factors (Ci – μg/kWh) and their TEF proposed by Nisbet and Lagoy [9] (**Table** 3.5), which are widely used by investigators to assess PAH toxicity as a metric to evaluate the toxic power of PAH species.

Aldehyde-induced cancer risk assessment

The International Agency for Research on Cancer (IARC) classified formaldehyde in group 1- carcinogenic to humans, acrolein in group 2A-probably carcinogenic to humans and acetaldehyde and crotonaldehyde in group 2B-possibly carcinogenic to humans. The first step in conducting an inhalation risk assessment is to estimate the

exposure concentrations (EC) and defining a specific exposure scenario. Toxicological data source to guide risk by the Integrated Risk Information System (IRIS) reports the quantitative estimate of carcinogenic risk from inhalation exposure for formaldehyde and acetaldehyde compounds. This data source does not include data for the rest of carbonyls analyzed. In this research, estimations of cancer risks from formaldehyde and acetaldehyde inhalation were performed in a specific exposure scenario: a person commuting 2 hours a day for 30 years, which U.S EPA calls trespasser/recreational receptor. The dilution factor of 20 was taken from the literature [10]. EC (μg/m^3) were calculated according to **Equation 3.2**.

$$EC = \frac{CA \times ET \times EF \times ED}{AT} \tag{3.2}$$

Where CA (μg/m^3) is the carbonyl concentration (diluted); ET (hours/day) the exposure time; EF (days/year) the exposure frequency; ED (years) the exposure duration; and AT (ED in years x 365 days/year x 24 hours/day) the averaging time.

The cancer risks (CR) from inhaled carbonyls were estimated according to **Equation 3.3**. This expression includes the inhalation unit risk (IUR) which according U.S EPA is the upper-bound excess lifetime cancer risk estimated to result from continuous exposure to an agent at a concentration of 1 μg/m^3 in air. The IUR for formaldehyde of 1.3E^{-5} (μg/m^3)$^{-1}$ and for acetaldehyde of 2.2E^{-6} (μg/m^3)$^{-1}$ were taken from the IRIS [11], assuming there were no synergistic or antagonistic chemical interactions. This simple additive approach is recommended by the Risk Assessment Guidance for Superfund when the total cancer risks is less than 0.1.

$$CR = IUR_{formaldehyde} \times EC + IUR_{acetaldehyde} \times EC \tag{3.3}$$

The carbonyl compounds measured in this thesis are part of the group of VOCs that contribute to OFP [12], and in turn to CR. However, IUR data is only available for formaldehyde and acetaldehyde; hence, the estimation of the CR is limited to the impact of these two pollutants.

3.3.5 Biological activity tests

In this section, the biological effects of SOF and WSF of PM were assessed. Cytotoxicity, genotoxicity, and oxidative DNA damage were evaluated on SOF using *in vitro* approach with a Human Hepatocarcinoma epithelial cell line, while acute eco-toxicity of WSF was evaluated *in vivo* using *D. Pulex*. Furthermore, 16 PAH emission factors were expressed as benzo[a]pyrene toxic equivalent.

These selected toxicity endpoints are only one piece of a comprehensive assessment of the health implications of vehicle emissions **Figure 3.6**. They allow comparing specific cell impacts between the tested fuels, but they are not sufficient for physiologically relevant toxicological assessments of such a complex mixture of pollutants as vehicle/engine exhaust.

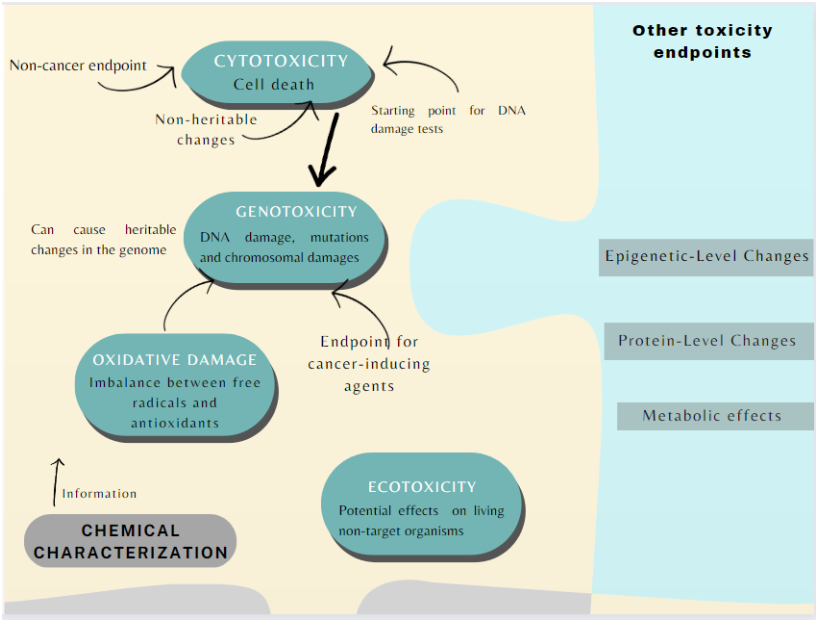

Figure 3.6: Selected toxicity endpoints.

Extraction of the organic and water-soluble fractions

The SOF was used for the cytotoxicity and DNA damage tests. All samples, including blank filter were placed in hermetically sealed stainless steel extraction cells and they were extracted through ASE 300 system (Dionex® Thermo Scientific, PA, USA) using dichloromethane as extraction solvent, and by pulses at a pressure of 1500 psi and 70 °C in two cycles of 5 min each. Subsequently, 50 mL of the extract was concentrated to approximately 2 mL in a rotary evaporator. On the other hand, for the ecotoxicity tests, WSF was used. The extraction of the WSF from the particles was carried out by ultrasonic waves for 3 hours, moderately hard reconstituted water was used as extraction solvent at a concentration of 10 mg PM/L. Moderately hard reconstituted water corresponds to deionized or glass-distilled water, free of contaminants [13] and with a total hardness of 80-90 mg/L $CaCO_3$, which is recommended for *D. pulex* culturing according to U.S. Environmental Protection Agency (U.S. EPA) methods [14]. All extracts were filtered. The reconstituted water was previously prepared as established by U.S. EPA [14] to ensure adequate conditions for the survival, growth and reproduction of the test specimens.

Cell cultures - HepG2 cell line and culture conditions

Cytotoxicity and genotoxicity assays were performed with the Human Hepatocarcinoma epithelial cell line HepG2 ATCC® CRL - 10741. This line was immortalized from human liver carcinoma cells derived from the liver tissue of a 15-year-old Caucasian male. These cells are of epithelial morphology with a set of 55 pairs of chromosomes. HePG2 is widely used for genotoxic studies because it expresses the P450 family of cytochromes (CYP-1A1, 1A2, 1B1, 2A6, 2A7, 2A13, 2C9, 2D6, 2E1, 3A4, 3A5, 3A7), involved in the metabolism of xenobiotics [15]. These cytochromes are also present in cells of the skin and lungs, the latter being a target organ for PM. These characteristics made HepG2 an ideal line for evaluating organic compounds from PM.

The cells were cultured in Dulbecco's Modified Eagle Medium (DMEM), supplemented with 10% fetal bovine serum and 10.000 U.I of penicillin -10 mg/mL of streptomycin in 75 cm^2 culture flasks at a humid atmosphere containing 5% CO_2 at 37 °C. The cell line was only worked in passages less than 15. Each test was carried out with a cell confluence of 80%.

Cytotoxicity in the HepG2 cell line

Cell viability was evaluated through the 3- (4,5-dimethylthiazol-2-yl) -2,5- diphenyltetrazole bromide (MTT) assay. To evaluate cytotoxicity, cell cultures with a viability greater than 90% were used. The cells were seeded in 96-well plates. They were treated with 20 serial dilutions of SOF (1:1), starting from a stock of 2.94 μgEq for 24 hours, after which 10 μL of MTT was added to the seeded cells and taken to an orbital shaker at 37 °C for 5 hours. After these hours, 100 μl of cold isopropanol were added per well, to dilute the formazan crystals, the culture plates were placed on an orbital vibrating plate for 24 hours. Analysis of the culture plates was performed using a Multiskan-go spectrophotometer at a wavelength of 570 nm.

Genotoxic activity and oxidative DNA damage through the comet assay modified with FPG and ENDO III enzymes

To evaluate the genotoxic effect of the SOF of fuel blends, HepG2 cells were seeded in 12-well plates. They were treated with 3 sublethal concentrations obtained from the MTT assay (0.735, 1.47, and 2.94 μgEq) for 24 hours, then the cells were soaked in low melting point agarose and seeded in Gelbond®. This process was done in two Gelbond®, one to be subjected to the enzymatic treatment and the other in a conventional way. Then the Gelbond® with the cells were subjected to a lysis solution (2.5 mol/L NaCl, 100 mmol/L EDTA- Na2, Tris 10 mmol/L (pH 10), DMSO 10%, Triton X-100 1%). After lysis, the two Gelbond® were soaked twice in Buffer (40 mM HEPES, 0.1 M KCl, 0.5 mM EDTA (pH 8.0)) for 5 min at room temperature.

The enzyme FPG or Endo III was added to one of the Gelbond® with a con-

centration of 1:1000. The Gelbond® was incubated in a humidified chamber for 45 min at 37°C. Finally, both Gelbond® were subjected to alkaline electrophoresis (pH<13) at 25 V and 300 mA. Cells were stained with GelRed ™ (Invitrogen Corp; CA, USA) and viewed under a Nikon® Eclipse 55i fluorescence microscope (Tokyo, Japan) with a 20X objective. The damage measurement parameter used was comet length, where DNA migration from each nucleus was measured with a eyepiece reticle [16, 17]. The parameters to evaluate DNA damage were the length of the comet, the percentage of damaged cells and the frequency of induction [18].

Acute ecotoxicity tests with *D. Pulex*

The *D. pulex* strain comes from "La Fe" reservoir (Antioquia-Colombia) and were cultivated under controlled ambient conditions and light intensity (16 light hours and 8 hours of darkness and lighting with 538 to 1076 Lux). The *D. Pulex* were fed with algae Ankistrodesmus falcatus and Pseudokirchneriella subcapitata. For each test, at least 160 neonates of 24-hour-old were captured and placed in a container with reconstituted water, in order to avoid feeding two hours before the start of the test. Neonates were exposed to four replicates of five different dilutions of WSF (6.25, 12, 25, 50 and 100% by volume). As a negative control the neonates were exposed to dilution water, and as a positive control, they were exposed to a potassium dichromate solution. After 24 of experimentation, immobile or dead neonates were quantified.

3.3.6 Statistical analysis

For particle and gaseous sampling and analysis, at least 3 replicates were performed, as mentioned in each section. All results presented show standard deviation bars. When evaluating results, the differences have been considered significant when the standard deviation bars do not overlap.

3.4 Transient State Tests

3.4.1 Engine test bench

These experiments were carried out in the engine test bench at the facilities of the Fuels and Engines Group (GCM) at the University of Castilla-La Mancha in Ciudad Real - Spain.

The experiments were carried out in an automotive, common rail direct injection, turbocharged and intercooled diesel engine, with Euro 6b technology manufactured by Nissan, model K9K (1.5 dCi). The engine was equipped with two exhaust gas recirculation loops, a low pressure cooled (LP-EGR) loop and a high pressure (HP-EGR) uncooled one, and with a diesel oxidation catalyst (DOC), a Lean NOx Trap (LNT), and a regenerative wall-flow-type diesel particle filter (DPF) located downstream the DOC and the LNT. The experimental installation is shown in **Figure** 3.7.

The resistive load, speed and torque was simulated and controlled by an asynchronous electric dynamometer (Schenck Pegasus Gmbh, Dynas model, LI250). The speed was taken from a digital tachometer attached to the rotor. The torque was measured from a torque meter cell and a signal conditioner from Gesellschaft für Industrieforschung GmbH, GIF. Finally, the accelerator position was controlled from the control and power module LRS 2003. This module acts over the accelerator sensor, which is connected to the Electronic Control Unit (ECU) of the engine. A Road Load Simulation (RLS) system from Horiba was used to emulate powertrain and body of a Nissan Qashqai 1.5 dCi vehicle. The main characteristics of the engine and simulated vehicle are listed in **Table** 3.7 and **Table** 3.8, respectively. The experiments were carried out following the WLTC driving cycle.

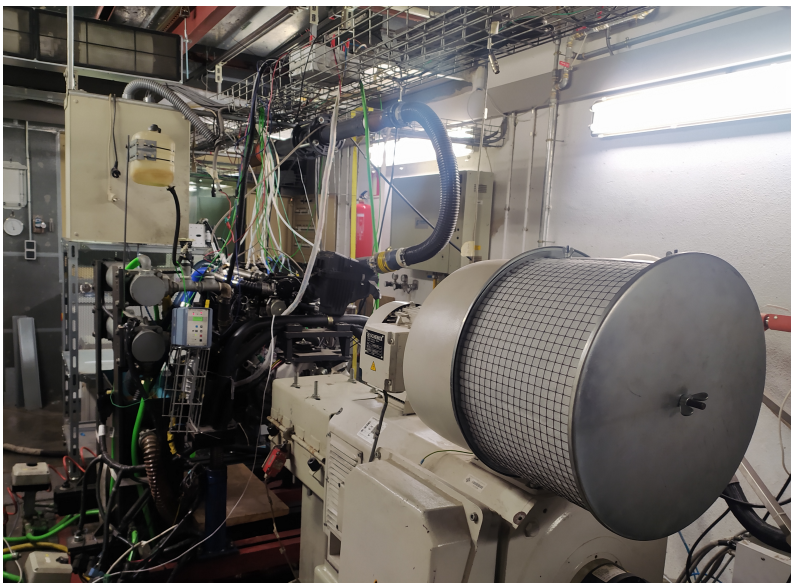

Figure 3.7: Engine configuration and sampling system

Table 3.7: Engine characteristics for transient state tests

Cylinders	4 (in line)
Valves/Cylinder	2
Displacement (cm^3)	1461
Stroke (mm)	80.5
Bore (mm)	76
Compression ratio	15.5:1
Injection	Common rail direct injection
Torque (max.)	260 Nm/1750 - 2500 r/min
Power (max.)	81 kW/4000 r/min
Aftertreatment system	DOC + DPF + LNT
Emission stardard	Euro 6b

Table 3.8: Characteristics of the simulated vehicle

Transmission	Manual, 6 gears
Differential ratio	4.13:1
Vehicle test mass (kg)	1470
1st:2nd:3rd:4th:5th:6th gear ratio	3.73:1; 1.95:1; 1.23:1; 0.84:1; 0.65:1; 0.56:1
Coast-down parameters	
F (N) = f_0 + $f_1\,V$ (km/h)	
+ $f_2\,V$ (km/h)^2	$f0$ = 89.6; f_1 = 0.0659;f_1 = 0.0391

The fuel and air consumption were measured with the original engine sensor (previously calibrated with an AVL 733s fuel gravimetric system) and hot-wire sensor, respectively. The data were registered with the INCA PC software. The regulated gaseous emissions (CO, CO_2, THC and NO_x=NO+ NO_2) were measured at the tailpipe with a gaseous emissions analyzer (Environement, France) with an accuracy of 1%. The total hydrocarbon emissions (THC) were measured with a flame ionization detector Graphite 52M-D. Carbon monoxide and carbon dioxide emissions were measured with a non-dispersive infrared (NDIR) detector MIR 2M. The infrared beam goes through an optical filter to differentiate between CO and CO_2 before passing through the sample. NOx emissions were measured using a chemiluminescence Topaze 3000 analyzer.

Solid particle emissions were measured upstream of the DPF with the Engine Exhaust Particle Sizer (EEPS) spectrometer model 3090 from TSI (USA). A first dilution with air was carried out on a rotating disc (RD) model MD19-2E at 150°C to avoid hydrocarbons condensation. After, when reaching 300°C, the diluted exhaust gas was introduced in the evaporating tube of the thermal conditioner (TC) model

ASET15-1. The aerosol flows into a mixing chamber for the second dilution to cool down. Primary dilution factor at RD was 107:1 and secondary dilution factor at the TC was 6.7:1, leading to a total dilution factor of 717:1. This high dilution factor is in order to prevent EEPS saturation during accelerations, and mainly, in the extra-high speed phase of the WLTC driving cycle.

Combustion diagnosis

For the thermodynamic combustion diagnosis, a Kistler Kibox instrument was used. In-cylinder pressure was measured with a piezoelectric pressure transducer (model 6056AU20, Kistler) coupled to a charge amplifier (5011B, Kistler). The crank angle signal was obtained with the original engine sensor. Using both signals the energy conservation equation was solved from in-cylinder experimental data providing characteristic parameters of the combustion process.

3.4.2 Test procedure

The WLTC was selected as driving cycle. WLTC is a chassis dynamometer test for the determination of emissions and fuel consumption from light-duty vehicles. This includes four driving sub-cycles, whose details are presented in **Table 3.9**.

Table 3.9: Characteristics of the WLTC

Phase	**Duration (s)**	**Stop duration (s)**	**Distance (m)**	**Maximum speed (km/h)**
Low	589	156	3095	56.5
Medium	433	48	4756	76.6
High	455	31	7162	97.4
Extra-high	323	7	8254	131.3
Total	1800	242	23266	-

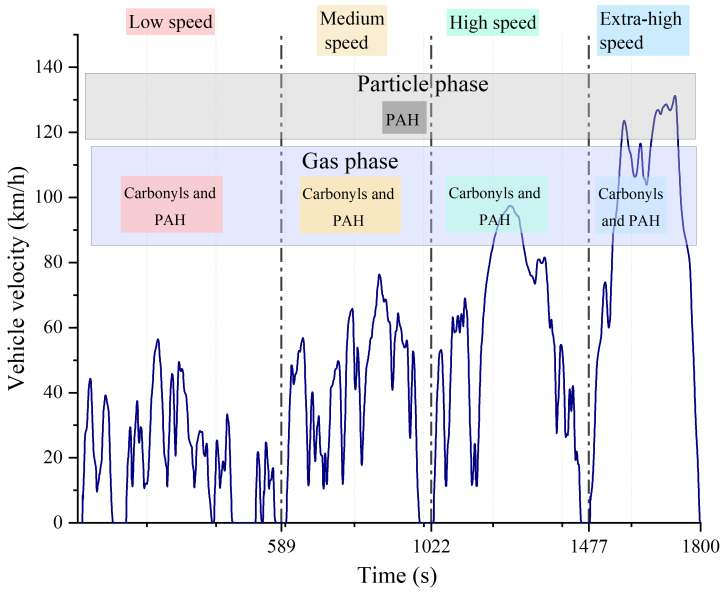

Figure 3.8: WLTC indicating sampling phase: gaseous (per phase) and PM (full cycle)

The tests were started from cold-engine conditions (19°C) (**Figure 3.8**), performed without any interruption, and repeated at least four times for all the tested blends at different days to evaluate the repeatability of the test and the results were averaged. The range of error corresponds to 90% confidence intervals and were shadowed around the average values. Preconditioning test, including LNT regenerations, were always performed the day before each test, to ensure that the initial conditions did not change from one test to another. DPF regeneration and fuel filter change were performed before each fuel tests. Unregulated gaseous pollutants were sampled and analyzed for each of the cycle phases, but in the particulate phase they were measured during the entire driving cycle as shown in **Figure** 3.8.

3.4.3 Unregulated pollutant sampling

Gaseous and particulate samples were collected in a homemade sampling system adapted to the exhaust pipe, upstream of the DOC/LNT/DPF, as shown in **Figure** 3.9.

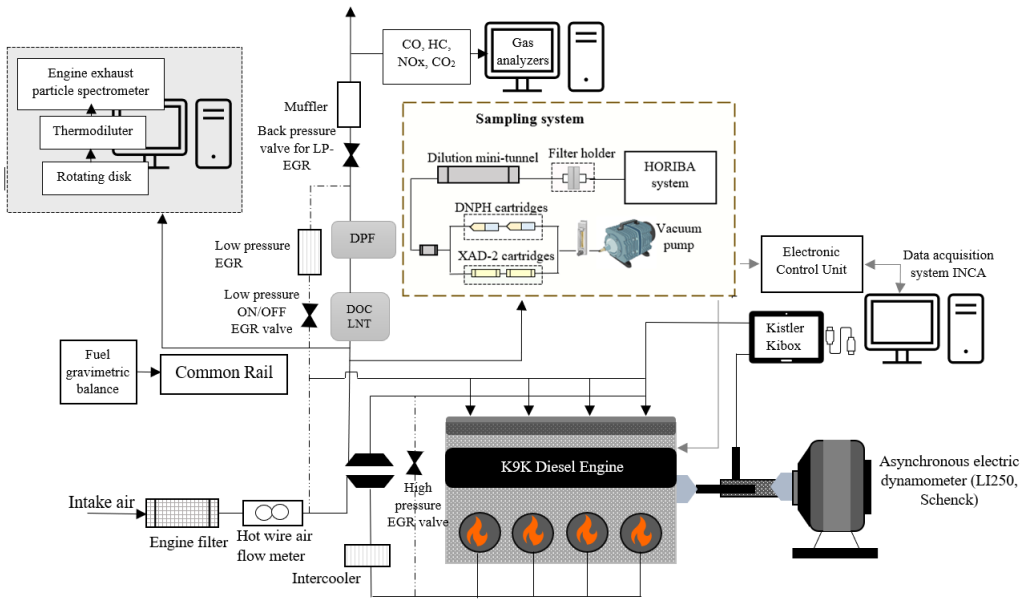

Figure 3.9: Engine configuration and sampling system

Gaseous pollutant sampling system

For gaseous sampling the line was kept at a temperature of 80°C to avoid condensation . A homemade sampling system (**Figure** 3.10) with the following characteristics was used to trap the target gaseous pollutants. At the intake of the sampling system a HEPA capsule filter (TSI®) was added to retain the particles > 0.3 μm. The system was divided into two identical parallel lines, from which samples were taken alternately. The parallel lines allowed sampling of carbonyls or PAH depending on the type of cartridge used, in each of the phases of the WLTC cycle. The flow rate was regulated and induced through a vacuum pump located at the end of the line. All pipes were covered with an insulating material to prevent gas condensation in the line. At the sampling point (location of the cartridges) the temperature was not sensed. However, it had to be slightly close to 80°C (temperature of the heat line).

For carbonyl sampling, commercial DNPH cartridges of 130 mg of 1,2-bis (2-pyridyl) ethylene (BPE) and 270 mg of 2,4-dinitrophenylhydrazine (Sigma-Aldrich) were used.

For PAH and apoptosis tests, stainless steel cartridges of 10 cm long and 1.3 cm in diameter were used, packed with 3.2 g of XAD-2 Amberlite® resin, previously washed with dichloromethane using a Soxhlet system for 8 hours with 8 to 10 cycles per hour.

Particle sampling system

PTFE 2.0 μm (47 mm, PALL) filters were used for particle sampling. These were weighed in triplicate and conditioned before sampling. The exhaust gas flow was passed through the MDLT 1304TM Mini Dilution Tunnel designed for the measurement of particulate mass in gases using the partial flow dilution method (dilution of 50x). The dilution unit was maintained at a constant temperature by means of a heated probe, with the dilution air, which was obtained from a compressed air line. The diluted sample was passed through a filter holder. The temperature at this point did not exceed 52ºC. The filters were placed in the filter holder and the pump was turned on immediately after the test began. Once the test was finished, the filter was removed, climatized for 48 hours, and weighed in triplicate. All samples, gaseous and particulate, were kept covered with aluminum foil and refrigerated until their subsequent extraction and analysis.

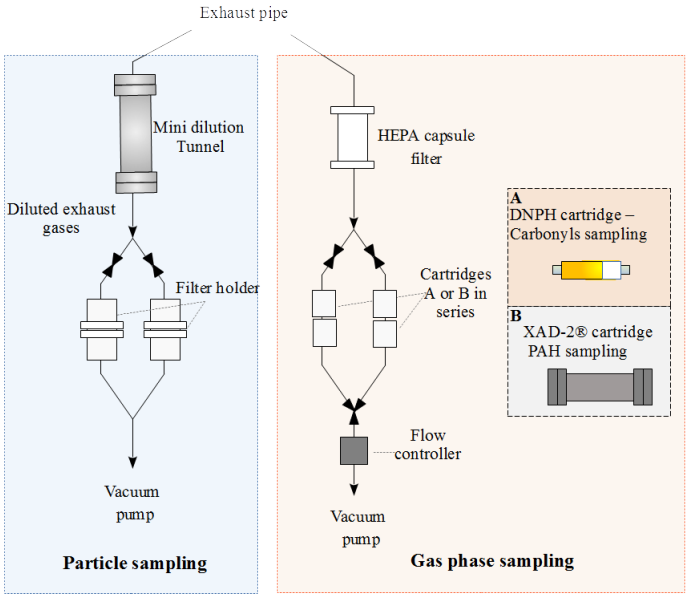

Figure 3.10: Gas phase and particle sampling systems -transient state tests

3.4.4 Chemical characterization of unregulated emissions

Extraction and sample analysis

All the glassware used in the extraction and handling of the samples was washed with acetone and solvents used for extraction and analysis were HPLC grade. The PAH samples (including field blanks) adsorbed on the amberlite resin, as well as the filters were extracted in a Soxhlet system with a 70:30 mixture of dichloromethane-methanol. The extraction was left for 8 hours with 8-10 cycles per hour. After ex-

traction, the samples were concentrated to 5 mL in a rotary evaporator and finally analyzed. Carbonyl samples were extracted with 4 mL of acetonitrile and passed through syringe filters to retain particles.

PAH and carbonyl compounds were quantified by HPLC-UV (Shimadzu®). For PAH, a standard calibration solution with 16 PAH (Supelco ®) was diluted with dichloromethane to 10, 25, 50, 150, 250 and 500 μg/mL. The calibration conditions were controlled before each analysis introducing a standard sample and an analytical blank. The separation was made by a Supelcosil PAH column (ID 5 μm, Ø 4.6 $\times$ 250 mm) and the gradient program was 40:60 - 100:0 - 40:60 (acetonitrile:water) during 60 min. The flow rate was constant at 1 mL/min and the injection volume was 10 μL. A UV–VIS detector (λ= 254 nm) was employed for detection. The PAH analyzed were: Naphthalene, acenaphthylene, acenaphthene, fluorene, phenanthrene, anthracene, fluoranthene, pyrene, benzo(a)anthracene, chrysene, benzo(b)fluoranthene, benzo(k) fluoranthene, benzo(a)pyrene, indeno(1,2,3-cd)pyrene, dibenz(a,h)anthracene, benzo(g,h,i)perylene.

For carbonyl analysis, a standard solution mix (Chem Service Inc) was used for calibration including formaldehyde, acetaldehyde, benzaldehyde, butyraldehyde, acetone, propionaldehyde, acrolein, crotonaldehyde, hexaldehyde, valeraldehyde, p-tolualdehyde, methacrolein, 2-butanone hydrazones. The calibration standard solution was prepared at concentrations of 0.6, 1, 5, 10, 20 and 40 μg/mL for formaldehyde and 0.3, 0.5, 2.5, 5, 10, and 20 μg/mL for the other 12 carbonyls.

The separation was made in a C18 column (ID 5 μm, Ø 4.6 $\times$ 250 mm) (Supelco ®). Acetonitrile and water with a 5% by volume of methanol were used as a mobile phase with gradient elution 50:50–65:35–100:0–50:50 during 37 min. The flow rate was maintained at 1 mL/min and the injection volume was 10 μL. A UV–VIS detector (λ= 360 nm) was employed for detection.

The target compounds were quantified by the regression method of their peak areas according to the standard curves. The emission factors were calculated from the concentrations obtained in the HPLC multiplied by the final extraction volume and the total volumetric flow of exhaust gases and divided by the travelled distance.

The OFP was also determined following the procedure described in **section** 3.3.4.

3.4.5 Biological activity test

Cellular study of Apoptosis

Hepatocellular carcinoma is one of the predominant causes of cancer-associated mortality worldwide [19]. Therefore, for the cellular study of apoptosis, HepG2 cells (HB-8065, human hepatocellular carcinoma cells) were selected. HepG2 were ob-

tained from American Type Culture Collection (ATCC, Manassas, VA, USA). HepG2 cells were maintained in RPMI-1640 medium (Sigma-Aldrich, Munich, Germany), supplemented with 10% sterile-filtered fetal bovine serum (FBS) (Sigma-Aldrich, Germany) and 1% antibiotic (l-glutamine-penicillin-streptomycin) (Sigma-Aldrich, Germany) solution.

Apoptosis tests were performed following the protocol reported previously by [20]. Briefly, after different treatments, cells were seeded in 96-well plates, and after 24 h, cells were treated with 10 μL of each sample (organic extract of particulate and gas samples) or 10 μL of the DMSO solvent (DMSO; Merck, Darmstadt, Germany) for 24 hours. The medium was removed, and cells were washed with 300 μL HANKs solution. Then, cells were fixed and permeabilized for 2 min in ice-cold methanol and stained with 1 μg/mL Hoechst (Sigma-Aldrich). Apoptotic nuclei were determined by fluorescence microscopy using a Cytation 5 system (BioTek). Image analysis was also conducted using ImageJ software (ImageJ) [21]. Apoptotic nuclei were determined according to morphological criteria [20]. The apoptotic index (AI) was then calculated using the **Equation 3.4**.

$$AI = \frac{A_{cc}}{N_{cc}} \times 100 \tag{3.4}$$

Where A_{cc} is the number of apoptotic carcinoma cells per section and N_{cc} is the total number of carcinoma cells per section.

3.4.6 Statistical analysis

For particle and gaseous sampling and analysis, at least 3 replicates were performed, as mentioned in each section. All results presented show standard deviation bars. When evaluating results, the differences have been considered significant when the standard deviation bars do not overlap.

Bibliography

[1] M. Lapuerta, Á. Ramos, J. Barba, and D. Fernández-Rodríguez. Cold- and warm-temperature emissions assessment of n-butanol blends in a euro 6 vehicle. *Applied Energy*, 218:173–183, 2018.

[2] David Donoso, David Bolonio, Rosario Ballesteros, Magín Lapuerta, and Laureano Canoira. Hydrogenated orange oil: A waste derived drop-in biojet fuel. *Renewable Energy*, 188:1049–1058, 2022.

[3] David Donoso, Rosario Ballesteros, David Bolonio, María-Jesús García-Martínez, Magín Lapuerta, and Laureano Canoira. Hydrogenated turpentine: A biobased component for jet fuel. *Energy & Fuels*, 35(2):1465–1475, 2021.

[4] Pedro N. Benjumea Hernández. Andrés F. Agudelo Santamaría, John R. Agudelo Santamaría. *Diagnóstico de la combustión de biocombustibles en motores*. Universidad de Antioquia, universidad de antioquia edition, 2007.

[5] Hamisu Adamu Dandajeh, Midhat Talibi, Nicos Ladommatos, and Paul Hellier. Polycyclic aromatic hydrocarbon and soot emissions in a diesel engine and from a tube reactor. *Journal of King Saud University - Engineering Sciences*, 34(6):435–444, 2022.

[6] OEHHA. Benzo[a]pyrene as a Toxic Air Contaminant. Part B. Health Effects of Benzo[a]pyrene. Technical report, Office of Environmental Health Hazard Assessment, California Environmental Protection Agency, Air Toxicology and Epidemiology Section: Berkeley, CA, 1993.

[7] W.P.L. Carter. Development of ozone reactivity scales for volatile organic compounds. *Journal of the Air and Waste Management Association*, 44(7):881–899, 1994.

[8] W.P.L. Carter. Updated maximum incremental reactivity scale and hydrocarbon bin reactivities for regulatory applications. *Updated Maximum Incremental Reactivity Scale and Hydrocarbon Bin Reactivities for Regulatory Applications*, 2010.

[9] I.C.T. Nisbet and P.K. LaGoy. Toxic equivalency factors (tefs) for polycyclic aromatic hydrocarbons (pahs). *Regulatory Toxicology and Pharmacology*, 16(3):290–300, 1992.

[10] A. Prokopowicz, M. Zaciera, A. Sobczak, P. Bielaczyc, and J. Woodburn. The effects of neat biodiesel and biodiesel and hvo blends in diesel fuel on exhaust emissions from a light duty vehicle with a diesel engine. *Environmental Science and Technology*, 49(12):7473–7482, 2015.

[11] U.S. EPA. Integrated Risk Information System US EPA, 2018.

[12] J. Duan, J. Tan, L. Yang, S. Wu, and J. Hao. Concentration, sources and ozone formation potential of volatile organic compounds (vocs) during ozone episode in beijing. *Atmospheric Research*, 88(1):25–35, 2008.

[13] M. Nordberg, D.M. Templeton, O. Andersen, and J.H. Duffus. Glossary of terms used in ecotoxicology (iupac recommendations 2009). *Pure and Applied Chemistry*, 81(5):829–970, 2009.

[14] *Methods for Measuring the Acute Toxicity of Effluents and Receiving Waters to Freshwater and Marine Organisms, 5th Ed.*, 2002.

[15] F. Nagai, Y. Hiyoshi, K. Sugimachi, and H.-O. Tamura. Cytochrome p450 (cyp) expression in human myeloblastic and lymphoid cell lines. *Biological and Pharmaceutical Bulletin*, 25(3):383–385, 2002.

[16] N.P. Singh, M.T. McCoy, R.R. Tice, and E.L. Schneider. A simple technique for quantitation of low levels of dna damage in individual cells. *Experimental Cell Research*, 175(1):184–191, 1988.

[17] A. Azqueta, J. Slyskova, S.A.S. Langie, I.O. Gaivão, and A. Collins. Comet assay to measure dna repair: Approach and applications. *Frontiers in Genetics*, 5(AUG), 2014.

[18] L.A.Z. Venegas. Optimizaciones metodológicas del ensayo del cometa y su aplicación en biomonitorización humana. 2009.

[19] Dan Tang, Baomu Sun, Hongyu Yu, Zhengde Yang, and Liang Zhu. Tumor-suppressing effect of MiR-4458 on human hepatocellular carcinoma. *Cellular Physiology and Biochemistry*, 35(5):1797–1807, 2015.

[20] Javier Frontiñán-Rubio, M. Victoria Gómez, Cristina Martín, Jose M. González-Domínguez, Mario Durán-Prado, and Ester Vázquez. Differential effects of graphene materials on the metabolism and function of human skin cells. *Nanoscale*, 10(24):11604–11615, 2018.

[21] Caroline A Schneider, Wayne S Rasband, and Kevin W Eliceiri. NIH Image to ImageJ: 25 years of image analysis. *Nature Methods*, 9(7):671–675, 2012.

Chapter 4

Steady state results

In this chapter, unregulated emissions (carbonyl compounds and PAH), the ozone formation potential and the biological response of soluble organic fraction and water-soluble fraction from biofuels-derived PM were investigated. The experiments were carried out in an automotive diesel engine fueled with butanol, pentanol and HVO blends and operating under two representative urban driving conditions.

4.1 Introduction

Among alcohols, butanol and pentanol have been considered prominent candidates as partial substitutes for diesel fuel as they have higher calorific value, lower vapor pressure, higher cetane number, as well as being less hydrophilic and greater miscibility than ethanol which allows increasing the butanol or pentanol percentage in the blends [1, 2, 3, 4, 5, 6]. Additionally, renewable diesel -HVO- fuel, composed mainly of paraffins and free of oxygen, sulfur and aromatics, has been identified as a prominent candidate to replace fossil diesel mainly due to its almost zero carbon footprint and its physicochemical properties similar to fossil diesel.

Although the effects of HVO, butanol, and pentanol on engine performance and regulated emissions have been widely reported in literature [7, 8, 9, 10], there are few and limited literature reports about their unregulated emissions and impact related to photochemical air pollution. Within unregulated emissions, PAH and carbonyls, have been of special interest due to their hazardous effects on human health and the environment [11, 12]. In addition, carbonyls, which are of major concern when blending alcohols with fossil fuels, are highly reactive in the atmosphere, contributing to formation of ozone and other photochemical air pollutants [13] and they serve as one of the major sources of free radicals causing an indirect negative impact on public

health [14].

Regarding the biological response, epidemiological studies have provided substantial evidence corroborating the ability of diesel derived particles to induce cytotoxicity, DNA damage and oxidative stress in cells through the production of ROS [15]. However, most of toxicological studies have been focused on fatty acid methyl esters (biodiesel) and on the evaluation of the toxicity of the SOF, very limited studies have assessed the WSF which might contribute significantly to toxicity due to potentially bioavailable soluble metals and ions [16].

Some of the results presented in this chapter have been published in indexed scientific journals ([17, 18, 19]).

4.2 Unregulated emissions from Butanol/diesel and HVO/diesel fuel blends

The effect of a representative butanol/ULSD fuel blends, and two HVO/ULSD blends on 18 PAH compounds (both in particles and gaseous phases) and 13 carbonyl compounds gathered from the exhaust gases. Details of the methodology are presented **section** 3.3.3. Briefly, the particle and gas phase sampling procedure for PAH and carbonyls characterization was carried out without any air dilution. 16 PAH requested by the US EPA + benzo[e]pyrene and dibenzo[a,l]pyrene which is acknowledged for its significant carcinogenic potential, were determined.

4.2.1 Engine performance parameters

Figures 4.1 and 4.2 show the thermodynamic combustion diagnosis for both engine operating modes. A greater influence of the biofuels was observed in the in–cylinder average bulk temperature and heat release rate curves suggesting differences in the combustion process leading to different unregulated emissions as discussed below.

In–cylinder average bulk temperature and heat release rate for the HVO blends could be influenced by their higher cetane number, which advanced the start of combustion as shown in the in–cylinder pressure curve (**Figure** 4.1), due to the shorter ignition delay in comparison with ULSD and Bu13. At high load, the difference in ignition delay between HVO blends and ULSD fuel is smaller, as the internal gas temperature rises at the start of combustion. The shorter ignition delay reduces the fuel vapor–air mixing time, leading to a lower peak of heat release rate at the premixed combustion phase (**Figure** 4.2) [20].

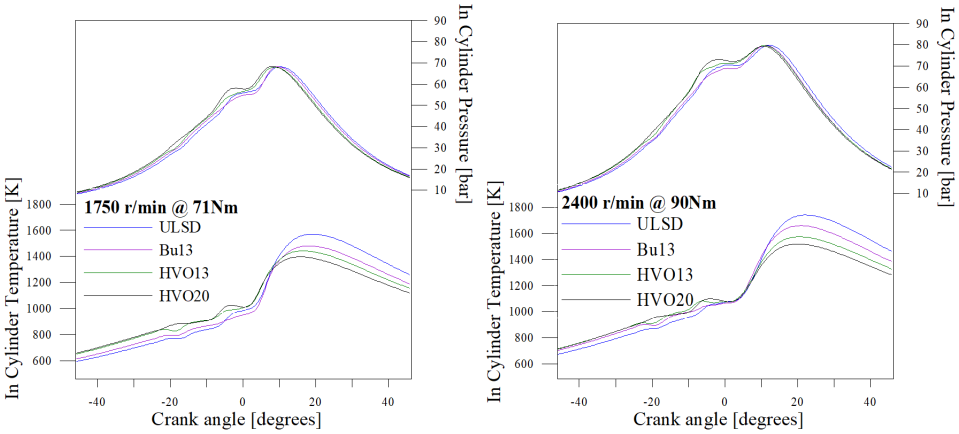

(a) In-cylinder temperature and pressure for M1. (b) In-cylinder temperature and pressure for M2.

Figure 4.1: In-cylinder pressure and average bulk temperature [21]

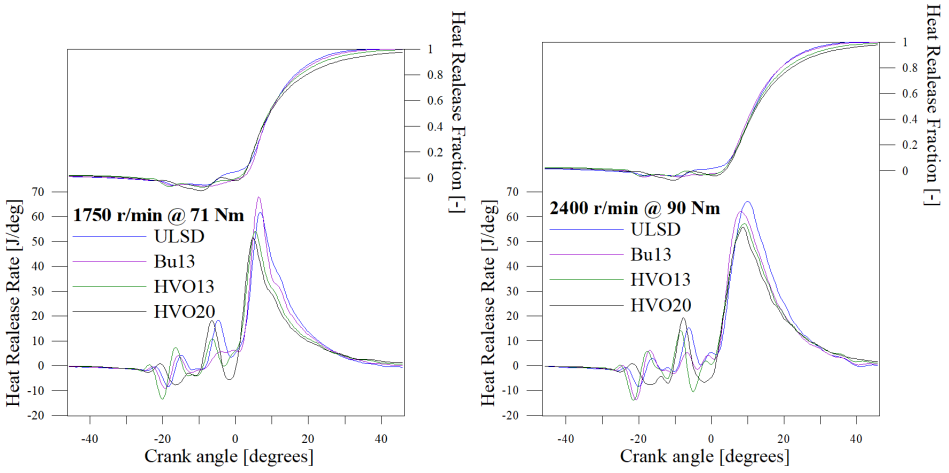

(a) Heat release rate and fraction for M1 (b) Heat release rate and fraction for M2.

Figure 4.2: Heat release rate and heat release fraction [21]

The pilot injection changed the thermodynamic conditions in the combustion chamber as reported by [22]. The rate of heat release during the pilot injection was higher for HVO blends (**Figure** 4.2), increasing in-cylinder pressure and temperature (**Figure** 4.1). Since tests were carried out at the same power output, then this explains the lower heat release rate of HVO blends during the main combustion phase (after 10 °CA) [23]. Furthermore, the high rate of heat release for ULSD and Bu13 can be explained by the reduction in cetane number with respect to blends with HVO, which enlarge the ignition delay and leads to more fuel being burned in the premixed phase. Moreover, it is hypothesized that the heat of evaporation and oxygen content of Bu13

could also improve the burning rate, which made the peak rate of heat release closer to that of ULSD. In addition, the lower density and viscosity of Bu13 might play a role in improving the air-fuel mixture [24].

The heat release fraction (cumulative heat release) in (**Figure** 4.2) shows similar average bulk in–cylinder combustion performance independently of the engine operating mode. However, for HVO the combustion performance was slightly lower than for other fuels. For ULSD, Bu13 and HVO the combustion reached above 99% of the total heat released after 50 crank angle degrees, which is common in diesel engine combustion. The rest of this unburned fuel could be one of the components conforming the particulate matter, which might contribute to explain the content of PAH with HVO. Other engine performance parameters are shown in **Table** 4.1. Regulated emissions are shown in **Appendix** B.

Table 4.1: Engine performance results

Parameter	**ULSD**		**Bu13**		**HVO13**		**HVO20**	
σ*	**M1**	**M2**	**M1**	**M2**	**M1**	**M2**	**M1**	**M2**
Engine power (kW)	13.0 (0.02)	22.7 (0.27)	13.0 (0.03)	22.6 (0.16)	13.0 (0.04)	22.6 (0.13)	13.0 (0.05)	22.4 (0.58)
Brake-specific fuel consumption (g/kWh)	273.9 (2.38)	272.7 (4.54)	280.8 (2.72)	273.9 (2.68)	269.4 (4.87)	279.6 (3.08)	268.4 (2.61)	277.1 (7.53)
Brake thermal efficiency (%)	30.6	30.8	30.9	31.7	31.0	29.9	31.1	30.1
Specific particulate matter emissions (mg/kWh)	39 (15)	46 (15)	35 (6)	40 (9)	37 (9)	42 (14)	36 (12)	39 (7)
Specific NOx emissions (g/kWh)	4.5 (0.09)	4.5 (0.06)	4.9 (0.09)	5.1 (0.12)	5.4 (0.14)	5.1 (0.18)	5.0 (0.07)	5.5 (0.13)

*Number in parenthesis represent standard deviation.
*M1= 1750 r/min @ 71 Nm; M2= 2400 r/min @ 90 Nm.

4.2.2 PAH emissions

PAH compounds have chemical structures of two or more fused benzene rings in linear, angular, or cluster arrangements [25]. **Figure** 4.3 shows the PAH emissions in gas phase (left) and particle phase (right) with different fuel blends in both operation modes. Apparently, similar PAH emission profiles can be observed, although their emission levels were different. For gas phase, Nap, Phen+Ant, are the three predominant compounds, when compared with the particle phase, Phen+Ant and Pyr reach the highest concentrations, which agrees with reports by Vojtisek-Lom et al. [26] for butanol and HVO and by Zhang et al. and Li et al. [27, 28] for diesel and biodiesel blends. In addition, De Souza and Correa [29] studied how during engine use, lubricating oil can accumulate significant amounts of PAH and therefore influence PAH

emissions. They reported NAP, Phen and Pyr, the same compounds with the highest concentrations in this study, as main PAH in the lubricating oil after 12,000 kilometers of use. In this case, PAH issued by the exhaust have mostly a pyrogenic origin. However, a fraction of those predominant PAH can also be contributed by PAH retained in the lubricant oil.

Emissions of NAP, the lowest molecular weight PAH, increased with both biofuel-diesel blends respect to ULSD results. While for Bu13 and HVO20, NAP concentrations were not statistically different, for HVO20 NAP reached the maximum concentration (between 150 and 190 μg/kWh) and was always higher in mode M2 than in mode M1 in both gas and particle phases. The emissions of Acy, B[a]A and Cry were the lowest and with similar magnitudes in both phases. However, HVO blends generated higher emissions of Phe + Ant, while for B[a]A, Flt, Flu and Acy, no significant differences were observed between tested fuels in any phases.

PAH with 5 and 6 rings (**Figure** 4.4) in the gas phase were detected in most of the conditions tested with concentrations much lower in magnitude than the congeners between 2 and 4 rings. BaP, considered the reference compound by US EPA, was higher for ULSD in M1 and HVO in M2. However, no clear trend can be identified with respect to butanol or HVO, i.e; no benefit is observed in terms of PAH emissions with these biofuels with respect to diesel under the conditions tested.

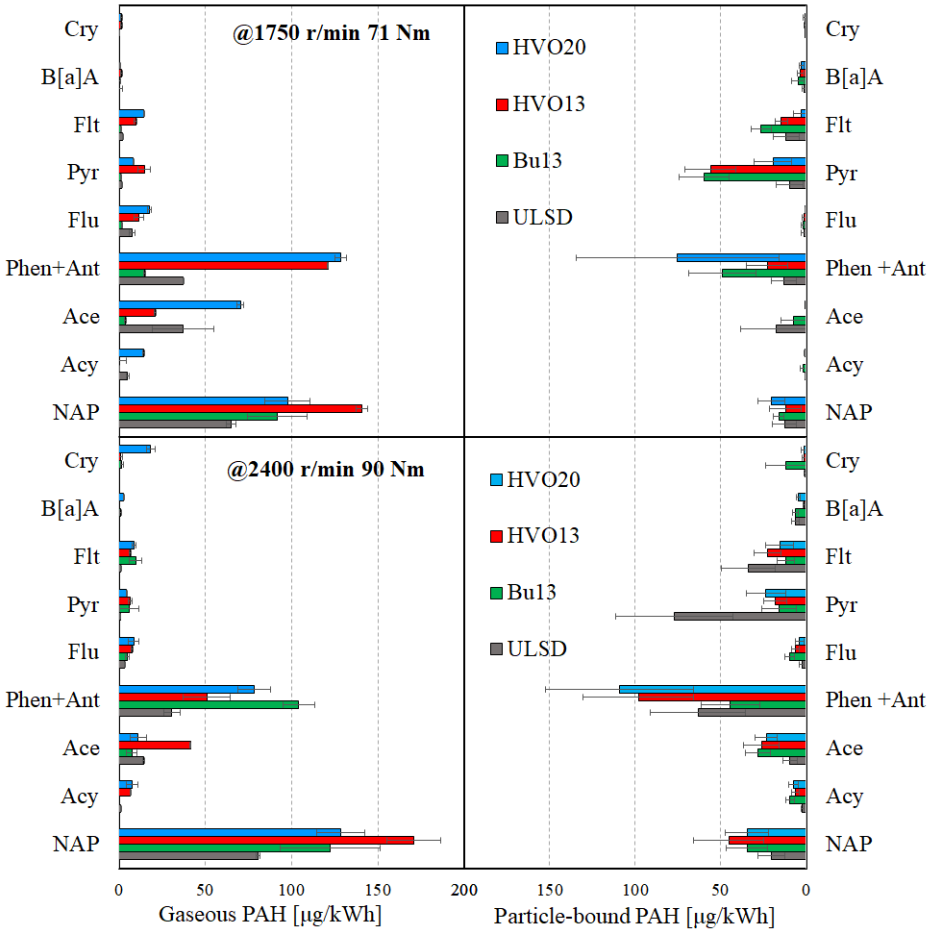

Figure 4.3: Light PAH specific emissions. Left: gaseous PAH, right: particulate PAH

Some researchers [30, 31] have suggested that PAH emissions are highly influenced by the PAH content in the fuel. In addition, Lima et al. [32] have also reported that PAH can be emitted regardless of their presence in the original fuel. In this case, the blended biofuels are aromatic-free, and the PAH concentrations were not significantly reduced with their use. Then, the presence of PAH in the exhaust for Bu13, HVO13 and HVO20, suggested that pyrolysis and pyrosynthesis processes of lower molecular weight hydrocarbon compounds were occurring during combustion, and free radicals formed during this process combined into acetylene resulting in the formation of aromatic rings through condensation products, leading to the formation of larger, more stable molecules, and in addition, the lubricant oil might be also contributing to these emissions [30, 33, 34].

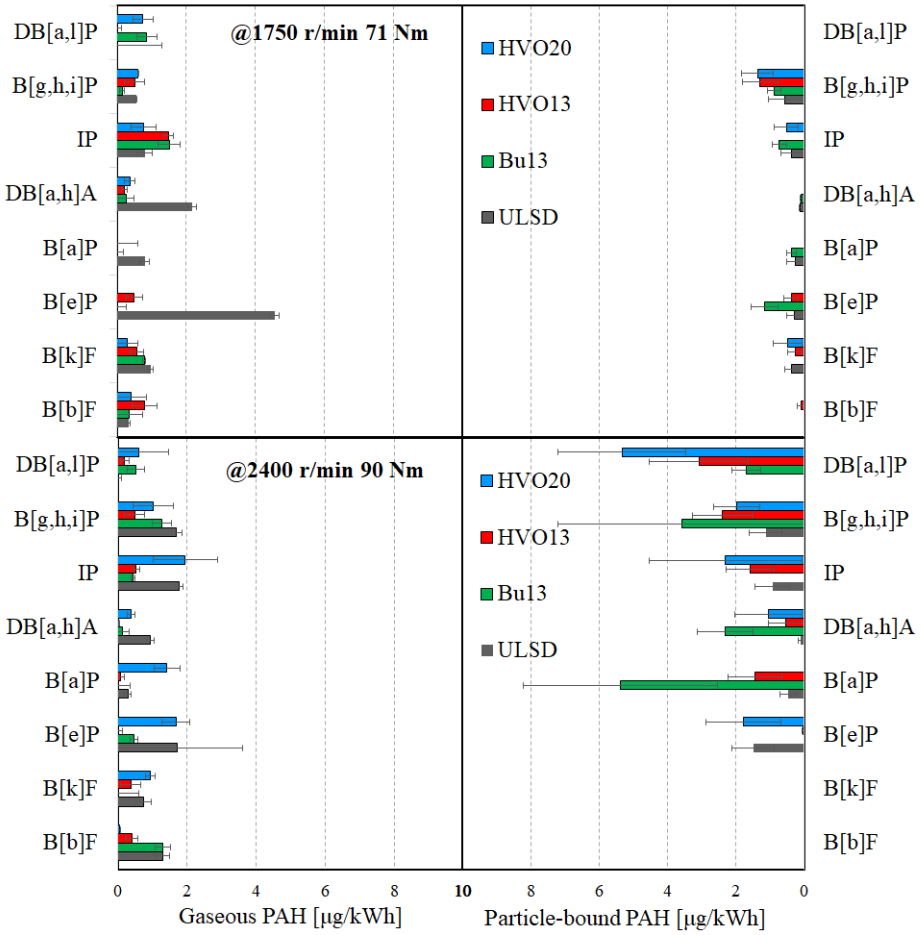

Figure 4.4: Heavy PAH specific emissions. Left: gaseous PAH, right: particulate PAH

In the particle phase, an increase in the concentrations of B[a]P and DB[a,h]A is observed with butanol. DB[a,l]P was only detected with Bu13, HVO13 and HVO20 in M2, increasing the concentration in this same order. It is important to note that DB[a,l]P has been reported to be even much more toxic than B[a]P [25, 35]. In general, low molecular weight PAH (containing two to four aromatic rings) are the most abundant compounds in the exhaust, which agrees well with the finding of Vojtisek-Lom et al. [26], these compounds are less toxic and degraded at reasonable rates in the presence of oxygen, unlike compounds with more than four rings, which are highly persistent in the environment. The high molecular weight PAH are usually found at low concentrations, especially at middle and high loads. Generally, thermodynamic stability of the molecule determines the ability of individual PAH to survive at high temperature environment [28].

The distribution between the gas and particle phases is observed in **Figure** 4.5. **Figure** 4.5a compares the distribution in each phase by rings. 2-ring compound was distributed mainly in the gas phase in all fuels and in both operation modes, however, a higher concentration was observed in M2. In 3-ring PAH there was an opposite trend between modes, for M1 the PAH in the gas phase dominate over the particle phase except for Bu13. However, in M2 the opposite occurs. As expected, from 4 to 6 rings, the PAH are observed mainly in the particle phase. **Figure** 4.5b shows the distribution between phases by fuel for total PAH emissions. Independently of the fuel used, it was observed that total PAH emissions were higher at the higher engine load (M2), corresponding to higher instantaneous in-cylinder pressure and temperature. Moreover, although the aromatic compounds decreased with the addition of both butanol and HVO, the total PAH emissions increased, which confirmed that the higher pressure and temperature favored the pyrosynthesis reactions. The total 18 PAH were dominated by 3- and 4-rings PAH with total proportion up to 70%, in agreement with Vojtisek-Lom et al. [26].

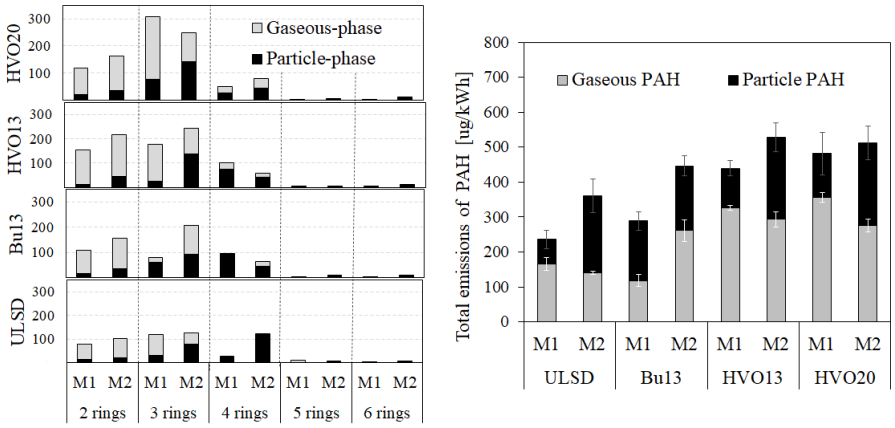

(a) PAH distribution by rings .

(b) Total PAH emissions between phases.

Figure 4.5: PAH distribution between the gaseous and particle phases

Variations in PAH emissions shown in **Figure** 4.3 to **Figure** 4.5, can be attributed to differences in fuel formulation and combustion characteristics, since engine performance parameters were similar as shown in **Table** 4.1. PAH emissions for Bu13 and ULSD were similar, which could be explained due to the high cetane number of the HVO blends (see **Table** 3.1) in agreement with [7, 36, 37]. The earlier start of main combustion of HVO blends resulted in an earlier end of combustion (**Figure** 4.2), and in lower bulk average in-cylinder temperatures (**Figure** 4.1), which might explain the higher PAH exhaust emissions. This could be expected since the total PAH were reported to increase with decreasing in-cylinder temperatures [38, 32]. Dandajeh et al. [39] reported that total PAH concentration decreased as the ignition delay increased. This was explained by the fact that the maximum average in-cylinder temperature

increased with ignition delay. For this reason, it is likely that the higher in-cylinder temperature of ULSD and Bu13 might explain the lower total PAH emissions in comparison with HVO blends.

With respect to the impact of fuel formulation, Jin et al [40] carried out experiments with coflow diffusion flames in order to study the n-butanol doping effect on PAH formation. They reported that while the mole fraction of n-butanol increased, benzene precursors, especially C3 radicals, also increased. This enhanced the formation of phenyl and benzyl radicals [41]. Furthermore, the increase in PAH with n-butanol blending has been reported in some studies [42, 43]. In addition to the mechanism of PAH formation by the combination of propargyl radicals producing benzene or phenyl as mentioned above, PAH from non-aromatic fuel blends with diesel can be explained from the reaction of adding vinyl to acetylene to produce vinylacetylene, where the formation of the first aromatic ring normally begins and is followed by acetylene addition to the n-C4H3 radical formed by the H abstraction from the vinylacetylene [44].

4.2.3 Carbonyl emissions

Seven carbonyl compounds were detected and quantified, acetone and acrolein, butyraldehyde and benzaldehyde were reported as the sum, because a total separation was not achieved in the chromatographic method. Crotonaldehyde, hexaldehyde, valeraldehyde, p-tolualdehyde, methacrolein and 2-butanone were not detected.

Figure 4.6 shows the percentage of leakage from each congener to the second cartridge, and for ULSD -M1 in which the highest sampling flow was used, leakage to a third cartridge was also quantified. Formaldehyde leaked less than 50% in all cases, contrary to acetaldehyde, which in most tests exceeded 50% except for butanol, indicating the great influence of the sampling flow. Regarding acetone, it was detected in most cases only in the second cartridge. This revealed the importance of using at least two cartridges in series to identify those compounds that do not react in the first cartridge to form complexes of DNPH, this can be mainly influenced by the sample flow. For ULSD M1, both acrolein and butyraldehyde + benzaldehyde, were fully detected only in the second cartridge. These measurements showed that, although the first cartridge was not saturated, there may be a fraction of the carbonyls that advance in the line and react in the second cartridge. If this cartridge is not located in series, the detected concentration could be underestimated. It is also important to note that even if sampling is optimized with a given flow and time, the change in fuel formulation can change the concentrations of the carbonyls generated. Therefore, always measuring with two cartridges in series becomes a recommended sampling practice.

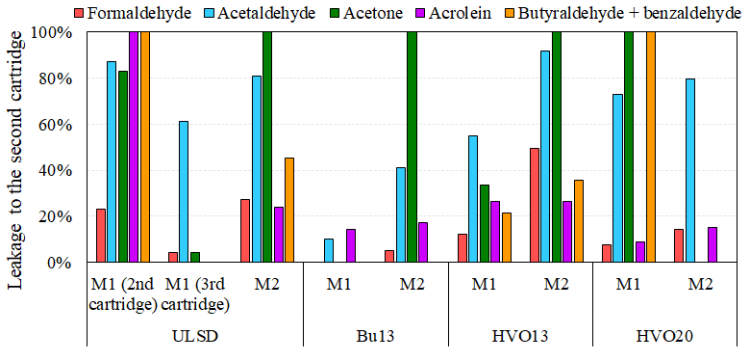

Figure 4.6: Percentage of leakage from each congener to the second cartridge

Carbonyl concentrations were consequently corrected according to the leaks. **Figure** 4.7 shows the specific emissions of the 7 carbonyls detected. Results show that the concentration of carbonyls was mainly influenced by the fuel and not by the operation mode. HVO showed lower carbonyl emission compared to Bu13. This may be due to the absence of oxygenated compounds. Formaldehyde was the most predominant compound among the carbonyls detected, except for the ULSD in M1 in which the acetone emission was the highest. The total contribution of formaldehyde and acetaldehyde to the carbonyl emissions ranged from 40% to 80%. The fuel blended with 13% butanol produced higher formaldehyde and acetaldehyde emissions than ULSD and HVO blends at both engine loads, enhanced oxidation of unburned hydrocarbons due to the addition of an oxygenated fuel such as butanol, would lead to the formation of carbonyl compounds, thereby agreeing with the results published by [24, 45, 46, 47]. This is consistent with some speciation studies that have shown that carbonyl emissions might be related to the hydroxyl group in alcohol fuels.

Formaldehyde and acetaldehyde emissions from C1-C5 alcohols are directly linked with molecular structure and combustion chemistry pathways [48]. During the alcohol combustion process, carbonyls can be formed at high temperatures, by H-atom abstraction and β-scission of the alcohol, and even at lower temperatures, the reaction of α-hydroxyalkyl radicals with O2 leads to carbonyls formation [48]. Another reason for the increase in carbonyl emissions with Bu13 could be caused by the longer ignition delay (**Figure** 4.1) due to the high latent heat of vaporization or high self-ignition temperature of butanol, the ignition delay promoted forming the premixed mixture and increased the availability of free oxygen available to react to form carbonyls [49].

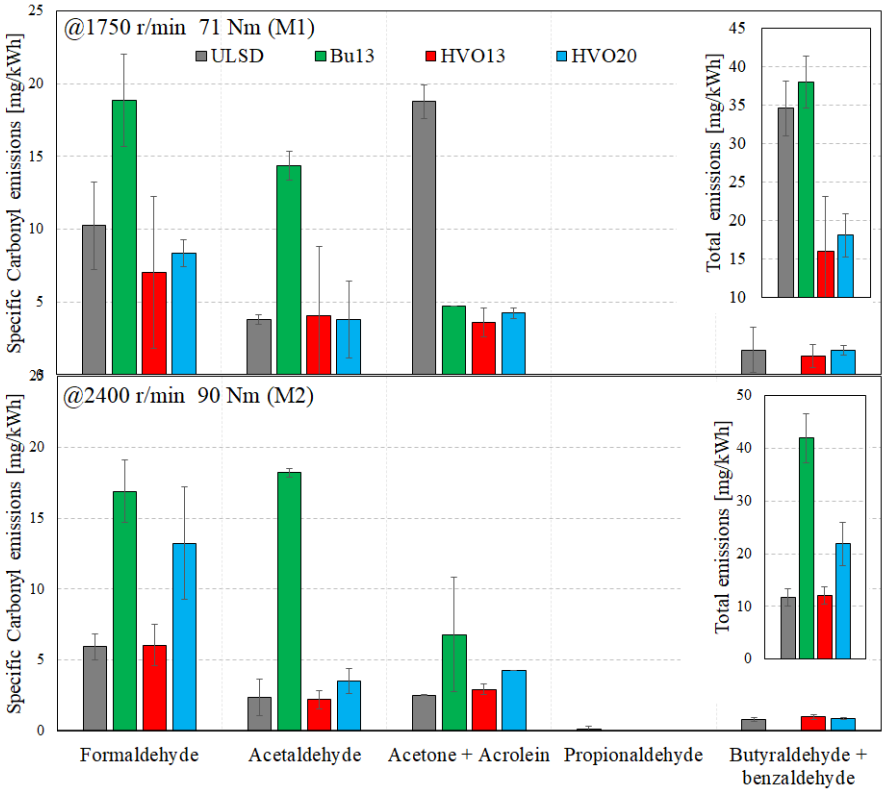

Figure 4.7: Specific carbonyl emissions

Carbonyl emissions were not significantly affected by the aromatic content of the fuel. Due to the higher level of aromatic compounds for ULSD, benzaldehyde and p-tolualdehyde emissions could be expected to be the highest for this fuel. However, p-tolualdehyde was no detected and benzaldehyde emissions were not significantly different from those of HVO blends. Similar conclusions were reached by Nelson et al. [50], who studied carbonyl emissions from twelve vehicles using a range of diesel fuel formulations and concluded that aldehydes such as formaldehyde and acetaldehyde were not affected by the aromatic content of the fuels. Carbonyls are largely formed in the combustion process from fuel fragments produced in the initial oxidative pyrolysis.

4.2.4 Ozone formation potential

In order to assess the contribution of the carbonyl emissions, the photochemical ozone production was calculated. **Figure** 4.8 shows the ozone equivalent production (designated with circles) for the fuel blends. Shaded bars in the background represent the contribution of each carbonyl to the total *OFP*. Results showed that there was no significant difference between ULSD and HVO13, although a slight decrease in M2 was exhibited by both fuels, and for the 20% HVO blend, a slight in-

crease was evident in comparison with 13% HVO. Bu13 exhibited the highest *OFP*, almost doubling the *OFP* of ULSD and HVO20. This is due to the emitted concentration of formaldehyde, acetaldehyde and acrolein, compounds with a high MIR. Formaldehyde was the major contributor to *OFP*, ranging from 50% to 65% among all carbonyl compounds. This is due to formaldehyde's high MIR value, and because it was the highest carbonyl emission among the 7 detected in exhaust samples.

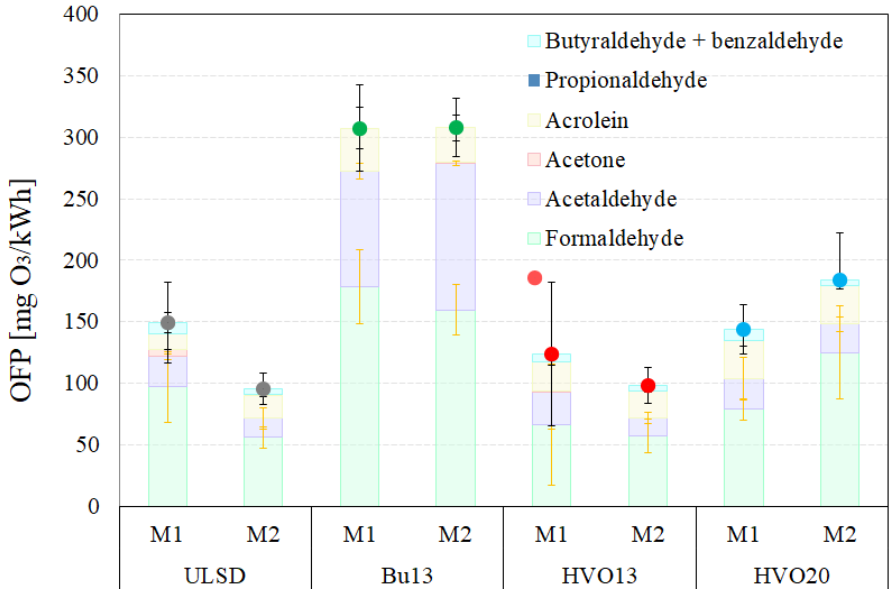

Figure 4.8: Ozone equivalent production (•) for the fuel blends

The *OFP* found in this work for ULSD was close to that reported by other researchers: Ballesteros et al. [51] reported 80 ± 5 mg O_3/kWh for diesel fuel supplied by Repsol, and 180 ± 70 mg O_3/kWh for a Spanish commercial diesel; Jhang et al. [52] reported an *OFP* increase from 30 mg O_3/kWh to 60 mg O_3/kWh, and 90 mg O_3/kWh as the load increases from 25% to 50% and 75% respectively. Those differences could be attributed to test conditions, engines technology, and variations in fuel composition, the latter being the most significant factor affecting the unregulated emissions. The *OFP* for butanol (16%) reported by Ballesteros et al. [53], was nearly six orders (6x) of magnitude lower than those found in this work, however, such difference can be because the authors reported the average *OFP* of three different operation modes (two urban and two extra-urban), although for the urban mode the emissions were high, the low emissions of the extra-urban mode offset the high ones. In addition to the reasons explained above (the type of engine and technology, etc.).

4.3 Unregulated emissions for Pentanol/diesel and fuel blends

4.3.1 Engine performance parameters

To evaluate the engine performance, BSFC and BTE were measured, and the results are shown in **Figure** 4.9a. At low load, BSFC increased slightly for all pentanol blends (8%) with respect to ULSD, due to the lower heating value of pentanol that resulted in an increased fuel mass needed to obtain the same power output. At high loads, BSFC showed no significant difference between fuels, implying that higher combustion temperatures and increased oxygen concentration in the fuel might lead to a better vaporization of fuel mixtures and faster evaporation rate [49], which improved the combustion speed.

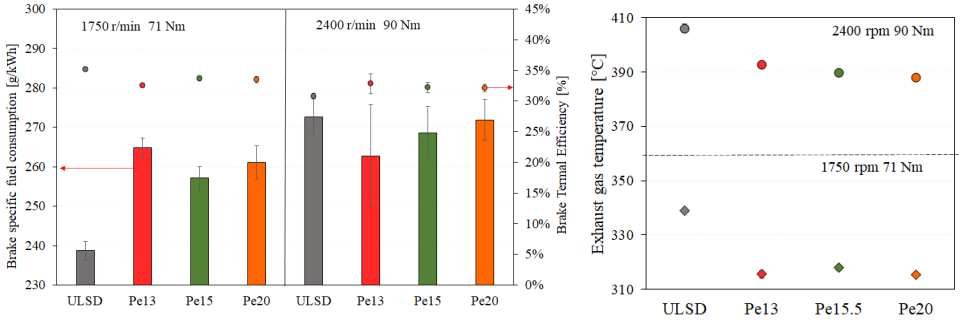

(a) Brake specific fuel consumption (bars-left axis) and brake thermal efficiency (points-right axis).

(b) Raw exhaust gas temperature .

Figure 4.9: Engine performance parameters

BTE for all fuels and engine loads were similar between 30% and 35%. The effect of the higher latent heat of evaporation of pentanol seemed to be compensated with the increased oxygen content and longer ignition delay associated with pentanol's lower cetane number, that both enhanced the combustion process and promoted the premixed burning phase [54]. The marginal differences between fuel blends in BSFC and BTE, indicated that pentanol blends up to 20% could keep combustion characteristics similar to ULSD fuel. Regulated emissions are shown in **Appendix** B.

4.3.2 Carbonyls

Figure 4.10 presents the specific and total carbonyl emissions for the pentanol/ULSD blends under the two load conditions tested. Due to the inability to identify the peaks separately for acetone and acrolein, butyraldehyde and benzaldehyde, they were quantified together.

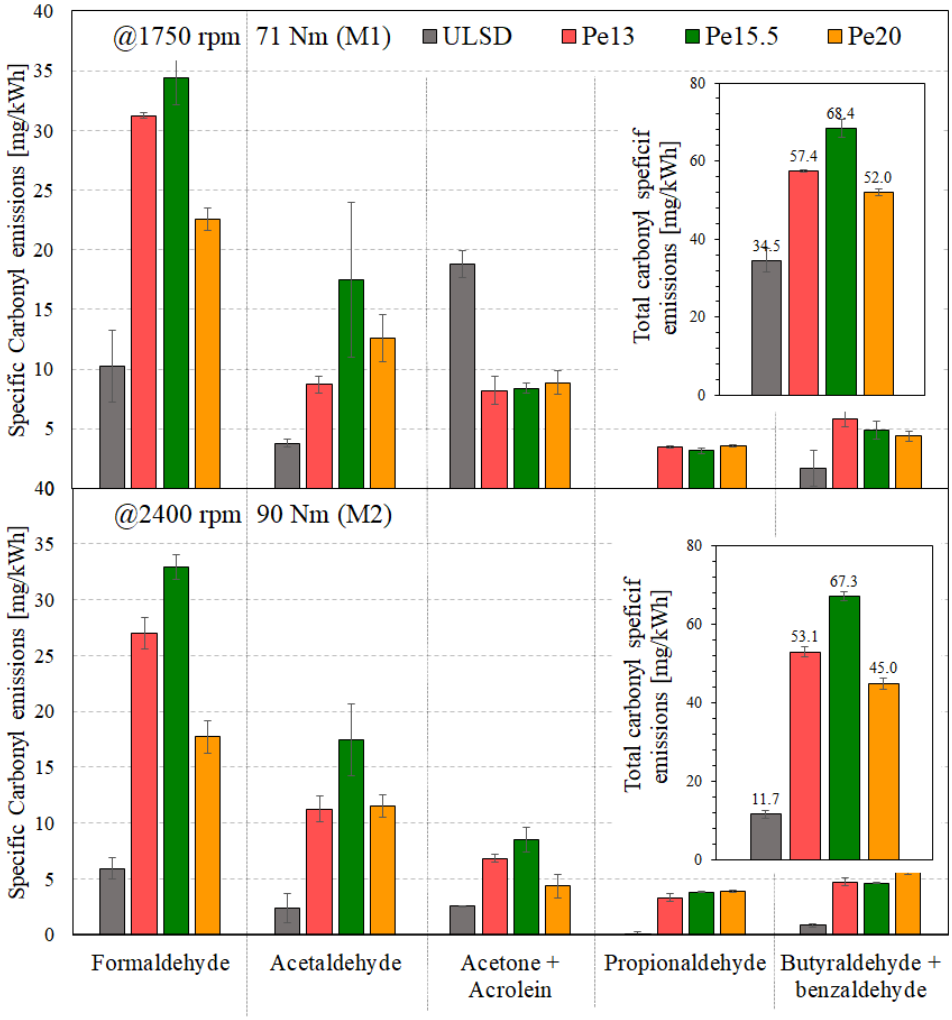

Figure 4.10: Specific carbonyl compounds emissions (mg/kWh) and total specific emissions (boxes on the right) for ULSD and the tested pentanol/diesel blends. Error bars correspond to standard deviation

At both engine loads carbonyl emissions were higher for the pentanol blends compared to ULSD. The incomplete combustion of alcohol fuels led to the formation of oxygenated hydrocarbons such as carbonyl compounds [55]. The hydroxyl group of pentanol might have an influence on the carbonyl's formation. Alkyl alcohols (R - O - H) can decompose by unimolecular dissociation via complex fission (multiple bonds break and form) or by simple fission (one bond breaks), the latter predominantly occurs at the C–C bonds and produces alkyl and hydroxyalkyl radicals that subsequently dissociate by β scission to alkenes and aldehydes, and ketones (carbonyl groups) [56]. In addition, the higher latent heat of vaporization of n-pentanol

can generate: a) a cooling effect due to the evaporation of pentanol [57], that caused a lower combustion temperature compared to ULSD, as can be inferred from the exhaust gas temperature in **Figure** 4.9b, and b) a longer ignition delay that increased the probability of deposition of unburned fuel on the walls of the combustion chamber [49].

Pe20 decreased the total emission of carbonyls compared with Pe13, may be due to the presence of additional oxygen, which improved combustion by diluting the mixture and removing fuel-rich zones in the cylinder. In addition, the lower viscosity of Pe20, compared to the other tested fuels, could favor the atomization and evaporation process of the fuel, for a better homogenization of the mixture [49].

Total carbonyl emissions decreased slightly with increasing load for all fuels, which agrees with results for blends with other oxygenated fuels [58, 59]. This has been attributed to increases in combustion temperature at such loads leading to a more complete oxidation of carbonyls. This trend was evident for ULSD, particularly for the emission of formaldehyde, acetone and acrolein, the lighter carbonyl products from incomplete oxidation of light hydrocarbons.

Formaldehyde showed the highest emission among the measured carbonyls for all pentanol blends at both engine loads. The relative weakness of the αC-H bonds in an alcohol molecule enhanced the reaction of pentanol with O_2 leading the formation of formaldehyde and HO_2 [55]. In addition, light hydrocarbons during combustion generate intermediate products such as formaldehyde rather than more fully oxidized species, especially in localized fuel-rich regions [58]. Valeraldehyde would be directly produced following H-atom abstraction at the αC site of pentanol; however, this species was not observed in the current measurements, perhaps due to its high reactivity and that through H-atom abstraction at the β site it can produce an alkene [55].

Table 4.2: Reported carbonyl emissions with alcohol/diesel blends

Ref	Engine	After-treatment	Fuel	SE*	Trend
Section 4.3.2	Four-cylinder, turbocharged and	DOC	Pentanol/ diesel	11-68 mg/kWh	↑
Section 4.2.3	intercooled Cummins ISF 2.8 L	DOC	Butanol/ diesel	35-43 mg/kWh	↑
[60] Tang et al. (2007)	Six cylinder Int.-Navistar DT466	DOC	Ethanol/ diesel	26–80 mg/kWh	↑
[61] Pang et al. (2008)	Four cylinders, DI Commins-4B	N.A.	Ethanol/ biodiesel/ diesel	≈300-300 mg/kWh	↑
[59] Song et al. (2010)	Heavy-duty diesel Engine	N.A.	Ethanol/ diesel	20-380 mg/kWh	↑
[24] Yang et al. (2015)	Single cylinder diesel engine	N.A.	Butanol/ biodiesel/ diesel	40-250 mg/kWh	↓
[58] Fan et al. (2018)	Four cylinders DI turbo-charged NRM diesel engine	None	Methanol/ diesel	222-322 mg/kWh	↑

SE:Total specific emission ranges for alcohol/diesel blends.
N.A.:Not available
↑: increased, ↓: decreased.

Total carbonyl concentrations in the exhaust from methanol, ethanol and butanol blends with diesel, and ternary diesel/biodiesel/alcohol blends were in the range of 20-380 mg/kWh (see **Table** 4.2). In this research the total specific emissions fell in the range of 11-68 mg/kWh. The specific emissions obtained in this work were higher than those obtained in a previous study with 13% of butanol blended with diesel under the same operating conditions [17]. These results suggest that pentanol increased carbonyl emissions compared to butanol.

4.3.3 Ozone formation potential

The estimated *OFP* for each fuel blend, and the contribution of each carbonyl, are presented in **Figure** 4.11. The *OFP* increased with the pentanol concentration because of the increase in the emission of carbonyl compounds with high MIR: formaldehyde, acetaldehyde, and propionaldehyde. At low load, with respect to ULSD, Pe13 and Pe20 increased OFP around 40%, and Pe15 doubled it (2x). At high load, the increase exceeded 100% and reached 430% for Pe15. ULSD and Pe20 decreased the *OFP* at high load, this was due the decrease in the emission of acetone and acrolein.

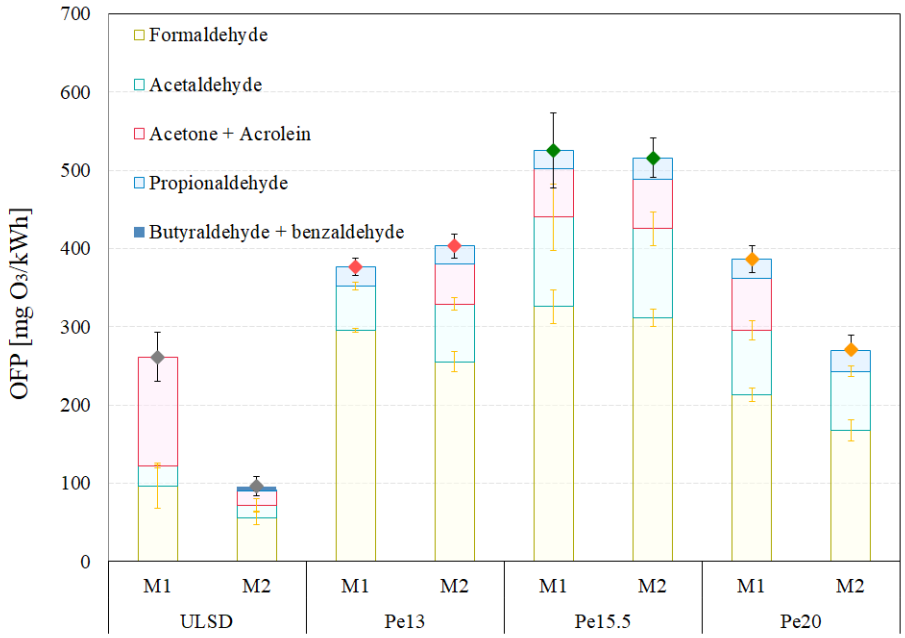

Figure 4.11: Ozone formation potential (rhombuses) and the contribution of each carbonyl compound (shaded bars) (M1= 1750 r/min @ 71 Nm; M2= 2400 r/min @ 90 Nm). Error bars correspond to standard deviation

.

Researchers have reported lower *OFP* for short chain alcohols, butanol, and biodiesel compared to those found in this work for pentanol blends. Ballesteros et al. [53] reported the carbonyl emissions and their derived *OFP* from an automotive diesel engine fueled with ULSD and its blends with ethanol (10%) and butanol (16%). They showed an *OFP* of 30 mg O_3/kWh for diesel and 45 mg O_3/kWh for ethanol and butanol blends. In their work, for ULSD and butanol blend, the most abundant carbonyl was formaldehyde with approximately 5 mg/kWh and 7 mg/kWh respectively (results after DOC). For ethanol blend, the highest emission was acetone with approximately 25 mg/kWh followed by formaldehyde with around 5 mg/kWh. In this study, acetaldehyde emissions, added to the high emission of acetone and acrolein, and the high MIR of acrolein as opposed to the low MIR of acetone, caused the differences in the *OFP* with regard to that reported by Ballesteros et al. [53]. In a subsequent study, Ballesteros et al.[51] reported the *OFP* for animal fat biodiesel (50% by volume) of 80 mg O_3/kWh and 150 mg O_3/kWh for ULSD. For both fuels, the most abundant compounds were acetone (16 and 5 mg/kWh), acetaldehyde (7.5 and 4 mg/kWh) and formaldehyde (3 and 2.5 mg/kWh). Although the total carbonyl emissions were dominated by acetone, this did not significantly affect the *OFP*. It is worth noting that *OFP* is not affected as much by the total emission of carbonyls as it is by the type of carbonyls and their respective MIR. Jhang et al. [52] measured the

carbonyl compounds in a diesel engine (Cummins B5.9-160) and they reported that the *OFP* for diesel fuel decreased from 90 mg O_3/kWh to 30 mg O_3/kWh with an increase in engine load from 25% to 75%. *OFP* is also affected by operating mode, engine technology, and fuel properties.

4.4 Biological activity

The biological response of SOF and WSF extracted from PM from Bu13, HVO13 and HVO20 was investigated. Cytotoxicity, genotoxicity, oxidative DNA damage, ecotoxicity and PAH equivalence toxicity are presented in this section. Details of the methodology are presented **section** 3.3.5. Briefly, The Hepatocarcinoma epithelial cell line (HepG2) was exposed to SOF for 24 h and analyzed using comet assay, with the inclusion of formamidopyrimidine DNA glycosylase (FPG) and endonuclease III (Endo III) to recognize oxidized DNA bases. The WSF was evaluated through acute ecotoxicity tests with the aquatic microcrustacean Daphnia pulex (*D. Pulex*).

4.4.1 Cytotoxicity and genotoxic activity

Results showed that there was no cytotoxic activity for all tested SOF concentrations, for this, Probit analysis for the 20 concentrations were used. Based on this, we decided to use three concentrations for genotoxic analyzes from a stock concentration of 2.94 μgEq.

Genotoxicity was evaluated through the alkaline comet assay and enzyme-modified comet assay for determination of oxidative damage. **Figure** 4.12 and **Figure** 4.13 show the results of the assay with and without FPG and Endo III enzymes, respectively. The significant differences of the reference material with respect to the negative control exhibited the sensitivity and specificity of our experimental conditions. The result of the comet assay (without FPG and Endo III enzymes) showed that for most fuels, only the 2.94 μgEq concentration produced direct genotoxic damage to the DNA strand. However, for HVO blends, the comet length increased with its concentration in the blend; and without FPG enzyme (**Figure** 4.12b), HVO20 fuel also caused cell fragmentation at the intermediate concentration (1.47 μgEq). With and without enzymes, DNA migration had no significant difference between fuels and negative control at the lowest PM concentration (0.735 μgEq). When considering the emission rate per kWh (**Figure** 4.14), the differences between the fuels are observed only at high doses, with a larger DNA fragmentation on the cells caused by HVO20 and followed by Bu13 and ULSD.

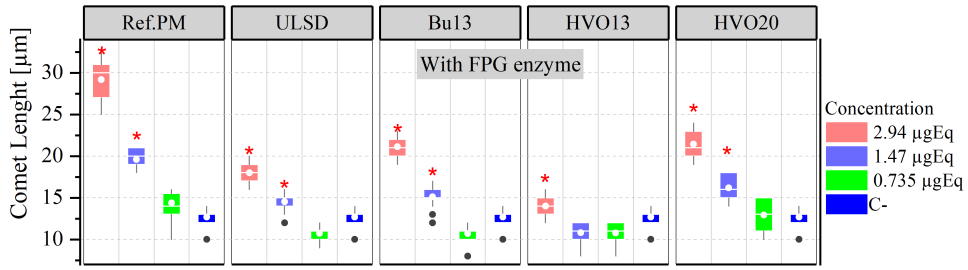

(a) Comet length in HepG2 cells in presence of FPG enzyme.

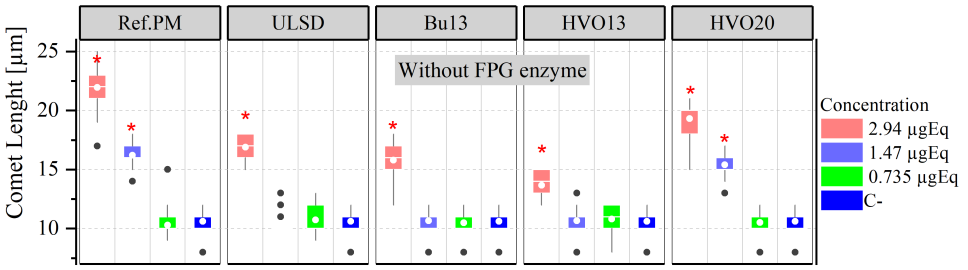

(b) Comet length in HepG2 cells in absence of FPG enzyme.

Figure 4.12: Comet length in HepG2 cells exposed to different fuels for 24 hours through the alkaline comet assay in the presence or absence of FPG enzyme. For all the experiments carried out in the presence and absence of the FPG enzyme, $KBrO_3$ (1.25mM) was used as a positive control, obtaining a median for the comet length of 26 (22, 29) μm without the enzyme and 51 (47, 55) μm with the enzyme FPG. Red asterisk ($*$): p<0.0001 compared to the negative control. ($\bullet$) correspond to atypical data

Similar results were found by Mendoza et al. [62], who reported an increase in the genotoxic activity by increasing the HVO concentration in the blend. They performed the comet assay on human lymphocyte cells exposed to PM gathered from a high emitter diesel engine in concentrations of 3.1, 6.2, and 12.5 μgEq. This might explain why in our work, significant damage was only observed at the highest concentration of 2.94 μgEq.

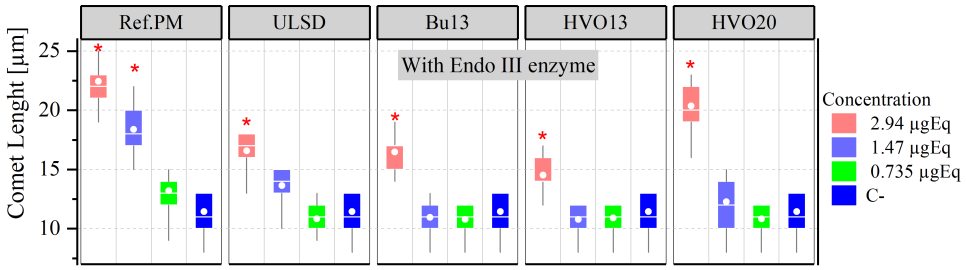

(a) Comet length in HepG2 cells in presence of Endo III enzyme.

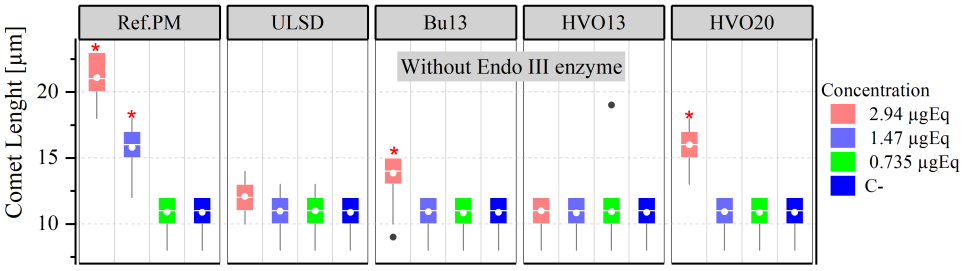

(b) Comet length in HepG2 cells in absence of Endo III enzyme.

Figure 4.13: Comet length in HepG2 cells exposed to different fuels for 24 hours through the alkaline comet assay in the presence or absence of Endo III enzyme. For all the experiments carried out in the presence and absence of the Endo III enzyme, H_2O_2 (100 μM) was used as a positive control, obtaining a median for the comet length of 35 (32,39) μm without the enzyme and 56 (53,59) μm with the enzyme Endo III. Red asterisk ($*$): p<0.0001 compared to the negative control. ($\bullet$) correspond to atypical data

Few studies have compared the genotoxic activity of the SOF from diesel/ HVO derived PM. In agreement with our results, Westphal et al.[63] and Jalava et al. [64] observed dose-dependent DNA strand breaks and toxicity of the extracts, but they did not report differences between diesel and HVO. Both studies used the comet assay to study the genotoxicity of emissions from diesel fuel, rapeseed methyl ester, and HVO in A549 lung cells and in a mouse macrophage cell line, respectively. In another study, Soriano et al. [65] reported genotoxic activity of SOF from Gas to Liquid fuel (a paraffinic hydrocarbon similar to HVO), and diesel fuel. However, they did not find significant differences between fuels. They evaluated DNA migration or genotoxicity at three PM concentrations using an alkaline comet assay in human lymphocytes. Although the impact of fuel composition might be relevant, other parameters such as engine technology, engine test modes, and other engine testing conditions should be considered. For example, Hemmingsen et al.[66] compared DNA damage of PM-SOF from two diesel engines complying with Euro 2 and Euro 4 emission standards using biodiesel blends and diesel fuel, and they found that the type of engine had

stronger effect than the fuel on the DNA damage.

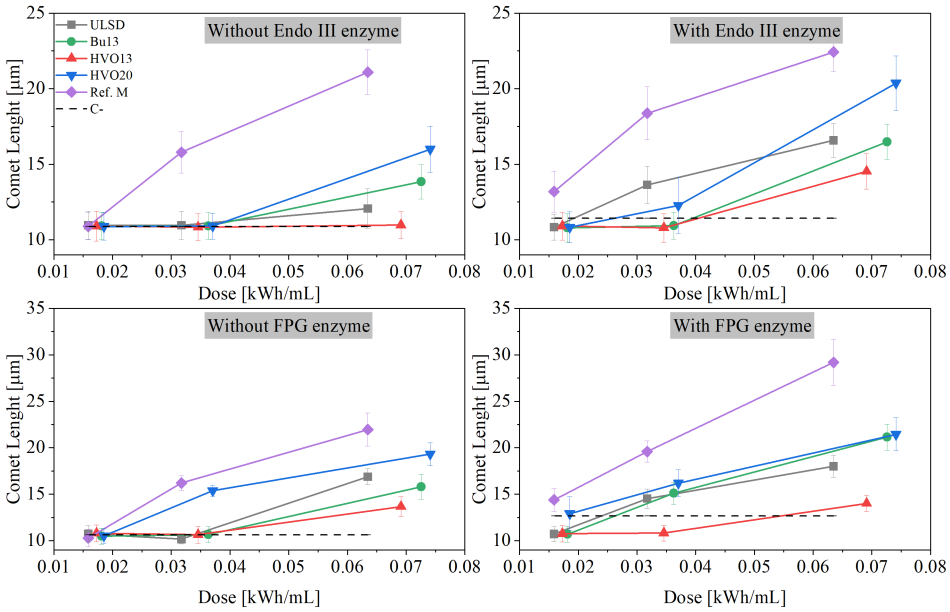

Figure 4.14: Fragmentation of DNA represented by comet tail length (um) at different sample doses. Dose as kWh per ml of culture medium (genotoxicity emission). The symbols correspond to the median comet length and the error bars to the standard deviation

There is a growing consensus that DNA damage involves oxidative damage caused by the ROS. The increase of ROS is one of the main known pathways of PM toxicity. One of the most common oxidation products of the DNA is 8-oxo-7,8-dihydroguanine (8-oxodG). Oxidatively damaged DNA bases, such as 8-oxodG, are repaired preferentially by the base excision repair pathway. While oxidative stress increases the levels of all types of oxidatively modified DNA bases, the accumulation of 8-oxodG in the DNA has been specifically linked to various inflammatory disease processes [67]. The modified comet assay using repair enzymes FPG, and Endo III is widely used for the assessment of oxidative DNA damage. The FPG is specific for 8-oxodG, and other ring-opened purines, and the Endo III, for the thymine glycol and the uracil glycol [68].

The addition of the FPG and Endo III enzymes resulted in a significant increase in the comet tail (p value <0.0001) with respect to the tests in the absence of them. With the addition of the enzyme FPG **Figure** 4.12a), the length of the comet increased around 42% for ULSD and Bu13 at the intermediate concentration, and around 34% for Bu13 at the highest exposure concentration after 24 hours. Regarding the oxidative damage that SOF could produce in the pyrimidine bases after incubation with the

enzyme Endo III, the results obtained also showed an increase in DNA damage after 24 h of exposure with respect to the negative control, and the length of the comet increased for all fuels, mainly for ULSD and HVO blends, which increased above 26%. These results indicate that the DNA damage from SOF of the tested fuels involved oxidative damage including oxidized purines and pyrimidines. The FPG and Endo III treatment showed a higher level of oxidized purines for ULSD and Bu13, and a slightly higher oxidized pyrimidines for HVO blends compared to Bu13. In addition to oxidation, DNA damage by alkylation should also be considered, because it is well documented that the FPG and Endo III restriction enzymes also detects some types of alkylation damage [68, 69].

The purine and pyrimidine serve as a form of energy for cells, and are essential for production of DNA and RNA, proteins, starch, regulations of enzymes, cell signaling bases. Therefore, alterations in their synthesis, catabolism, and concentrations may lead to significant functional consequences [32]. Oxidized purine and pyrimidine are part of tandem base lesions [33], and as a consequence, they could generate the same damage, regardless of the oxidized base (puric or pyrimidine). One possible damage could be nucleotide misincorporation during DNA replication (mismatches in DNA bases).

The results indicated that the ROS played an important role in the genotoxic effects of SOF from HVO and Bu13-derived PM. The ROS could be induced by different mechanisms, i.e., through transition metals contained in the particles, which were measured in this thesis, but they were under the detection limits of our method; through processes that metabolize xenobiotics in PM [70], and through some xenobiotics, such as PAH, which are contained in the SOF from the tested fuels [17]. However, there are other mechanisms that might be also involved in oxidative damage. For example, Tokiwa et al. [71] suggested that the oxidative damage could be also induced by carbonaceous particles instead of mutagenic and carcinogenic substances. They used a test *in vivo* doing intratracheal injections of the carbonaceous part of diesel particles in mice, and this resulted in an increase in 8-oxodG adduct levels in the lung tissue, but it was not increased when PAH such as benzo[a]pyrene, 1,8-dinitropyrene, and 1-nitropyrene were used.

Regarding the percentage of damaged cells (**Table** 4.3), all samples showed fragmentation. However, the magnitude of this damage was different among them, and was classified into two categories: a) no damage, and b) low damage. No concentration-response relationship was found in the percentage of cell damage in the absence of FPG and Endo III enzymes. Almost 100% of the cells showed low damage at the highest PM concentration for all fuels without FPG enzyme, and only for HVO20, 98% of the cells showed a low damage at 2.94 μgEq without the Endo III enzyme.

From these results, it was possible to conclude that part of the DNA breaks was

induced due to oxidative damage to the nitrogenous bases (puric or pyrimidine) that are part of the DNA, caused by SOF from ULSD and its blends with the renewable fuels tested. With the addition of the enzymes a concentration-response effect was observed for ULSD and HVO20. The oxidative damaged increased with the concentration of HVO in the fuel blend.

Table 4.3: Percentage of damaged cells in the HepG2 cell line, exposed to different fuels for 24 hours through the alkaline comet assay in the presence or absence of FPG and Endo III enzymes

		FPG				**Endo III**			
Extract	**Conc.**	**Absence**		**Presence**		**Absence**		**Presence**	
	(μgEq)	**No**	**Low**	**No**	**Low**	**No**	**Low**	**No**	**Low**
		Damage (%)							
Ref. PM	0	100	0	100	0	100	0	100	0
	0.735	99.6	0.4	51	49	100	0	80	20
	1.47	0	100	0	100	0	100	0	100
	2.94	0	100	0	100	0	100	0	100
ULSD	0	100	0	100	0	100	0	100	0
	0.735	99.6	0.4	100	0	100	0	100	0
	1.47	99.6	0.4	44	56	100	0	66	34
	2.94	0	100	0	100	83	17	1	99
Bu13	0	100	0	100	0	100	0	100	0
	0.735	100	0	100	0	100	0	100	0
	1.47	100	0	24	76	100	0	100	0
	2.94	7.3	92.7	0	100	34	66	1	99
HVO13	0	100	0	100	0	100	0	100	0
	0.735	100	0	100	0	100	0	100	0
	1.47	99.3	0.7	100	0	100	0	100	0
	2.94	17	83	66	34	100	0	50	50
HVO20	0	100	0	100	0	100	0	100	0
	0.735	100	0	73	27	100	0	100	0
	1.47	0	100	16	84	100	0	87	13
	2.94	0	100	0	100	2	98	0	100

Figure 4.15 shows the induction frequency (IF) with absence and presence of the enzyme FPG (**Figure** 4.15a), and Endo III (**Figure** 4.15b). The IF, which indicates how many times the treatment exceeded the negative control, was higher for the FPG compared to Endo III. The DNA damage occurred at 1.47 μgEq and in the presence of the enzymes, while no damage occurred in the absence of enzymes, except for HVO20 with FPG.

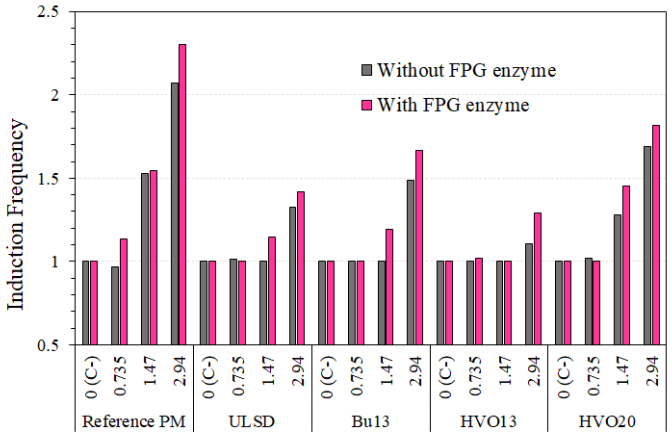

(a) Induction frequency in the presence or absence of FPG .

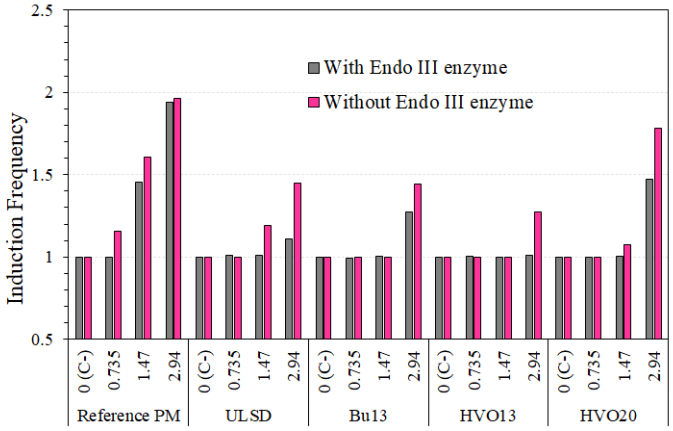

(b) Induction frequency in the presence or absence of Endo III.

Figure 4.15: Induction frequency in HepG2 cells exposed to different fuels for 24 hours through alkaline comet assay. For all the experiments carried out in the presence and absence of the FPG enzyme, $KBrO_3$ (1.25mM) was used as a positive control obtaining an IF of 2.42 without the enzyme and 4.7 with the FPG enzyme. For all the experiments carried out in the presence and absence of the Endo III enzyme, H_2O_2 (100 μM) was used as a positive control obtaining an IF of 3.3 without the enzyme and 5.2 with the Endo III enzyme

These results advised that the DNA damage was induced, by one side due to the direct effects of the SOF, and on the other hand, due to indirect effects such as the oxidative damage (apurinic > pyrimidine). It was notable that even though Bu13, HVO13 and HVO20 fuel blends possess lower aromatic content than neat diesel fuel, they did not exhibit significant genotoxic response differences compared to the ULSD, however, the HVO blends generated a higher DNA damage than ULSD.

4.4.2 Acute ecotoxicity tests with *D. Pulex*

Table 4.4 shows the results regarding the dead or immobile *D. Pulex* neonates specimens exposed.

Table 4.4: Immobility or mortality of neonates of *D. pulex* exposed to different dilutions of the sample during 48 hours of the sample

Fuel	**Sample fraction (%)**	**N° immobile or dead specimens**	**LC_{50} result (%)**
ULSD	6.25	2	Not calculable
	12.5	1	
	25	1	
	50	3	
	100	3	
	(+)	11	N.A.
	(-)	2	N.A.
Bu13	6.25	2	No calculable
	12.5	0	
	25	4	
	50	1	
	100	3	
	(+)	9	N.A.
	(-)	0	N.A.
HVO13	6.25	0	Not calculable
	12.5	0	
	25	0	
	50	2	
	100	1	
	(+)	12	N.A.
	(-)	0	N.A.
HVO20	6.25	1	Not calculable
	12.5	2	
	25	3	
	50	1	
	100	2	
	(+)	10	N.A.
	(-)	1	N.A.

N.A.:Not applicable

Ecotoxicity results are expressed by the LC_{50} value that was the calculated effective concentration that causes 50% of ecological effect (mortality or immobility). For none of the fuel PM samples it was possible to calculate LC_{50}. In all the dilutions and for all the extracts, the number of dead or immobile neonates was significantly lower than the positive control. These results indicated that the WSF of the PM at the prepared concentrations did not imply acute toxicity to these organisms.

Figure 4.16 shows the percentage of mortality for each sample dilution, which allows establishing a concentration-response relationship. For all PM fuel samples tested, the mortality was not significantly different from the negative control; therefore, it was not possible to determine the acute ecotoxicological effects. Our results indicated that the chronic effects of PM samples were highly significant and fuel dependent (genotoxic assessment above), which are commonly related to some specific PM components, such as PAH and their nitro and oxy derivatives. However, the cytotoxicity and ecotoxicity, which are related to the acute effects of the PM samples, were not significant in this work [72, 73].

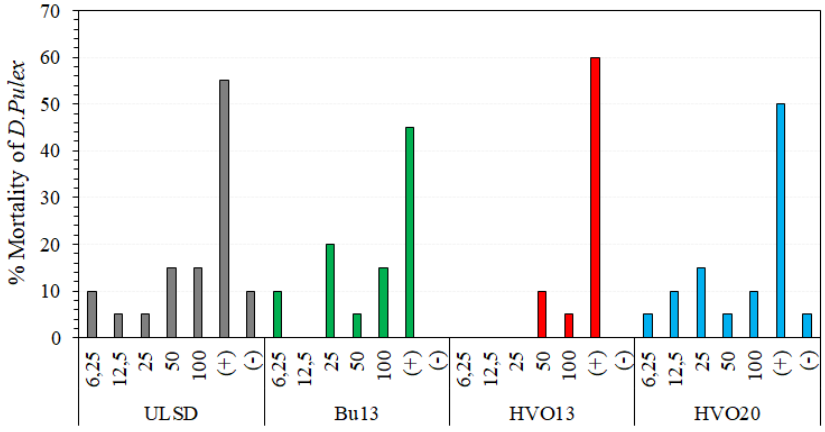

Figure 4.16: Mortality of D.Pulex neonates in 48 h for PM extracts

Few published studies have investigated the role of WSF on PM ecotoxicity, and they have focused from the environment PM. The ecological effects of PM-WSF from the combustion of bio-based fuels have been less studied. In our previous study [74], the WSF of PM from ULSD blended with palm biodiesel (10%, 20% blends and 100%) caused an increase in the death of exposed individuals which meant an increase in ecotoxicity. The WSF has also been used to investigate health effects using cell lines, for example, Zerboni et al. [75] evaluated the biological effects in human bronchial BEAS-2B cells exposed to 50 μg/mL of WSF- PM from Euro 3 and Euro 6 diesel vehicles using fossil diesel. They found inflammatory and pro-carcinogenic pathways induced by the older engine technology. It is worth noting that the concentration used for *in vitro* analysis was 5 times higher than that used in the present study. Regarding ambient PM, Tao et al. [76] and Xu et al. [77] evaluated adverse health effects with intratracheal instillation on mice using the WSF and SOF of diesel exhaust particles and they found the SOF contributed most to induced pulmonary inflammation and other adverse cellular effects. However, it is well known that ambient PM composition is markedly different from those of diesel exhaust particles.

4.4.3 PAH equivalence toxicity

Several studies have identified mutagenic and carcinogenic PAH compounds in diesel PM. However, since the toxic potency of the different PAH is not the same, the toxicity comparison is usually carried out by the BaP-TEQ. Although this index is widely used to assess the toxicity of several materials containing PAH, this might underestimate total toxicity since it does not consider the impact of other carcinogens and xenobiotics associated with PM. In addition, other carcinogenic PAH which are not included in the 16 prioritized by the U.S. EPA, would be present in the PM samples as shown in **section** 4.2.2.

Figure 4.17 shows the BaP-TEQ for the PM samples tested. The BaP-TEQ ranged from 2 μg BaP-TEQ/kWh to 8 μg BaP-TEQ/kWh. Bu13 exhibited the highest BaP TEQ value, while HVO blends were not significantly different from ULSD. Although Bu13, HVO13 and HVO20 PM samples decreased the percentage of aromatics in the parent fuel blend from 31.5% (ULSD) to 27.4% (Bu13, HVO13) and 25.2% (HVO20), this did not imply a lower BaP TEQ. This might be due to the formation of PAH in the combustion process, and to the emission of compounds with high TEF, mainly Bu13. Although butanol is an aromatic-free fuel, PAH could be produced in the combustion process as discussed above. In a recent study, Khan et al. [78] investigated the effect of alcohol size and hydroxyl group position on the growth of PAH from the pyrolysis of ethanol, 1-propanol, 2-propanol,1-butanol, and 2-butanol in a laminar flow reactor. They observed that increasing the alcohol carbon number increased the concentration of PAH. The pyrolysis of C3 and C4 alcohol fuels produced considerably higher concentrations of three ring PAH which played an important role in the growth of 4 to 6 rings PAH. Jin et al. [79] studied the formation of PAH with butanol in laminar co-flow non-premixed flames. They found that the presence of allene and propyne precursors promoted the formation of benzene, and consequently the PAH formation through the additions of C2 and C3 species to benzyl or phenyl radicals. Similar results were reported by Tran et al.[80], who investigated the impact of n-butanol addition into n-butane on PAH formation. They reported that n-butanol reactions released C3 and C4 intermediate species promoting the formation of benzene.

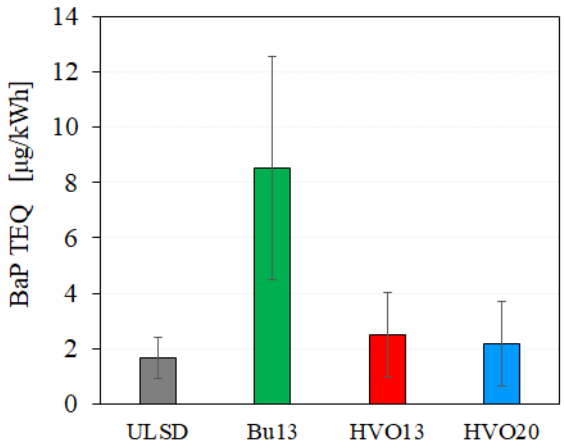

Figure 4.17: The total toxic equivalent concentrations of PAH in SOF from PM of the tested fuels. Error bars correspond to the standard deviation

Since the BaP-TEQ results did not correlate with the genotoxicity and oxidative DNA damage, it means that the biological response could be generated also by other PM toxic compounds which were not included in the BaP-TEQ index. Due to the large PM specific surface, various organic substances different to PAH such as some metals, nitro and oxy-PAH [81, 82] can be adsorbed. Numerous studies linking ROS production and PAH metabolism had been reported, however, they often lead to conflicting conclusions [70].

In summary, results showed that there was no cytotoxic activity for all tested SOF concentrations. Genotoxic responses by all the SOF samples were at same level, except for the HVO13 which was weaker in the absence of the enzymes. The addition of the FPG and Endo III enzymes resulted in a significant increase in the comet tail, indicating that the DNA damage from SOF for all tested fuel blends involved oxidative damage including a higher level of oxidized purines for ULSD and Bu13 in comparison with HVO blends, but the oxidized pyrimidines for HVO blends were slightly higher compared to Bu13. The WSF did not show acute ecotoxicity for any of the fuels. Unlike other samples, Bu13-derived particles significantly increased the BaP-TEQ. The contribution to the genotoxic activity and oxidative DNA from SOF was not correlated to BaP-TEQ, which means that the biological activity of PM might be affected also by other toxic compounds not measured here, present in particulate phase.

4.4.4 Inhalation cancer risk from aldehydes

The concentrations in mg/m^3 of formaldehyde and acetaldehyde for each fuel are shown in **Figure** 4.18 (left axis). Formaldehyde was the predominant compound and also the one with the highest toxic potential by inhalation. As shown in **Figure** 4.18

(right axis), the CR resulting from 2-h daily exposure to formaldehyde and acetaldehyde from exhaust emissions of the tested fuels in the most critical case (dilution factor of 20), ranged from 0.97×10^{-8} for ULSD to 5.7×10^{-8} for Pe15.5, they were all below the threshold of 10^{-6} (1 in 1 million chance of the occurrence of additional human cancer over a 70-year lifetime) suggested by the U.S EPA for carcinogenic chemicals. Pentanol blends exhibited the highest CR with respect to ULSD, due to the higher formaldehyde emissions. However, by applying U.S EPA criteria, the CR from the inhalation of these two aldehydes was considerably low: approximately 1 in 100 million people could eventually develop cancer related to inhalation exposure to formaldehyde and acetaldehyde over 30 years on a 2-hours morning work route. Notice that the above results for the CR were only considering two aldehydes. To obtain the representative cancer risk assessment, the greatest possible quantity of VOCs and semi-VOCs with a high potential for affecting health should be measured.

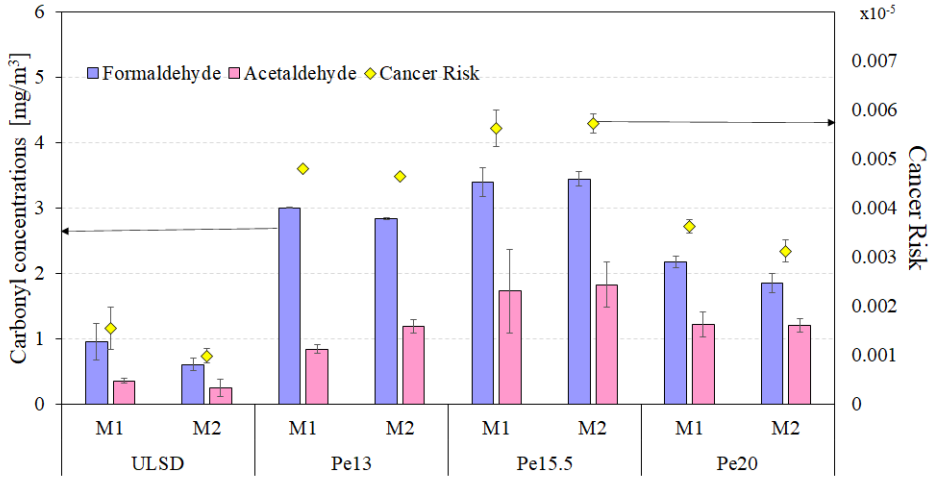

Figure 4.18: Concentrations of formaldehyde and acetaldehyde in mg/m^3 (bars - left axis) and cancer risk from 2-h daily exposure to formaldehyde and acetaldehyde emissions (diamonds- right axis). Error bars correspond to standard deviation

4.5 Conclusions

From the results presented in this chapter and under the test conditions and engine configuration used in this experimental research, the following conclusions can be drawn:

Regarding unregulated emissions

- Independently of engine load and fuel tested, most of the PAH were present in the gas-phase, with predominance of those between 3 and 4 rings. However,

DB[a,l]P and B[a]P, were predominant in the particle phase, instead of gas phase. A leakage assessment is mandatory to study unregulated gaseous PAH and carbonyl compounds.

- Total PAH emissions, including the Dibenzo[a,l]pyrene, increased with the use of n-butanol and HVO blended with ULSD. This suggested that although both, renewable diesel and butanol, are aromatic-free biofuels, the in-cylinder combustion process, and the pyrolysis and pyrosynthesis reactions of lower molecular weight hydrocarbon compounds induced the formation of aromatic rings through condensation products.

- Carbonyl emissions for pentanol were the highest among all tested fuels followed by butanol blend. This was explained by the hydroxyl-group of the linear alcohol. As a consequence, pentanol fuel blends exhibited the highest ozone formation potential. The *OFP* of renewable diesel, ULSD and their blends was similar.

Regarding biological activity

- All PM samples exhibited genotoxic effects, however none of them showed cytotoxicity nor ecotoxicity effects.

- ULSD, Bu13, and HVO20-derived PM, showed the similar genotoxic response. However, the genotoxic response and oxidative damage of DNA increased with the concentration of HVO fuel in the blend.

- The SOF from all PM samples induced oxidative DNA damage which is at least partly responsible for the genotoxic activity with a higher level of oxidized purines for ULSD and Bu13, and slightly higher oxidized pyrimidines for HVO.

- The contribution to genotoxic activity and oxidative DNA damage of the SOF samples did not correlate with PAH equivalent toxicity.

- The lower aromatic content of the fuel did not imply a lower BaP-TEQ. Bu13 exhibited the highest BaP-TEQ value, while HVO blends were not significantly different from ULSD.

- The higher carbonyl emissions resulted in higher cancer risk for pentanol/diesel blends compared to ULSD. However, the CR for trespasser/ recreational receptor was below the threshold suggested by the U.S EPA for carcinogenic chemicals. Although the CR was estimated by considering the two most abundant aldehydes measured in this work, it might not reflect the CR of the full range

of all VOCs emitted by an engine.

- The set of tests carried out provides valuable information on the cellular impact of the emissions, but under very specific conditions of cell line, concentration exposures, etc. Therefore, it needs to be complemented with other types of tests, in other types of cells, and under different conditions.

Bibliography

[1] M. Lapuerta, R. García-Contreras, J. Campos-Fernández, and M.P. Dorado. Stability, lubricity, viscosity, and cold-flow properties of alcohol-diesel blends. *Energy and Fuels*, 24(8):4497–4502, 2010.

[2] A. Gómez, J.A. Soriano, and O. Armas. Evaluation of sooting tendency of different oxygenated and paraffinic fuels blended with diesel fuel. *Fuel*, 184:536–543, 2016.

[3] A.F. López, M. Cadrazco, A.F. Agudelo, L.A. Corredor, J.A. Vélez, and J.R. Agudelo. Impact of n-butanol and hydrous ethanol fumigation on the performance and pollutant emissions of an automotive diesel engine. *Fuel*, 153:483–491, 2015.

[4] M. Lapuerta, J. Rodríguez-Fernández, D. Fernández-Rodríguez, and R. Patiño-Camino. Cold flow and filterability properties of n-butanol and ethanol blends with diesel and biodiesel fuels. *Fuel*, 224:552–559, 2018.

[5] J. Liang, Q. Zhang, Z. Chen, and Z. Zheng. The effects of EGR rates and ternary blends of biodiesel/n-pentanol/diesel on the combustion and emission characteristics of a CRDI diesel engine. *Fuel*, 286, 2021.

[6] W. Zhao, J. Yan, S. Gao, T.H. Lee, and X. Li. The combustion and emission characteristics of a common-rail diesel engine fueled with diesel, propanol, and pentanol blends under low intake pressures. *Fuel*, 307, 2022.

[7] O. Armas, R. García-Contreras, Á. Ramos, and A.F. López. Impact of animal fat biodiesel, gtl, and hvo fuels on combustion, performance, and pollutant emissions of a light-duty diesel vehicle tested under the nedc. *Journal of Energy Engineering*, 141(2), 2015.

[8] K. Sugiyama, I. Goto, K. Kitano, K. Mogi, and M. Honkanen. Effects of hydrotreated vegetable oil (hvo) as renewable diesel fuel on combustion and exhaust emissions in diesel engine. *SAE International Journal of Fuels and Lubricants*, 5(1):205–217, 2012.

[9] M. Kousoulidou, A. Dimaratos, A. Karvountzis-Kontakiotis, and Z. Samaras. Combustion and emissions of a common-rail diesel engine fueled with hwco. *Journal of Energy Engineering*, 140(3), 2014.

[10] D. Singh, K.A. Subramanian, and M.O. Garg. Comprehensive review of combustion, performance and emissions characteristics of a compression ignition engine fueled with hydroprocessed renewable diesel. *Renewable and Sustainable Energy Reviews*, 81:2947–2954, 2018.

[11] M.A. Danzon, F.X.R. Van Leeuwen, and M. Krzyzanowski. Air quality guidelines: For europe. *World Health Organization Regional Publications - European Series*, (91):vii–x+1–273, 2001.

[12] C.-E. Boström, P. Gerde, A. Hanberg, B. Jernström, C. Johansson, T. Kyrklund, A. Rannug, M. Törnqvist, K. Victorin, and R. Westerholm. Cancer risk assessment, indicators, and guidelines for polycyclic aromatic hydrocarbons in the ambient air. *Environmental Health Perspectives*, 110(SUPPL. 3):451–488, 2002.

[13] D. Dong, M. Shao, Y. Li, S. Lu, Y. Wang, Z. Ji, and D. Tang. Carbonyl emissions from heavy-duty diesel vehicle exhaust in china and the contribution to ozone formation potential. *Journal of Environmental Sciences (China)*, 26(1):122–128, 2014.

[14] R. van Zelm, M.A.J. Huijbregts, H.A. den Hollander, H.A. van Jaarsveld, F.J. Sauter, J. Struijs, H.J. van Wijnen, and D. van de Meent. European characterization factors for human health damage of pm10 and ozone in life cycle impact assessment. *Atmospheric Environment*, 42(3):441–453, 2008.

[15] B Halliwell. Free radicals, reactive oxygen species and human disease: a critical evaluation with special reference to atherosclerosis. *British journal of experimental pathology*, 70(6):737–757, dec 1989.

[16] S. Mbengue, L.Y. Alleman, and P. Flament. Bioaccessibility of trace elements in fine and ultrafine atmospheric particles in an industrial environment. *Environmental Geochemistry and Health*, 37(5):875–889, 2015.

[17] S. Arias, F. Molina, R. Palacio, D. López, and J.R. Agudelo. Assessment of carbonyl and pah emissions in an automotive diesel engine fueled with butanol and renewable diesel fuel blends. *Fuel*, 316, 2022.

[18] Silvana Arias, Verónica Estrada, Isabel C. Ortiz, Francisco J. Molina, and John R. Agudelo. Biological toxicity risk assessment of two potential neutral carbon diesel fuel substitutes. *Environmental Pollution*, 308(52):119677, 2022.

[19] Silvana Arias, Maria L. Botero, Francisco Molina, and John R. Agudelo. Pentanol/diesel fuel blends: Assessment of inhalation cancer risk and ozone formation potential from carbonyl emissions emitted by an automotive diesel engine. *Fuel*, 321(March):124054, 2022.

[20] Q. Cheng, H. Tuomo, O. Kaario, and L. Martti. Hvo, rme, and diesel fuel combustion in an optically accessible compression ignition engine. *Energy and Fuels*, 33(3):2489–2501, 2019.

[21] Pedro N. Benjumea Hernández. Andrés F. Agudelo Santamaría, John R. Agudelo Santamaría. *Diagnóstico de la combustión de biocombustibles en motores*. Universidad de Antioquia, universidad de antioquia edition, 2007.

[22] M. Badami, F. Millo, and D.D. D'Amato. Experimental investigation on soot and nox formation in a di common rail diesel engine with pilot injection. *SAE Technical Papers*, 2001.

[23] J. Jeon, Y.H. Park, S.I. Kwon, and S. Park. Effect of pilot injection timings on the combustion temperature distribution in a single-cylinder ci engine fueled with dme and ulsd. *Oil and Gas Science and Technology*, 71(1), 2016.

[24] P.-M. Yang, Y.-C. Lin, K.C. Lin, S.-R. Jhang, S.-C. Chen, C.-C. Wang, and Y.-C. Lin. Comparison of carbonyl compound emissions from a diesel engine generator fueled with blends of n-butanol, biodiesel and diesel. *Energy*, 90:266–273, 2015.

[25] E.L. Cavalieri, E.G. Rogan, S. Higginbotham, P. Cremonesi, and S. Salmasi. Tumor-initiating activity in mouse skin and carcinogenicity in rat mammary gland of dibenzo[a]pyrenes: the very potent environmental carcinogen dibenzo[a, l]pyrene. *Journal of Cancer Research and Clinical Oncology*, 115(1):67–72, 1989.

[26] M. Vojtisek-Lom, V. Beránek, P. Mikuška, K. Křůmal, P. Coufalík, J. Sikorová, and J. Topinka. Blends of butanol and hydrotreated vegetable oils as drop-in replacement for diesel engines: Effects on combustion and emissions. *Fuel*, 197:407–421, 2017.

[27] Y. Zhang, D. Lou, Z. Hu, and P. Tan. Particle number, size distribution, carbons, polycyclic aromatic hydrocarbons and inorganic ions of exhaust particles from a diesel bus fueled with biodiesel blends. *Journal of Cleaner Production*, 225:627–636, 2019.

[28] X. Li, Y. Zheng, C. Guan, C.S. Cheung, and Z. Huang. Effect of biodiesel on pah, opah, and npah emissions from a direct injection diesel engine. *Environmental Science and Pollution Research*, 25(34):34131–34138, 2018.

[29] C.V. de Souza and S.M. Corrêa. Polycyclic aromatic hydrocarbons in diesel emission, diesel fuel and lubricant oil. *Fuel*, 185:925–931, 2016.

[30] H.-H. Mi, W.-J. Lee, C.-B. Chen, H.-H. Yang, and S.-J. Wu. Effect of fuel aromatic content on pah emission from a heavy-duty diesel engine. *Chemosphere*, 41(11):1783–1790, 2000.

[31] A.R. Collier, M.M. Rhead, C.J. Trier, and M.A. Bell. Polycyclic aromatic compound profiles from a light-duty direct-injection diesel engine. *Fuel*, 74(3):362–367, 1995.

[32] A.L.C. Lima, J.W. Farrington, and C.M. Reddy. Combustion-derived polycyclic aromatic hydrocarbons in the environment - a review. *Environmental Forensics*, 6(2):109–131, 2005.

[33] K. Ravindra, R. Sokhi, and R. Van Grieken. Atmospheric polycyclic aromatic hydrocarbons: Source attribution, emission factors and regulation. *Atmospheric Environment*, 42(13):2895–2921, 2008.

[34] W.J. Shields, S. Ahn, J. Pietari, K. Robrock, and L. Royer. *Atmospheric Fate and Behavior of POPs*. 2013.

[35] E.L. Cavalieri, S. Higginbotham, N.V.S. Ramakrishna, P.D. Devanesan, R. Todorovic, E.G. Rogan, and S. Salmasi. Comparative dose-response tumorigenicity studies of dibenzo[a,l]pyrene versus 7, 12-dimethylbenz[a]anthracene, benzo[a and two dibenzo[a,l]pyrene dihydrodiols in mouse skin and rat mammary gland. *Carcinogenesis*, 12(10):1939–1944, 1991.

[36] J.M.S. Mattson and C. Depcik. First and second law heat release analysis in a single cylinder engine. *SAE International Journal of Engines*, 9(1):536–545, 2016.

[37] H. Aatola, M. Larmi, T. Sarjovaara, and S. Mikkonen. Hydrotreated vegetable oil (hvo) as a renewable diesel fuel: Trade-off between nox, particulate emission, and fuel consumption of a heavy duty engine. *SAE International Journal of Engines*, 1(1):1251–1262, 2009.

[38] T.E. Jensen and R.A. Hites. Aromatic diesel emissions as a function of engine conditions. *Analytical Chemistry*, 55(4):594–599, 1983.

[39] H.A. Dandajeh, M. Talibi, N. Ladommatos, and P. Hellier. Influence of combustion characteristics and fuel composition on exhaust pahs in a compression ignition engine. *Energies*, 12(13), 2019.

[40] H. Jin, A. Cuoci, A. Frassoldati, T. Faravelli, Y. Wang, Y. Li, and F. Qi. Experimental and kinetic modeling study of pah formation in methane coflow diffusion flames doped with n-butanol. *Combustion and Flame*, 161(3):657–670, 2014.

[41] J.A. Miller and C.F. Melius. Kinetic and thermodynamic issues in the formation of aromatic compounds in flames of aliphatic fuels. *Combustion and Flame*, 91(1):21–39, 1992.

[42] N. Yilmaz and S.M. Davis. Polycyclic aromatic hydrocarbon (pah) formation in a diesel engine fueled with diesel, biodiesel and biodiesel/n-butanol blends. *Fuel*, 181:729–740, 2016.

[43] Z.-H. Zhang and R. Balasubramanian. Influence of butanol addition to diesel-biodiesel blend on engine performance and particulate emissions of a stationary diesel engine. *Applied Energy*, 119:530–536, 2014.

[44] Michael Frenklach and Hai Wang. *Detailed mechanism and modeling of soot particle formation*. Number 59. 1994.

[45] M. Gowtham, C.G. Mohan, and R. Prakash. Effect of n-butanol fumigation on the regulated and unregulated emission characteristics of a diesel engine. *Fuel*, 242:84–95, 2019.

[46] B. Choi, X. Jiang, Y.K. Kim, G. Jung, C. Lee, I. Choi, and C.S. Song. Effect of diesel fuel blend with n-butanol on the emission of a turbocharged common rail direct injection diesel engine. *Applied Energy*, 146:20–28, 2015.

[47] K.H. Kim, B. Choi, S. Park, E. Kim, and D. Chiaramonti. Emission characteristics of compression ignition (ci) engine using diesel blended with hydrated butanol. *Fuel*, 257, 2019.

[48] S.M. Sarathy, P. Oßwald, N. Hansen, and K. Kohse-Höinghaus. Alcohol combustion chemistry. *Progress in Energy and Combustion Science*, 44:40–102, 2014.

[49] Arkadiusz Jamrozik, Wojciech Tutak, and Karol Grab-Rogaliński. Combustion stability, performance and emission characteristics of a ci engine fueled with diesel/n-butanol blends. *Energies*, 14(10), 2021.

[50] P.F. Nelson, A.R. Tibbett, and S.J. Day. Effects of vehicle type and fuel quality on real world toxic emissions from diesel vehicles. *Atmospheric Environment*, 42(21):5291–5303, 2008.

[51] R. Ballesteros, J. Guillén-Flores, and J.D. Martínez. Carbonyl emission and toxicity profile of diesel blends with an animal-fat biodiesel and a tire pyrolysis liquid fuel. *Chemosphere*, 96:155–166, 2014.

[52] S.-R. Jhang, K.-S. Chen, S.-L. Lin, Y.-C. Lin, K.T.T. Amesho, and C.-B. Chen. Evaluation of the reduction in carbonyl emissions and ozone formation potential from the exhaust of a heavy-duty diesel engine by hydrogen-diesel dual fuel combustion. *Applied Thermal Engineering*, 132:586–594, 2018.

[53] R. Ballesteros, J.J. Hernández, and J. Guillén-Flores. Carbonyls speciation in a typical european automotive diesel engine using bioethanol/butanol-diesel blends. *Fuel*, 95:136–145, 2012.

[54] B. Choi and X. Jiang. Individual hydrocarbons and particulate matter emission from a turbocharged crdi diesel engine fueled with n-butanol/diesel blends. *Fuel*, 154:188–195, 2015.

[55] T.S. Norton and F.L. Dryer. The flow reactor oxidation of c1-c4 alcohols and mtbe. *Symposium (International) on Combustion*, 23(1):179–185, 1991.

[56] C.S. McEnally and L.D. Pfefferle. Fuel decomposition and hydrocarbon growth processes for oxygenated hydrocarbons: Butyl alcohols. *Proceedings of the Combustion Institute*, 30(1):1363–1370, 2005.

[57] Radheshyam, K. Santhosh, and G.N. Kumar. Effect of 1-pentanol addition and egr on the combustion, performance and emission characteristic of a crdi diesel engine. *Renewable Energy*, 145:925–936, 2020.

[58] C. Fan, C. Song, G. Lv, G. Wang, H. Zhou, and X. Jing. Evaluation of carbonyl compound emissions from a non-road machinery diesel engine fueled with a methanol/diesel blend. *Applied Thermal Engineering*, 129:1382–1391, 2018.

[59] C. Song, Z. Zhao, G. Lv, J. Song, L. Liu, and R. Zhao. Carbonyl compound emissions from a heavy-duty diesel engine fueled with diesel fuel and ethanol-diesel blend. *Chemosphere*, 79(11):1033–1039, 2010.

[60] S. Tang, B.P. Frank, T. Lanni, G. Rideout, N. Meyer, and C. Beregszaszy. Unregulated emissions from a heavy-duty diesel engine with various fuels and emission control systems. *Environmental Science and Technology*, 41(14):5037–5043, 2007.

[61] X. Pang, Y. Mu, J. Yuan, and H. He. Carbonyls emission from ethanol-blended gasoline and biodiesel-ethanol-diesel used in engines. *Atmospheric Environment*, 42(6):1349–1358, 2008.

[62] C. Mendoza, L.Y. Orozco, J. Palacio, A.F. López, and J.R. Agudelo. Genotoxic and mutagenic activity of particulate matter gathered in a high emitter automotive diesel engine operated with different palm oil-derived biofuels. *Journal of Energy Resources Technology, Transactions of the ASME*, 143(6), 2021.

[63] G.A. Westphal, J. Krahl, A. Munack, N. Rosenkranz, O. Schröder, J. Schaak, C. Pabst, T. Brüning, and J. Bünger. Combustion of hydrotreated vegetable oil and jatropha methyl ester in a heavy duty engine: Emissions and bacterial mutagenicity. *Environmental Science and Technology*, 47(11):6038–6046, 2013.

[64] P.I. Jalava, M. Tapanainen, K. Kuuspalo, A. Markkanen, P. Hakulinen, M.S. Happo, A.S. Pennanen, M. Ihalainen, P. Yli-Pirilä, U. Makkonen, K. Teinilä, J. Mäki-Paakkanen, R.O. Salonen, J. Jokiniemi, and M.-R. Hirvonen. Toxicological effects of emission particles from fossil- and biodiesel-fueled diesel engine with and without doc/poc catalytic converter. *Inhalation Toxicology*, 22(SUPPL. 2):48–58, 2010.

[65] J.A. Soriano, R. García-Contreras, J. de la Fuente, O. Armas, L.Y. Orozco-Jiménez, and J.R. Agudelo. Genotoxicity and mutagenicity of particulate matter emitted from diesel, gas to liquid, biodiesel, and farnesane fuels: A toxicological risk assessment. *Fuel*, 282, 2020.

[66] J.G. Hemmingsen, P. Møller, J.K. Nøjgaard, M. Roursgaard, and S. Loft. Oxidative stress, genotoxicity, and vascular cell adhesion molecule expression in cells exposed to particulate matter from combustion of conventional diesel and methyl ester biodiesel blends. *Environmental Science and Technology*, 45(19):8545–8551, 2011.

[67] X. Ba, L. Aguilera-Aguirre, Q.T.A.N. Rashid, A. Bacsi, Z. Radak, S. Sur, K. Hosoki, M.L. Hegde, and I. Boldogh. The role of 8-oxoguanine dna glycosylase-1 in inflammation. *International Journal of Molecular Sciences*, 15(9):16975–16997, 2014.

[68] C.C. Smith, M.R. O'Donovan, and E.A. Martin. hogg1 recognizes oxidative damage using the comet assay with greater specificity than fpg or endoiii. *Mutagenesis*, 21(3):185–190, 2006.

[69] B. Tudek, A.A. VanZeeland, J.T. Kusmierek, and J. Laval. Activity of escherichia coli dna-glycosylases on dna damaged by methylating and ethylating agents and influence of 3-substituted adenine derivatives. *Mutation Research - DNA Repair*, 407(2):169–176, 1998.

[70] R. Singh, R.J. Sram, B. Binkova, I. Kalina, T.A. Popov, T. Georgieva, S. Garte, E. Taioli, and P.B. Farmer. The relationship between biomarkers of oxidative dna damage, polycyclic aromatic hydrocarbon dna adducts, antioxidant status and genetic susceptibility following exposure to environmental air pollution in humans. *Mutation Research - Fundamental and Molecular Mechanisms of Mutagenesis*, 620(1-2):83–92, 2007.

[71] H. Tokiwa, N. Sera, Y. Nakanishi, and M. Sagai. 8-hydroxyguanosine formed in human lung tissues and the association with diesel exhaust particles. *Free Radical Biology and Medicine*, 27(11-12):1251–1258, 1999.

[72] M. Vojtisek-Lom, M. Pechout, L. Dittrich, V. Beránek, M. Kotek, J. Schwarz, P. Vodička, A. Milcová, A. Rossnerová, A. Ambrož, and J. Topinka. Polycyclic aromatic hydrocarbons (pah) and their genotoxicity in exhaust emissions from a diesel engine during extended low-load operation on diesel and biodiesel fuels. *Atmospheric Environment*, 109:9–18, 2015.

[73] F.D.L. Gondim, M.F. Moura, R.M. Ferreira, D.S. Serra, R.S. Araújo, M.L.M.D. Oliveira, and F.S.Á. Cavalcante. Exposure to total particulate matter obtained from combustion of diesel vehicles (euro 3 and euro 5): Effects on the respiratory systems of emphysematous mice. *Environmental Toxicology and Pharmacology*, 83, 2021.

[74] S. Arias, F. Molina, and J.R. Agudelo. Palm oil biodiesel: An assessment of pah emissions, oxidative potential and ecotoxicity of particulate matter. *Journal of Environmental Sciences (China)*, 101:326–338, 2021.

[75] A. Zerboni, T. Rossi, R. Bengalli, T. Catelani, C. Rizzi, M. Priola, S. Casadei, and P. Mantecca. Diesel exhaust particulate emissions and in vitro toxicity from euro 3 and euro 6 vehicles. *Environmental Pollution*, 297, 2022.

[76] S. Tao, Y. Xu, M. Chen, H. Zhang, X. Huang, Z. Li, B. Pan, R. Peng, Y. Zhu, H. Kan, W. Li, and Z. Ying. Exposure to different fractions of diesel exhaust pm2.5 induces different levels of pulmonary inflammation and acute phase response. *Ecotoxicology and Environmental Safety*, 210, 2021.

[77] Y. Xu, Z. Li, Y. Liu, B. Pan, R. Peng, W. Shao, W. Yang, M. Chen, H. Kan, Z. Ying, and Y. Zhang. Differential roles of water-insoluble and water-soluble fractions of diesel exhaust particles in the development of adverse health effects due to chronic instillation of diesel exhaust particles. *Chemical Research in Toxicology*, 34(12):2450–2459, 2021.

[78] Z.A. Khan, P. Hellier, and N. Ladommatos. Measurement of soot mass and pahs during the pyrolysis of c2–c4 alcohols at high temperatures. *Combustion and Flame*, 236, 2022.

[79] H. Jin, Y. Wang, K. Zhang, H. Guo, and F. Qi. An experimental study on the formation of polycyclic aromatic hydrocarbons in laminar coflow non-premixed methane/air flames doped with four isomeric butanols. *Proceedings of the Combustion Institute*, 34(1):779–786, 2013.

[80] L.-S. Tran, J. Pieper, M. Zeng, Y. Li, X. Zhang, W. Li, I. Graf, F. Qi, and K. Kohse-Höinghaus. Influence of the biofuel isomers diethyl ether and n-butanol on flame structure and pollutant formation in premixed n-butane flames. *Combustion and Flame*, 175:47–59, 2017.

[81] G. Karavalakis, G. Deves, G. Fontaras, S. Stournas, Z. Samaras, and E. Bakeas. The impact of soy-based biodiesel on pah, nitro-pah and oxy-pah emissions from a passenger car operated over regulated and nonregulated driving cycles. *Fuel*, 89(12):3876–3883, 2010.

[82] L. Huang, S.V. Bohac, S.M. Chernyak, and S.A. Batterman. Composition and integrity of pahs, nitro-pahs, hopanes, and steranes in diesel exhaust particulate matter. *Water, Air, and Soil Pollution*, 224(8), 2013.

Chapter 5

Transient state results

In this chapter, unregulated emissions in gas and particles from a Euro 6b diesel engine, operated with four unconventional and advanced biofuels blended with diesel fuel and pure HVO as base biofuel were investigated. The engine was operated following WLTC driving cycle starting from cold-engine conditions. The apoptotic index induced by gas and particle emissions was determined as biological response. Furthermore, since polyoxymethylene dimethyl ethers (DME) are becoming a promising solution for transportation because they can be categorized as e-fuels, the effect of a diesel fuel blend with 20% of OME, on the performance, combustion characteristics, regulated emissions, particle number, and particle size distribution were also investigated

5.1 Introduction

In literature there are several studies on unregulated emissions (PAH and mainly formaldehyde) with HVO and slightly less with OME blends as shown in **Chapter** 2. However, most of them have been conducted under steady state or with small size engines. To my knowledge, there is no study in the literature that has reported the emissions of both PAH and carbonyls for each phase of the WLTC driving cycle in a modern engine.

This chapter presents the effect of five promising alternative fuels (see **section** 3.2.1) blended with diesel or HVO, on 16 PAH compounds (both particle-bound and gaseous phases) and 13 carbonyl compounds emitted by an automotive diesel engine under the WLTC, starting from cold-engine conditions as a realistic scenario to evaluate their impact on unregulated and harmful emissions. Ozone formation potential was quantified from carbonyl emission factors to provide potential implications

of ozone pollution with the tested fuels. The biological response through the apoptotic index induced by the samples derived from the gas phase and the particles was determined. Furthermore, at the end of this chapter, the effect of a diesel fuel blend with 20% of OME on the performance and pollutant emissions (CO, NO_2, NO, THC) is presented. Moreover, due to the links between PM emissions and health effects, measurements of particle number and particle size distribution are also presented here.

5.2 Unregulated emissions

5.2.1 PAH emissions

Figure 5.1 shows the total average gaseous and particle-bound PAH emission factors. For gaseous phase, the results are presented by driving cycle phase and for the PM as total emissions along the cycle.

Total PAH emissions in the gaseous phase were higher in the low-speed phase for all fuels and ranged from 20.7±1.5 μg/km to 51.7±8.9 μg/km. All fuels maintained a similar total average emissions in both medium and high-speed phases, and OME20 and HVO fuels showed the lowest total average emissions (16±2.5 μg/km and 11± 2.5 μg/km, respectively). At the extra high-speed phase, the total emissions increase significantly for the HT20 fuel blend compared to previous phases, while the other fuel blends presented the lowest emissions of the entire driving cycle, except diesel and OME20, which remained almost unchanged in the high and extra high-speed phases (24±2.0 μg/km and 16±2.5 μg/km, respectively).

The low-speed phase significantly influenced the total PAH gaseous emissions. Diesel and HT20 exhibited the highest emissions (around 118 μg/km and 138 μg/km, respectively), HO20 decreased by 25% compared to diesel, followed by OME20, HVO and SLB100 which decreased around 48±8%.

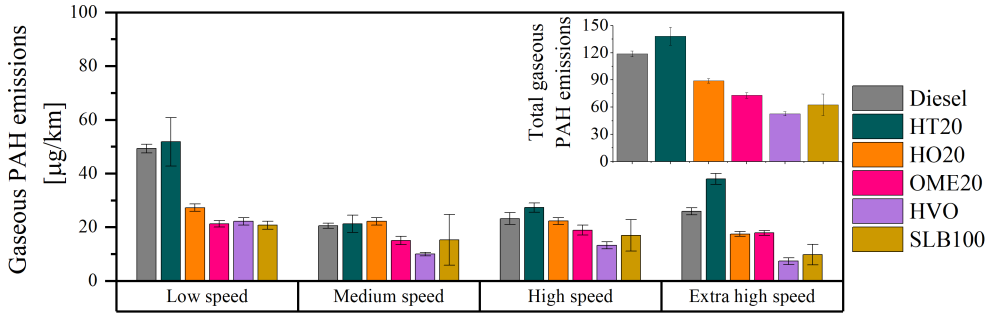

(a) Total average gaseous PAH emission factors.

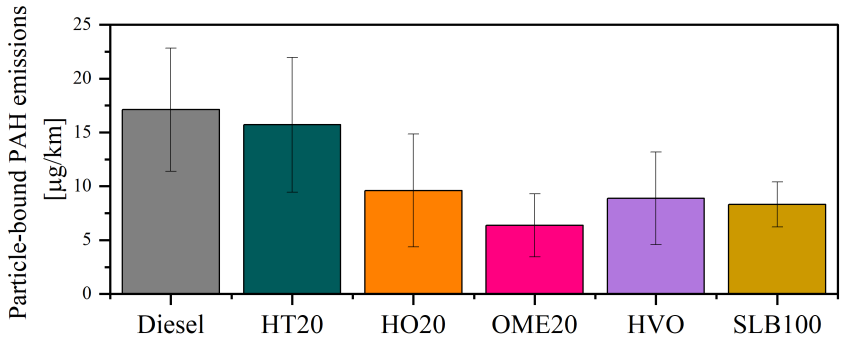

(b) Total average particle-bound PAH emission factors.

Figure 5.1: Total average PAH emission factors. Error bars correspond to standard deviations.

As expected, total average gaseous PAH emission factors were higher under cold-engine start conditions at low-speed phase, which can be explained by: a) when the engine is cold the amount of unburned PAH is high because of the reduced combustion efficiency, and as the cycle progresses, the in-cylinder temperature increases, which improves combustion efficiency and leads to relatively lower unburned PAH emissions. These results are in agreement with the results reported by Karavalakis et al. [1] who studied the cold-start influence on PAH emissions, b) the temperature affects the two competing processes, the rate of PAH formation through fuel pyrolysis and the rate of oxidative attack on these compounds. Both rates increase with temperature, but the oxidative attack rate increases faster [2], c) some diesel fuel blends such as HT20 and HO20 with higher volatility than diesel might cause better dilution of the more volatile fractions with air, leading to low local equivalence ratios that might be below the lower flammability limit. HT20 and HO20 also have lower cetane numbers compared to diesel and other blends, resulting in a longer ignition delay, and providing the fuel more time to dilute. Based on the above, there is a time when the flame front does not progress anymore (misfiring), as it remains below the lower flammability limit, which could increase unburned PAH emissions at cold start in the low-speed driving cycle phase.

At extra high speed it was expected that the increase in the combustion temperatures would lead to a better oxidation of aromatics thus limiting PAH growth. However, the gaseous PAH emissions with HT20 showed an increase when moving from the high to the extra high-speed phase, suggesting that the formation of combustion-derived PAH was favored by increasing the average mean speed. This result is unexpected, and the reason is probably associated with the pyrosynthesis of the fuel fragments (formation of alkynes and alkadienes through the decomposition of olefins and olefinic radicals) due to the higher fuel/air ratio and high in-cylinder temperature [3], which could contribute to the formation of aromatic species. Oxygenated fuel blends have been reported to help reduce gaseous PAH emissions [4]. It was suggested that the oxygenated fuel blends modifies the combustion chemistry by affecting the PAH and soot oxidation reaction rates through an alteration of the concentration of OH radicals [2]. In addition, they promote more complete combustion, suppressing the formation of low-ring PAH and accelerating the degradation of PAH with high rings. This explains the low PAH emissions of SLB100 and OME20 compared to diesel at high and extra high speed.

HVO emissions remained among the lowest in all driving cycle phases. Since HVO has the highest lower heating value, neat HVO exhibited the lowest fuel consumption. Additionally, neat HVO burns more slowly than other fuels and blends because of the absence of oxygen content in its composition, and shows better indicated thermal efficiency at both lower and higher loads caused by the more centered combustion around top dead center [5]. These combustion characteristics and the absence of aromatics in this fuel, which, as mentioned above, are precursors in the formation reactions of higher molecular weight PAH, are related to lower PAH emissions throughout the driving cycle compared to the other fuel blends tested. These results differ from the steady-state results with 13% and 20% HVO blends, in which gas-phase PAH increased compared to diesel fuel. However, in the steady-state tests there was more than 80% of the fossil fuel containing aromatics, precursors of PAH-forming reactions. Additionally, engine technology and operating conditions were different.

Particle-bound PAH emissions range from 6.3 ± 4.3 μg/km to 17.1± 5.7 μg/km, which is significantly lower than gaseous emissions. No significant differences were found in total particle-bound PAH emissions from HT20 and HO20 compared to diesel, while OME20, pure HVO and SLB100 reduced particle-bound PAH emissions more than 50%. It has long been postulated that the dominant pathway for the formation of PAH is hydrogen-abstraction/acetylene-addition (HACA), acetylene (and other soot precursor species) can react with molecular oxygen or oxygen-containing radicals from the oxygenated fuels and eventually can produce CO rather than PAH and soot [6].

Compared with previous studies, the PAH emission factors in this study are comparable to those reported in literature for diesel engines operating with diesel and

biodiesel and under different driving cycles as can be observed in **Table** 5.1. The results reported in [1] show that particle-bound PAH emission factors under cold start conditions were up to three orders of magnitudes higher than those reported in hot start under the same driving cycle. Most of the studies were performed on particles and our results are relatively low compared to the others. This may reflect the great influence of the driving cycle, the engine technology as well as the aftertreatment system.

The speciated PAH emission factors in the gas phase and particle bound have been illustrated in **Figure** 5.2. Low-molecular weight PAH (containing 2–4 aromatic rings) were the most prominent PAH compounds emitted from the gaseous phase while higher molecular weight PAH (with 5 or more rings) were prominent in the particle phase, in agreement to the findings of other studies [7, 8, 9]. Indeno[1,2,3-c,d]pyrene, benzo[g,h,i]perylene and dibenzo[a,h]anthracene were not detected in gas phase and indeno[1,2,3-c,d]pyrene were below the detection limit in PM. These results suggested that particle-bound PAH were mainly generated through pyrosynthesis reactions of lower molecular weight aromatic compounds, since fuel formulation did not contain high molecular weight PAH [10]. Although in the gas phase, part of the PAH (low-molecular weight PAH) might derive from the fuel, a significant percentage of PAH emissions were formed in the combustion process, since large amount of fuel-related PAH was decomposed [11].

Table 5.1: PAH specific emissions for diesel, HVO and biodiesel

Ref	Cycle	Fuel	PAH [μg/km]	Engine	After-treatment	Phase
This work	WLTC (cold start)	Diesel	118.9 ± 3.2 (gas) 17.1 ± 5.7 (particles)	Euro 6b Nissan 1.5 dCi (model K9K)	—	Particles + gas
This work	WLTC (cold start)	HVO	52.7 ± 2.3 (gas) 8.9 ± 4.3 (particles)	Euro 6 Nissan 1.5 dCi (model K9K)	—	Particles + gas
[1]	UDC (cold start) UDC (hot start) NEDC	Diesel Biodiesel Diesel Biodiesel Diesel Biodiesel	84 75 31 24 52 45	Euro 1VW Golf 1.9 TDi	DOC	Particles
[10]	Four modes selected from the standard thirteen- mode SAE test cycle for HDV Diesel	Diesel	1850 ± 1339	Volvo and MAN SL200 diesel city council buses	—	Particles + gas
[12]	Two road types with distinctive conditions	Diesel	155± 120 60±70 30±15 25± 20	China II emission standard China III emission standard China IV emission standard China V emission standard	SCR (China IV – China V)	Particles
[13]	Urban, suburban and freeway routes	Diesel	10 15 37 65	CMC 4D34-3AT3A (2006) Isuzu 4HE1XN (2001) CMC FK457MS (1995) Fuso FM657MS (1995)	—	Particles

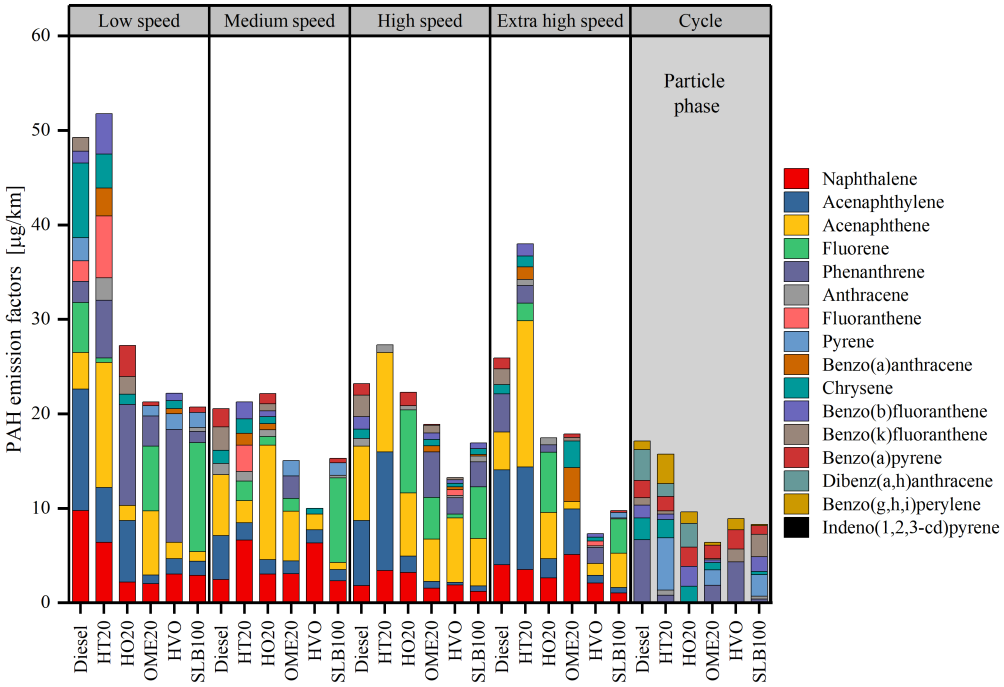

Figure 5.2: Speciated PAH emission factors in the gas phase (per phase of the WLTC driving cycle) and particle-bound (all the driving cycle) for all the fuels tested

Remarkable increases and reductions were observed in some compounds with respect to the diesel emission profile. Some compounds not-detected when operating with diesel fuel, such as the carcinogenic benzo(a)pyrene were detected in the low-speed phase when operating with HO20, OME20 and SLB100. The individual compounds emitted in relatively large amounts in the gaseous phase were two, three and four-ring PAH such as naphthalene, acenaphthylene, acenaphthene, fluorene and phenanthrene, most of them have been identified also as major PAH present in diesel fuel emissions [10, 11, 14].

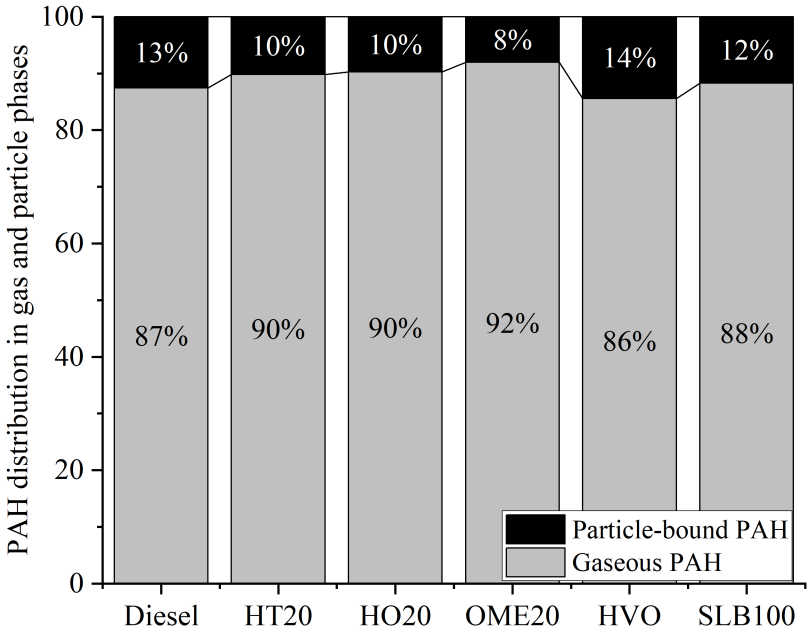

Figure 5.3: Gas-particle partitioning of PAH

Figure 5.3 shows the PAH distribution in gas and particle phases. For all tested fuels, gas-phase PAH contributed 86%–92% to the total PAH exhaust emissions, more than particle-phase PAH, these results agree with those of previous studies [10, 15, 16, 17] that reported gas-phase PAH as the most dominant in diesel engine exhaust. Although the gas/particle partitioning of PAH is an integrated complex process due to its formation and growth concurrently with particles, high molecular-weight-PAH showed a stronger trend to condensate and adhere to particles according to their physicochemical properties. Since low and medium molecular-weight-PAH are commonly more prominent, the gaseous phase comprises to more than 80% of the total PAH emissions.

PAH equivalence toxicity

Figure 5.4 shows the total toxic equivalent concentrations of PAH in gas and particle phases. Although particle-bound PAH comprise only a small fraction of total PAH emissions, they comprise a high fraction of the BaP-TEQ due to the higher presence of high molecular weight PAH compared to the gas phase, which are classified with high toxicity (high TEF values) among the priority PAH. It is worth noting that although the emission factors in the gaseous phase were notably higher (more than

double in some cases) than emissions in the particle phase, the BaP-TEQ emission factors are around the same magnitude for both phases, which means that both phases contribute approximately equal to the toxicity associated with carcinogenic PAH with the fuels tested at the WLTC.

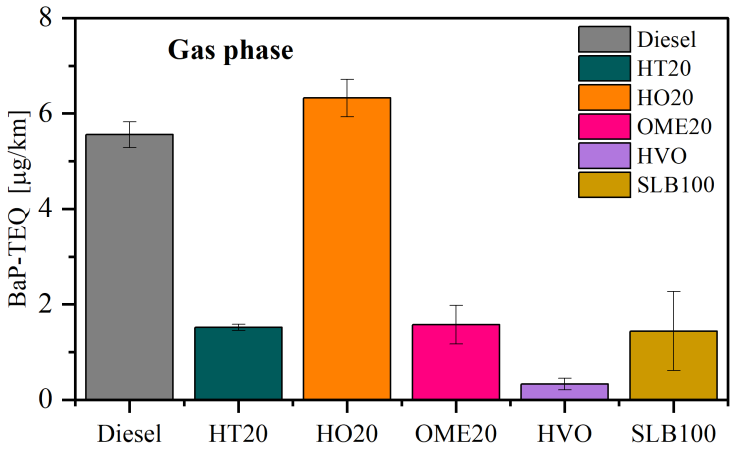

(a) Total toxic equivalent concentrations of PAH in gas phase.

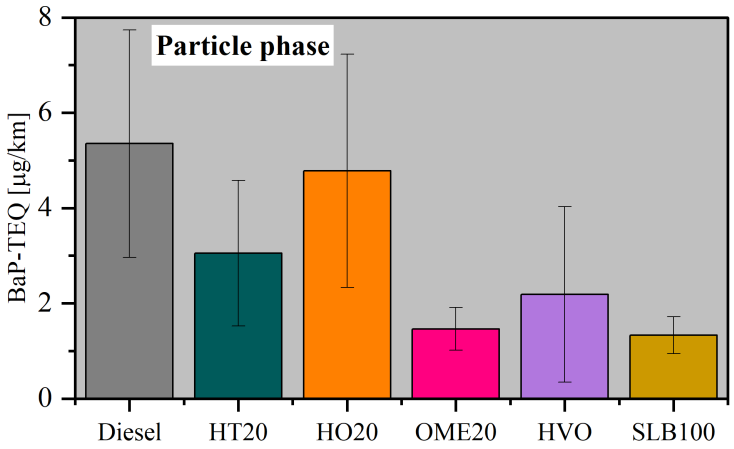

(b) Total toxic equivalent concentrations of particle-bound PAH.

Figure 5.4: Total toxic equivalent concentrations of PAH. Error bars correspond to the standard deviation

The BaP-TEQ in the particle phase followed the same trend as the emission factors. Both HT20 and HO20 did not show significant differences compared to diesel, while the rest of the tested fuels decreased the BaP-TEQ around 50% (or more) and they did not show significant difference between them. However, in the gaseous phase, HO20 exhibited the highest toxicity (6.3± 0.4 μg/km), followed by diesel, due to the emission of benzo(a) pyrene in the low-speed phase. HT20, OME20

and SLB100 did not show significant difference, while HVO exhibited the lowest toxicity.

It should be noted that although it is widely used to assess toxicity, this index is only associated with the concentration of 16 prioritized PAH. This could underestimate the total toxicity associated with other carcinogens and xenobiotics, and therefore, it does not represent a measure of overall toxicity, for which biological tests and further physicochemical characterization are needed.

5.2.2 Carbonyl emissions

Figure 5.5 shows total carbonyl emissions per phase (distance-based). At the beginning, in the low-speed driving cycle phase, higher carbonyl emissions were associated with low engine temperature. As the cycle progressed and the engine warmed up, the total carbonyl emissions decreased. The increase of in-cylinder temperature and pressure promoted better combustion, which could further oxidize the carbonyl compounds. When comparing between different fuels, it was observed that in the low-speed phase, diesel showed the highest emissions followed by the two oxygenated fuels, OME20 and SLB100. In the medium speed HT20 showed the highest carbonyl emissions followed by diesel fuel. No significant differences were found between fuels in phases 3 and 4 for any of the fuels.Pure diesel is mainly composed of saturated and aromatic aliphatic hydrocarbons. During combustion (oxidative conditions), alkanes, which are the simplest hydrocarbons, are converted through the oxidation process into carbon dioxide -CO_2- (the most oxidized substance). During this reaction, alcohols, carbonyls, carboxylic acids, and esters are formed as intermediate products [18]. Light carbonyls derive mainly from incomplete combustion of aliphatic hydrocarbons, which explains the higher emission of this compound in the low-speed phase.

Since aldehydes were not present in the reference diesel fuel, any aldehyde and ketone appearing in exhaust gases was formed in the engine and exhaust system. They are largely formed in the combustion process from fuel fragments produced in the initial oxidative pyrolysis of the fuel [19]. Aldehyde formation reactions are mainly based on alkyl radicals (R•), which are formed by cleavages of C-C or C-H bonds of hydrocarbons and are important carriers of the chain reaction in the combustion of hydrocarbons (straight chain aliphatic hydrocarbons and related species) [19, 20, 21]. Hence, aldehyde formation was largely determined by combustion conditions such as local stoichiometry and temperatures. Nelson et al. [19] studied emissions of aldehydes from two vehicles following the urban driving cycle using a range of diesel fuel formulations. The fuels ranged in sulfur content from 24 to 1700 ppm, and in total aromatics from 7.7 to 33 mass%. They found that aldehyde emission rates vary considerably, and they were not significantly affected by diesel properties, but were possibly related to engine operating conditions.

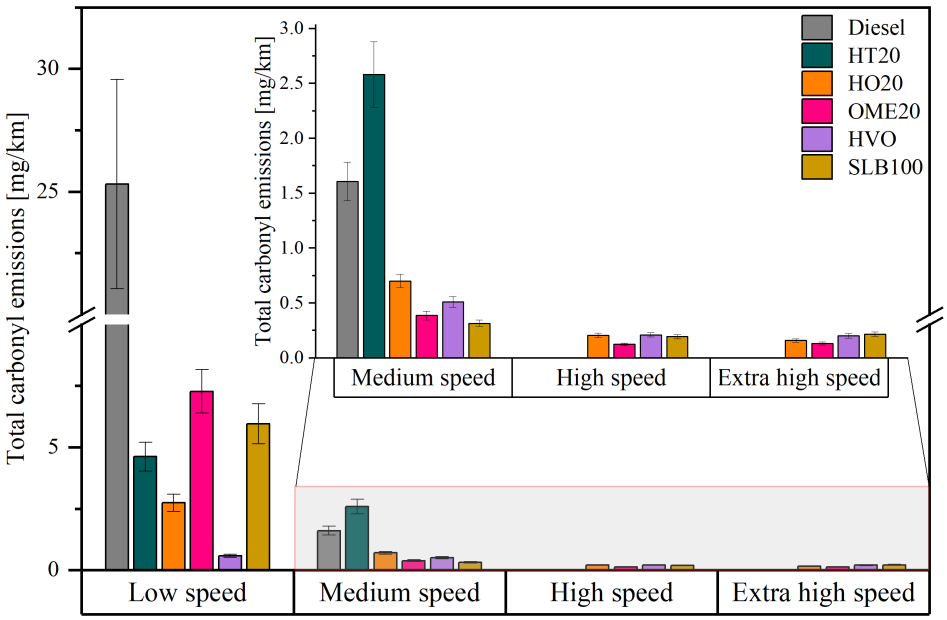

Figure 5.5: Total carbonyl emissions per driving cycle phase. Error bars correspond to the standard deviation

Other researchers have found correlation between carbonyl emissions and engine temperature. Wagner et al. [20] reviewed carbonyl formation in internal combustion engines. They pointed out that aldehyde formation is most pronounced at low temperatures, for example at engine start, although it continues to some extent at higher temperatures. Takada et al. [22] found a negative correlation between formaldehyde emission and in-cylinder temperature. The experiments were carried out with an 8 L, 6-cylinder, 4-stroke-cycle, turbocharged DI diesel engine with a common rail fuel injection system fueled with commercial diesel fuel, using steady state operation.

All fuel blends reduced carbonyl emissions in the low-speed phase by more than 80% compared to diesel. Regarding oxygenated fuels, both SLB100 and OME20 emitted the highest total carbonyl compounds compared to the other blends (not including pure diesel) in the low-speed phase. Although SLB100 fuel has 6.16% of linoleic acid in its composition, which could promote the formation of lower carbonyl compounds (because of its double bonds), this fuel blend reduced total carbonyls in the low-speed phase by 86% and even more in the other driving cycle phases. In OME20 combustion process, more oxygen is delivered (11% of the fuel mass), which improves the combustion efficiency, favoring the oxidation of THC, including carbonyls. In the low-speed phase, OME20 reduced total carbonyl emissions by 83% compared to diesel.

HT20 and HO20 fuels reduced carbonyl emissions by 89 and 93%, respectively,

compared to diesel in the low-speed driving cycle phase. Although HT and HO have terpenes in their composition derived from hydrogenated orange oil and turpentine [23, 24] and they have one or more carbon-carbon double bonds in their molecular structures, which makes them highly reactive to oxidation to form carbonyls [25], both HT20 and HO20 fuel blends significantly reduced the emissions of these compounds in the first phase of the driving cycle. On the contrary, in the medium speed phase, HT20 increased total carbonyl emissions by 60% compared to diesel. This reduction may be due to the fact that both blends, HT20 and HO20, are more volatile than diesel. The more volatile fractions diffuse much more and they are better diluted with air than diesel, which could improve oxidation of the intermediate compounds.

HVO showed the lowest total emissions compared to the other fuel blends, compared to diesel, the lack of aromatics allows to reduce more intermediates during combustion [26]. Thus, aldehyde emissions were significantly reduced with HVO. This reduction has been previously reported for Gas to Liquid (GTL), a fuel with a very similar composition to HVO [27, 28]. These results were similar to those obtained in steady state with HVO blends (HVO13 and HVO20) in **Section** 4.2.3, which showed significant reductions of carbonyls with these fuel blends.

For phases 3 and 4, no obvious differences were observed in the emissions from all the fuel blends except for diesel and HT20, for which no emissions were detected at all. After the medium-speed phase of the driving cycle, the difference in total carbonyl emissions between the fuel blends and diesel stabilizes, indicating that the cold-engine start affects more carbonyl formation in combustion processes than fuel properties.

Figure 5.6 presents the emission factors for 11 carbonyls detected in each of the four phases of the WLTC. Acetone and 2-butanone were not detected or were below the detection limit. Formaldehyde and acetaldehyde were the most abundant compounds, which derived mainly from incomplete combustion of aliphatic hydrocarbons. Since higher hydrocarbons are more unstable and easier to decompose than lower hydrocarbons, lower molecular weight carbonyls are more abundant in the exhaust gas [29].

OME20 and SLB100 reduced carbonyl emissions in the low and medium-speed WLTC phases compared to diesel. Even though formaldehyde and acetaldehyde increased in the first phase compared to other renewable fuel blends tested, emissions continued being much lower than diesel. The use of oxygenated fuel blends can influence carbonyl emissions due to combustion related factors and fuel properties. The oxygen content can promote more complete combustion [30] and consequently, decrease carbonyl emissions. However, apart from combustion factors, carbonyl compounds can be formed as secondary products during the oxidation process [21]. These results suggested that combustion-related factors could influence carbonyl formation even more than fuel composition.

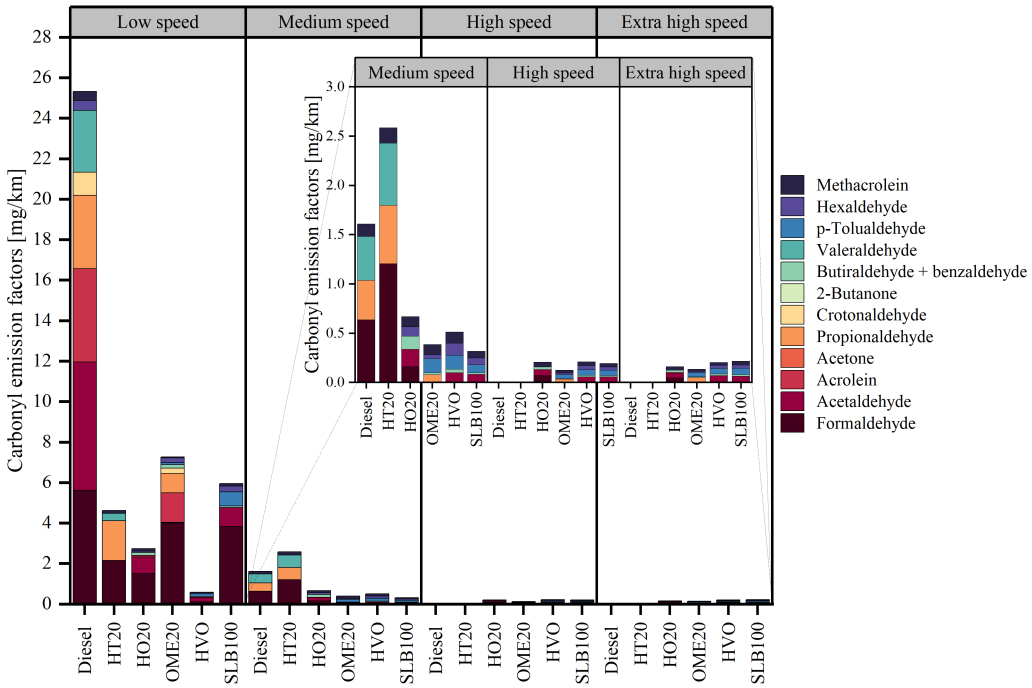

Figure 5.6: Emission of carbonyl compounds for each phase

The use of other oxygenated fuels such as alcohols and biodiesel in diesel engines have given discordant results. Some studies have reported that alcohol and biodiesel increase carbonyl emissions [31, 32, 33], while other studies have shown carbonyl emission reductions, explained by the increase of fuel–bonded oxygen atoms that enhance combustion compared to diesel [34, 35]. Li et al.[36] found an increase in formaldehyde and acetaldehyde blending diesel-ethyl tert-butyl ether compared to diesel in a common rail direct injection diesel engine. They attributed the increase in carbonyl emissions to the high EGR rate, which suggests that there are other factors related to engine mapping that may affect unregulated emissions and that were not analyzed in this study.

Diesel and HT20 showed the highest emissions of formaldehyde, propionaldehyde and valeraldehyde at medium speed phase. However, both diesel and HT20 fuels did not emit any carbonyl in the high and extra high-speed phases. Emissions from the other fuel blends in the last two driving cycle phases were much less than 0.1 mg/km, probably due to the higher combustion temperature during an increased engine speed which help oxidizing the aldehydes to CO [37].

The constant emission of other aldehydes throughout the drive cycle, such as hexaldehyde, may correspond specifically to the composition of the fuel. For example, SLB100 emitted approximately the same concentration of hexaldehyde throughout the entire driving cycle. The linoleic acid content in SLB100 may explain this trend due to this acid is the main precursor of hexaldehyde when oxidized [38].

5.2.3 Ozone formation potential

Figure 5.7 shows the total ozone formation potential for each fuel under the WLTC. In addition, it shows the contribution of each phase of the cycle to the total *OFP*. Compounds such as formaldehyde, acetaldehyde, and acrolein that have a high propensity to react in the atmosphere (high MIR), increase *OFP*. This is clearly evidenced for all fuels in the low-speed phase, since due to the high emissions of formaldehyde, acetaldehyde, and acrolein, this phase contributes the most to the total *OFP*.

Diesel fuel exhibited the highest *OFP* of 140 mg O_3/km, as expected, given its high carbonyl specific emission compared to all other fuels. Other studies have also evaluated *OFP* for diesel fuel. Dong et al. [39] reported a total average *OFP* value associated with carbonyls of 537 mg O_3/km. They tested 15 vehicles including medium and large bus, medium-duty truck and heavy-duty truck fueled with diesel and operating under two driving cycles representative of driving conditions in China. All tested vehicles with Euro II and III. Bermudez et al. [40] reported a *OFP* of 983 mg O_3/km and 967–1741 mg O_3/km for diesel and three different biodiesel fuels, respectively. They used a 4-cylinder, light-duty diesel Euro 4 without any exhaust treatment device and operating under NEDC. Tsai et al. [41] reported a *OFP* value of 140 mg O_3/km and 70 mg O_3/km when followed the federal test procedure-75 (FTP-75) and highway fuel economy cycle, respectively. The experiments were carried out in eight in-use light-duty diesel vehicles without aftertreatment system and fueled with diesel. Although most of these studies reported higher *OFP* values than the one found in this study for diesel, this may be related to the engine technology and the test cycle. On the other hand, the HT20, OME20 and SLB100 decreased by 65% the *OFP* compared to diesel without a significant difference between them. The *OFP* with HO20 decreased to 28 mg O_3/km and the lowest was reached with HVO of 7 mg O_3/km. For these fuels it is difficult to make a comparison with the literature, since no *OFP* data (distance-based- mg O_3/km) were found.

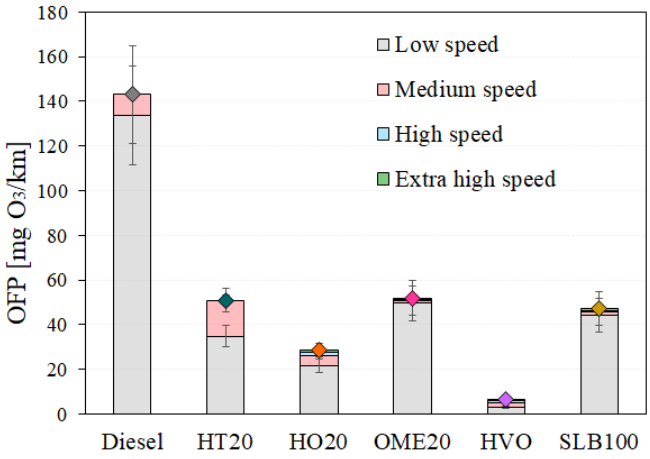

Figure 5.7: Ozone formation potential (diamonds) and the contribution of each driving cycle phase (shaded bars) for the tested fuels. Error bars correspond to standard deviations

5.3 Biological activity

5.3.1 Apoptosis induced by gas and particle emissions

Apoptosis is an active and physiological mode of cell death. Mitochondria, Bcl-2 protein, cytochrome c and caspases, are essential components of the intracellular apoptotic signaling pathways. Some PAH compounds may cause an accumulation of the tumor suppressor protein p53 which may be important for the induction of apoptosis. In addition, some PAH induce cellular toxicity by regulating the generation of reactive oxygen species (ROS), which mediate apoptosis [42]. Similarly, some aldehydes, such as formaldehyde, have shown to cause oxidative stress inside the cells and the alteration of mitochondrial energy metabolism resulting in nuclear fragmentation and apoptosis. The apoptosis results obtained in the present study can be caused partly by PAH and partly by carbonyl emissions, in addition to other organic compounds emitted, since the exhaust gas is composed by a complex mixture of pollutants, some of them classified as carcinogenic.

A higher apoptotic index implies that the sample induced very serious damage in the exposed cells, which triggers a series of molecular processes capable of finally leading to their programmed death. However, apoptosis is a method that the body uses to get rid of damaged or abnormal cells.

Figure 5.8a presents the results of apoptotic index induced by gaseous emissions (above) and particles (bellow). The cell exposure doses (concentration of organic extracts) varied according to the evaluated phase since it was not possible to obtain

enough particles to increase the concentration to the equivalent in the gaseous emissions.

The amount of apoptotic cells, and thus the apoptotic index, increased in a dose-dependent manner and was significantly higher in cells exposed to gas phase-derived samples from HT20, HO20, OME20 and SLB10 fuels. No significant differences in apoptotic index were observed at the highest exposure concentration. Nevertheless, Diesel and HVO did not show significant differences in the AI for all exposure doses, which indicated that even at the lowest concentration the induced apoptosis did not decrease, suggesting a high toxicity of the gas-derived samples from these fuels.

On the other hand, the AI induced by particulate matter samples did not show a concentration-response effect for any of the samples. OME20, HVO, and SLB100 derived samples did not show significant difference from control, while diesel, HT20 and HO20 showed an apoptotic index equal to DMSO. However, if the response was induced only by DMSO, it would be expected that as the exposure concentration decreased (from 0.05 to 0.00005 gPM/mL), which means an increase of DMSO (dilution solvent), the apoptotic index would increase, but this was not observed. Therefore, the results obtained by the particle-derived samples did not allow a clear conclusion to be drawn on the particle-induced apoptosis of the tested fuels. One of the possible causes may be the low particle concentration in the sample, given the limited number of particles obtained in every WLTC.

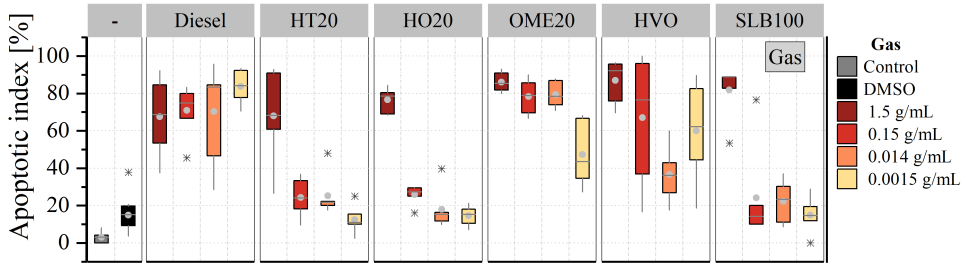

(a) Apoptotic index induced by gaseous emissions.

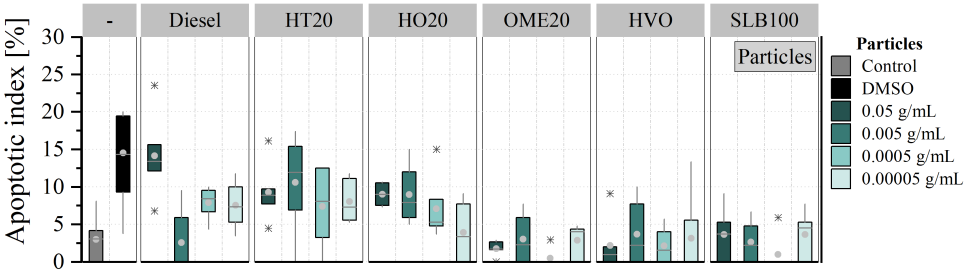

(b) Apoptotic index induced by particles

Figure 5.8: Apoptotic index induced by gaseous and particle emissions

Although various studies highlighted that acute exposure to exhaust emissions induced a biological response in different cell types *in vivo* and *in vitro* [43], the related induced apoptotic pathway after acute exposure of HepG2 cells to the organic fraction from diesel exhaust emissions has not been reported. Further research is needed to highlight the detailed mechanisms of exhaust gas pollutant-mediated apoptosis as well as a detailed physicochemical characterization of exhaust gases to determine which specific compounds of might be causing the biological effects.

5.4 OME20: Chemical effects vs mapping strategy

As mentioned in **Chapter** 1, new fuel technologies, such as electrofuels, are an attractive alternative to meet the energy demand and emission regulations, with sustainable electricity being the primary source of energy. Recently, there is increasing interest in using polyoxymethylene dimethyl ether (OME) as a diesel substitute. Since the results of unregulated emissions with the OME20 blend showed significant benefits with respect to diesel (**section** 5.2), it was decided to study the effect of OME20 (diesel fuel blend with 20% of OME with 3 to 5 oxymethylene groups), on the performance, combustion characteristics, regulated emissions, particle number (PN), and particle size distribution in a compression ignition Euro 6b engine following the WLTC. Unlike unregulated emissions, regulated emissions were measured downstream of the aftertreatment system, while PN emissions were measured upstream of the particulate filter.

5.4.1 Engine performance

Figure 5.9 shows the instantaneous fuel consumption. Sharp consumption peaks were associated with accelerations for both fuels. At the end of the driving cycle, the accumulated fuel consumption was 11 % higher for OME20 compared to diesel (929 and 826 g, respectively), equivalent to the same percent decrease (11%) in the LHV of OME20 with respect to diesel. This is due to the oxygen content in the blend (11%) and implies that the engine would require more fuel to maintain the same power output. At idle and low load no significant differences were observed, while for high and extra high-speed phases, the higher consumption for OME20 became evident.

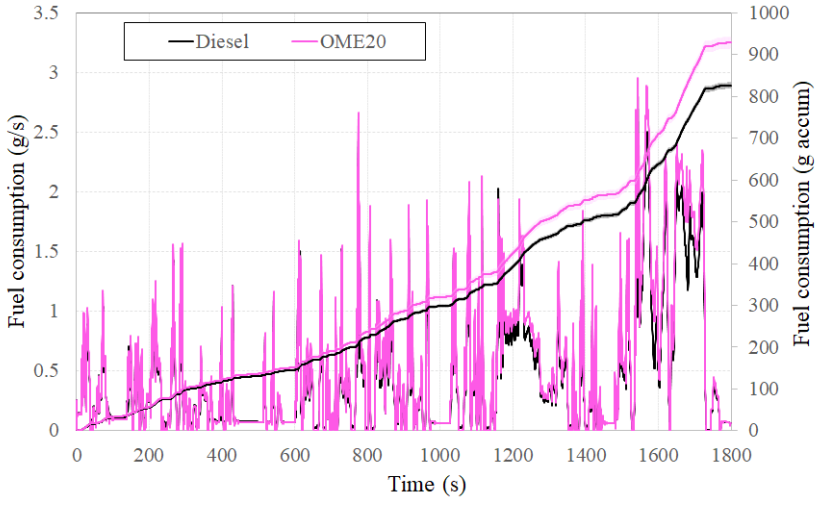

Figure 5.9: Fuel consumption of the tested fuels

Average values of brake specific efficiency are shown in **Figure** 5.10 for each driving cycle phase. As expected, the worst efficiency was observed in the first phase for all fuels, when the engine was cold [44, 45]. As the driving cycle progressed, the brake thermal efficiency (*bte*) increased as a result of the higher engine temperature, and the reduction in mechanical losses. The *bte* was slightly higher for OME20 than for diesel fuel in the low and medium-speed driving cycle phases. This increase can be explained because the OME intramolecular oxygen increased the combustion velocity, as detailed below. However, as the driving cycle advanced, the *bte* was not significantly affected by the type of fuel, and in the extra high-speed driving cycle phase, diesel shows a slightly higher efficiency than OME20 due to a second regeneration of the LNT system, which occurred only for this fuel blend, as a consequence of its higher ECU-modelled NOx emissions (see **section** 5.4.3). The total *bte* at the end of the driving cycle was not significantly different between fuels because the higher efficiency for OME20 at the initial driving cycle phases was compensated by the lower efficiency at the extra high-speed phase.

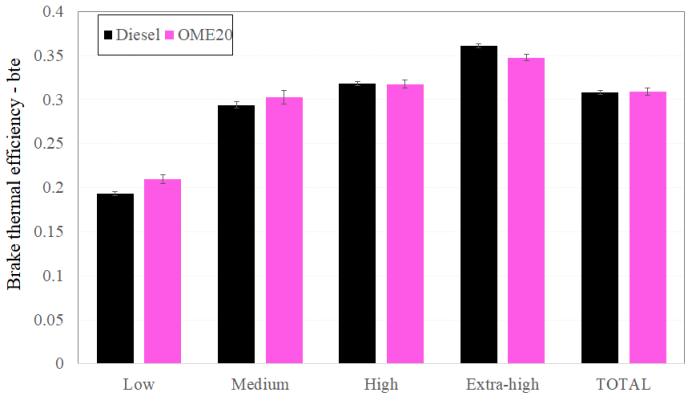

Figure 5.10: Brake thermal efficiency (*bte*) of the tested fuels

Exhaust pollutant emissions were markedly affected by the equivalence ratio and the EGR rate. Slight increases in both equivalence ratio and EGR led to sharp increases in CO, THC and PN emissions, which are not attributable to differences in fuel formulation. The instantaneous equivalence ratio (**Figure** 5.11) was high during accelerations and low at idle condition (although nil during decelerations). In both cases it decreased as the driving cycle progressed because the engine turned warmer. However, the mean equivalence ratio was significantly higher at high and extra high-speed driving cycle phases than at the previous phases, as observed in **Figure** 5.12. The instantaneous equivalence ratio higher than 1 at 1220 s corresponded to the LNT regeneration.

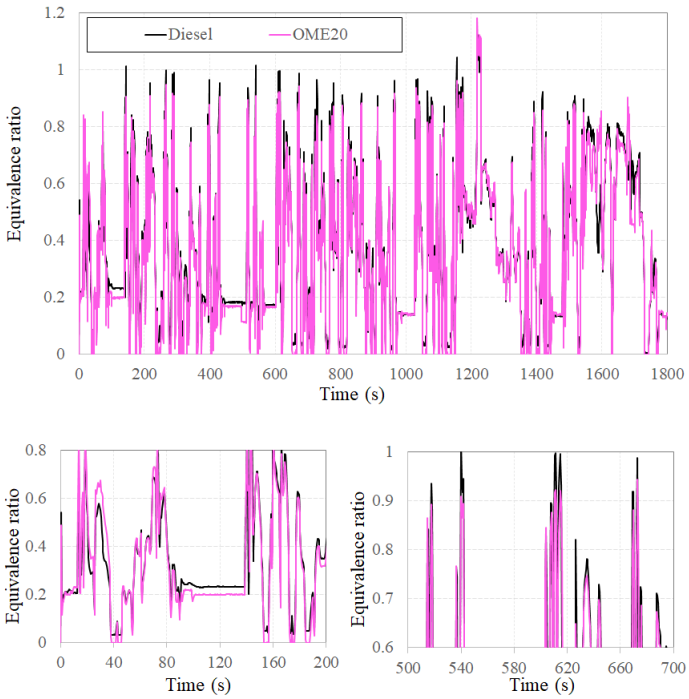

Figure 5.11: Instantaneous equivalence ratio

For the low and medium speed driving cycle phases, a slightly lower mean equivalence ratio was observed for OME20. This was especially noticeable at the initial idle period (**Figure** 5.11). However, in the high and extra high-speed driving cycle phases no significant differences were observed. It is worth noting that the average differences shown in **Figure** 5.12 derived mainly from specific acceleration points (see detailed example in **Figure** 5.11) in which the equivalence ratio was higher for diesel fuel. These high equivalence ratio points were closely related to particle number, THC and CO emissions, as discussed below. In most instants of high equivalence ratio, higher peaks were observed for diesel fuel.

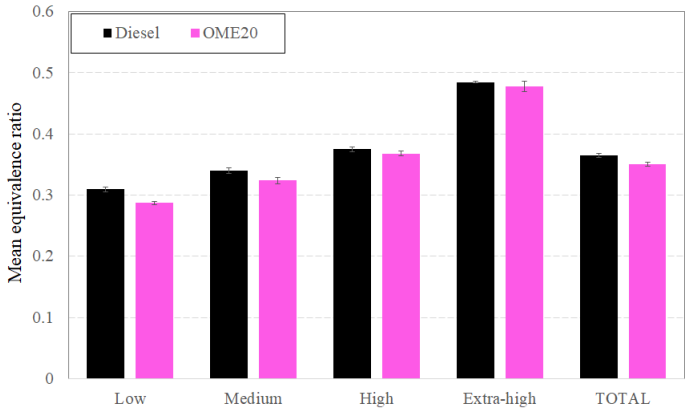

Figure 5.12: Mean equivalence ratio for each phase of the WLTC

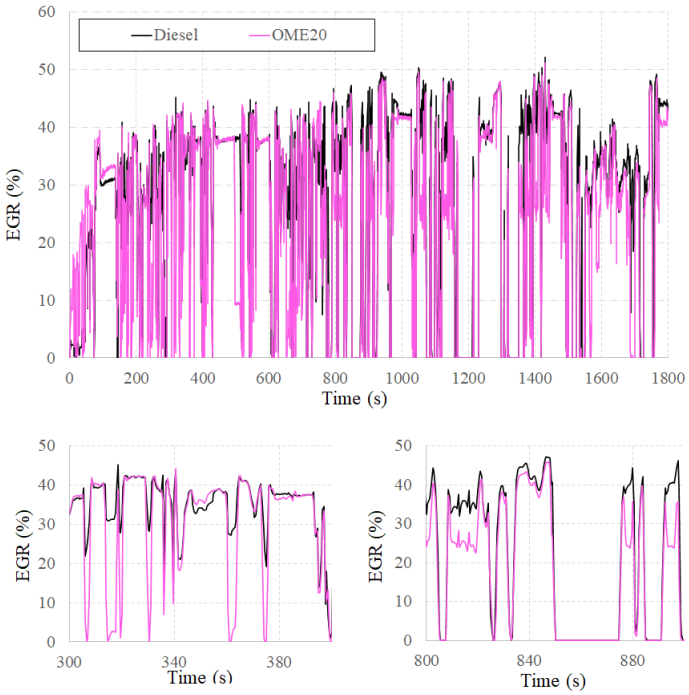

Figure 5.13: Instantaneous exhaust gas recirculation rate

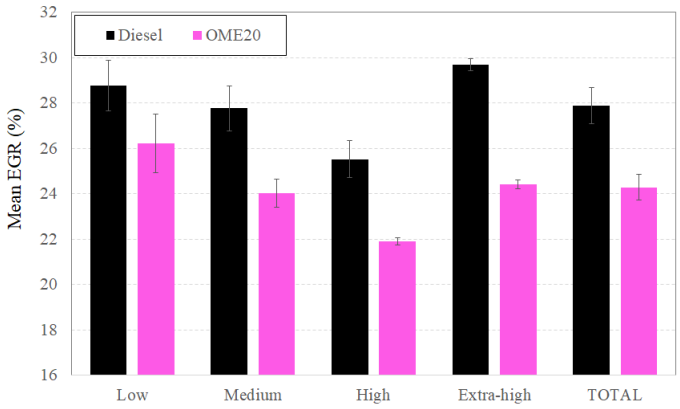

Figure 5.14: (Mean exhaust gas recirculation for each phase of the WLTC

Figures 5.13 and 5.14 show the instantaneous and mean EGR per each driving cycle phase. Engine emissions were markedly sensitive to the EGR rate, since small decreases in EGR lead to significant increases in NO formation and decreases in particle emissions, as discussed below. The EGR was inactive during both accelerations and decelerations. As the engine load increased, OME20 caused reduction in the EGR rate (**Figure** 5.13) due to its lower heating value which implied more fuel injected compared to diesel to reach the demanded power (**Figures** 5.9), thus modifying the accelerator position. This induced the EGR to decrease (see detailed example in **Figure** 5.13), either closing the EGR valves or opening the back-pressure valve, following the engine mapping strategy. Even more, during many accelerations, the EGR rate was nil for OME20 while it was not for diesel fuel (see detailed example in **Figure** 5.13), thus this explains the significant difference in the mean EGR rate per driving cycle phase (**Figure** 5.14).

5.4.2 Combustion diagnosis

Figure 5.15a shows the average instantaneous in-cylinder pressure and the average heat release rate (HRR) for each driving cycle phase. For OME20 the maximum combustion pressure was the highest, and both pressure rate and HRR peaks were advanced as the driving cycle progressed. In **Figure** 5.15b significant differences in the heat release rate for high speeds in the pilot injection and the main injection are noted. Due to the lower energy content for OME20, the amount of heat release during the pilot injection was lower compared to diesel. Therefore, for OME20, the peak of HRR in the main injection was higher than that of diesel fuel, causing an increase in the combustion rate, and consequently, shortening the combustion duration.

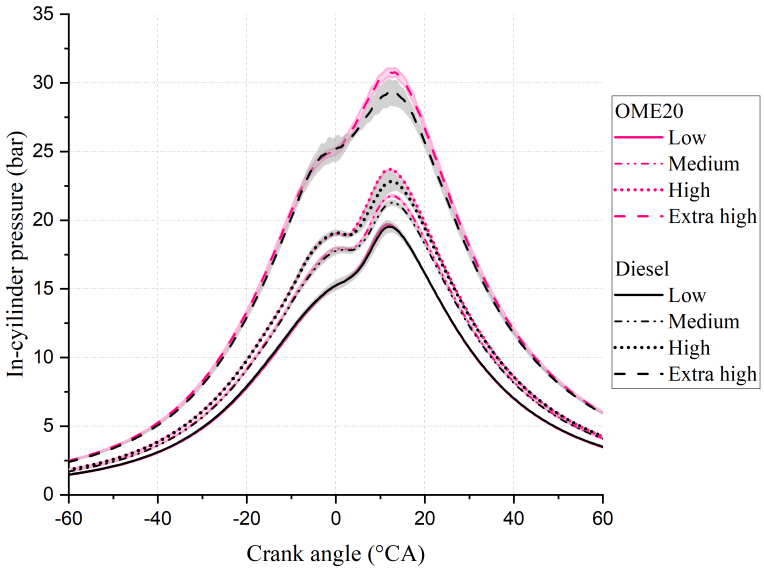

(a) In-cylinder pressure.

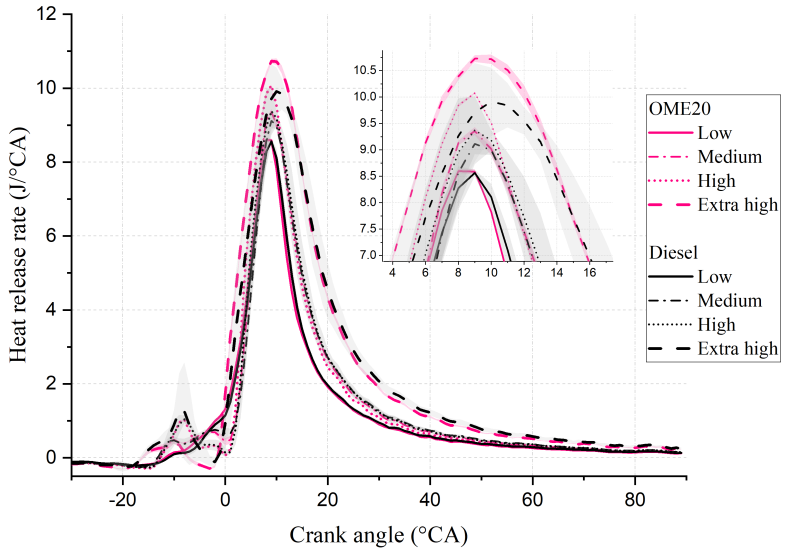

(b) Heat release rate.

Figure 5.15: In-cylinder pressure and heat release rate for each phase of the WLTC

It is believed that the OME's oxygen content and its high volatility promoted the combustion reaction leading to the increase of the burning rate, which increased

the peak of HRR for OME20 compared to diesel fuel. This effect could also be partially attributed to the lower EGR rate for OME20, as mentioned above. In fact, the highest difference between pressure peaks was found in the extra high-speed driving cycle phase and the smallest difference was in the low-speed phase, coincidently with the difference in the EGR rate (**Figure** 5.13). The resulting shortened combustion duration would explain the increased brake thermal efficiencies.

5.4.3 Gaseous emissions

The gaseous emissions, including NOx, CO and THC are shown in **Figures** 5.16, 5.17 and 5.18, respectively. **Figure** 5.16 shows the instantaneous (left) and accumulated (right) emissions of nitrogen oxides (NOx) and dioxide (NO2). The NOx emissions varied considerably during the driving cycle. For both fuels, NOx peaks were observed mainly during accelerations, because the EGR was not active since more fuel was injected. The highest differences in NOx emission peaks and in the increasing rate of accumulated NOx emissions occurred in the medium-speed phase, corresponding to the highest EGR rate peaks (**Figure** 5.13).

The highest NOx emissions for OME20 can be explained by both chemical and engine mapping effects. Chemical effects are related to fuel properties: both the oxygen content and high volatility facilitate oxygen-rich zones, which, together with high temperatures, promote the formation of NO. The engine mapping effects involve thermal and kinetic mechanisms. The thermal mechanism occurs because more OME20 fuel was required to achieve the demanded engine power. Since the accelerator pedal position was higher, leading to lower EGR rate compared to diesel fuel (**Figure** 5.13). This caused an increase in local combustion temperature and consequently high NO emissions formation. Finally, the lower EGR rate of OME20 increased the combustion velocity (EGR is a flame retarder), leading to higher pressure and thus higher temperature peaks which favor the NO formation.

At the end of the driving cycle, OME20 increased NOx emissions by 42% with respect to diesel fuel. Similar differences in both instantaneous and accumulated NO_2 emissions were observed, indicating that NO/NO_2 ratio remained constant regardless the engine operating conditions.

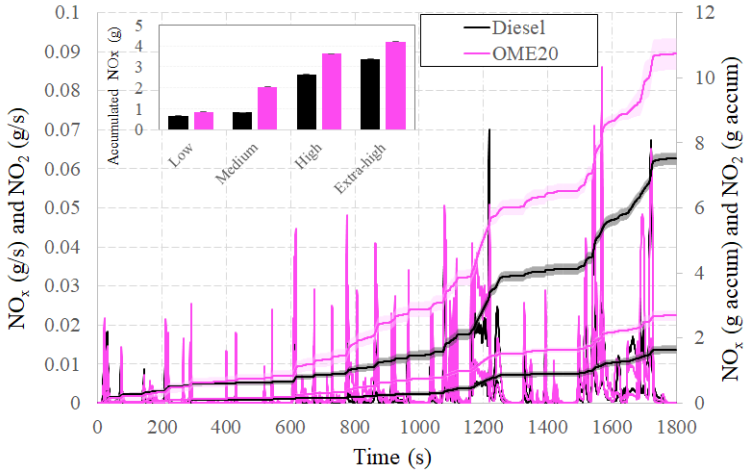

Figure 5.16: NOx and NO_2 emissions (left) instantaneous and (right) accumulated. Box inside represents the accumulated NOx emissions per driving cycle phase of the WLTC

Figure 5.17 shows the CO instantaneous (left) and accumulated emissions with both OME20 and diesel fuel. CO is mainly formed during cold-engine start conditions, since 58% of the CO was emitted in the low-speed driving cycle phase for both fuels. Increasing load increased combustion temperature leading to higher conversion efficiency in the diesel oxidation catalyst. It is for this reason that accelerations such as those around second 1000 resulted in lower CO emissions than at seconds 280 and 600. Additionally, a sharp increase in accumulated CO emissions can be observed in second 1200, which was caused by the LNT regeneration. The addition of OME to diesel fuel resulted in a 52% reduction in CO accumulated emissions compared to diesel because the additional oxygen in the fuel led to a better oxidation of CO to CO_2. When analyzing CO_2 emissions (not shown here), no significant differences were found between fuels, amounting around 2840 ± 40 g for both fuels at the end of the cycle.

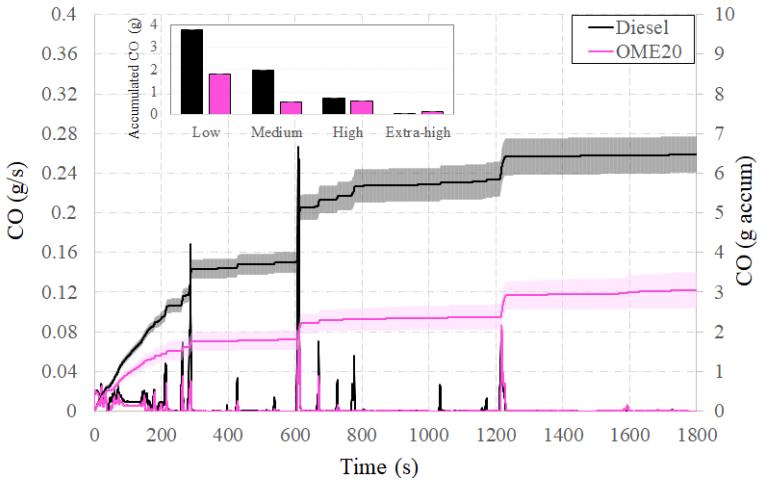

Figure 5.17: CO emissions (left) instantaneous and (right) accumulated. Box inside represents the accumulated CO emissions per driving cycle phase of the WLTC

Figure 5.18 shows the THC instantaneous (left) and accumulated emissions for both tested fuels. THC emissions followed the same trend than CO. At the beginning of the cycle, in the low-speed driving cycle phase, high THC emissions were associated with low in-cylinder temperature. However, although both CO and THC emissions are related to cold engine conditions, one difference between them is that CO is more sensitive to accelerations, while THC are permanently emitted throughout the driving cycle. After approximately 1200 s of the cycle, there is a peak of emissions with both fuels due to the LNT regeneration.

With OME20 an additional LNT regeneration occurred in the latest part of the extra high-speed phase because NOx emissions were high, therefore the LNT was saturated earlier than in the case of diesel, (as observed in **Figure** 5.16) leading to an increase in THC emissions (**Figure** 5.18). Such increase did not always take place at the same time in the cycle (either at second 1600 or at second 1680) which led to an apparent double peak of THC when averaging. This additional regeneration with OME20 partially compensated the reduction in THC emissions at the end of the cycle. Accumulated THC emissions were 17% lower for OME20 than for diesel fuel. This decrease can be mainly explained by the reduction in EGR, and the lower equivalent ratio of OME20, which implied an excess of air, promoting a better THC and CO oxidation. However, it is likely that THC emissions were also influenced by the fuel formulation, since the oxygen content facilitated the combustion of fuel-rich areas, preventing the emission of unburned hydrocarbons.

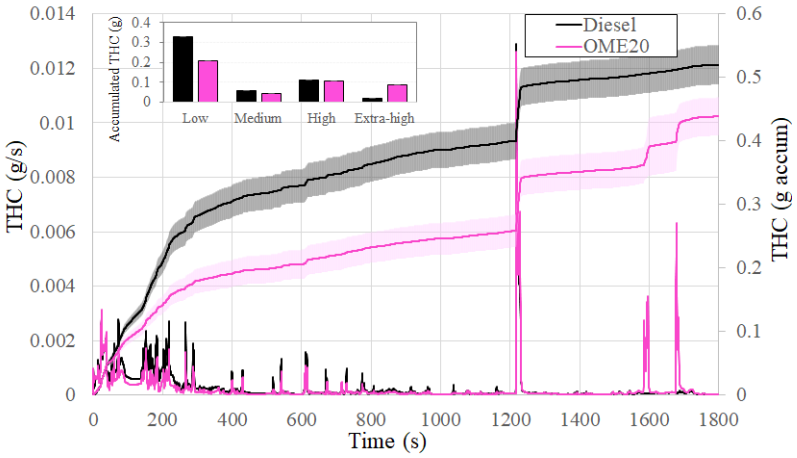

Figure 5.18: THC emissions (left) instantaneous and (right) accumulated. Box inside represents the accumulated THC emissions per driving cycle phase of the WLTC

5.4.4 Particle number emissions

Figure 5.19 shows both instantaneous and accumulated particle number (PN). The PN was higher in the acceleration periods, due to the higher equivalence ratio, resulting in a local lack of oxygen and poor combustion [46]. In these conditions, soot emissions increased and the solid particles in the accumulation mode increased. OME20 showed a marked effect on reducing PN compared to diesel fuel during the whole driving cycle, especially at the extra-high speed where the equivalence ratio is much higher. The total reduction in PN with OME20 was about 60% and can be explained by both chemical effects and engine mapping strategy. Chemical effects are mainly related to the fuel formulation since OME20 has lower aromatic content, fewer C-C bonds, and much higher oxygen content (11%) compared to neat diesel, thus promoting complete combustion and high in-cylinder temperature, which was favorable for soot oxidation. Previous studies have demonstrated that oxygenated fuels with higher number of C–C bonds promoted soot emissions even with similar oxygen content [47]. Regarding the engine mapping strategy, the deeper accelerator pedal position induced lower EGR rate (see **section** 5.4.1), which may have the following implications: a) it increases the combustion velocity, leading to higher temperature peaks, favoring the oxidation of the soot (kinetic effects), b) it increases the oxygen concentration in the intake charge, reducing the formation of soot and facilitating its oxidation. However, such deeper pedal acceleration does not compensate the higher stoichiometric fuel/air ratio, leading to a leaner combustion condition. These effects enhanced the PN reduction, and together with the OME20 properties, reduced PN emissions more than other equally oxygenated fuels (11% oxygen by weight) [48].

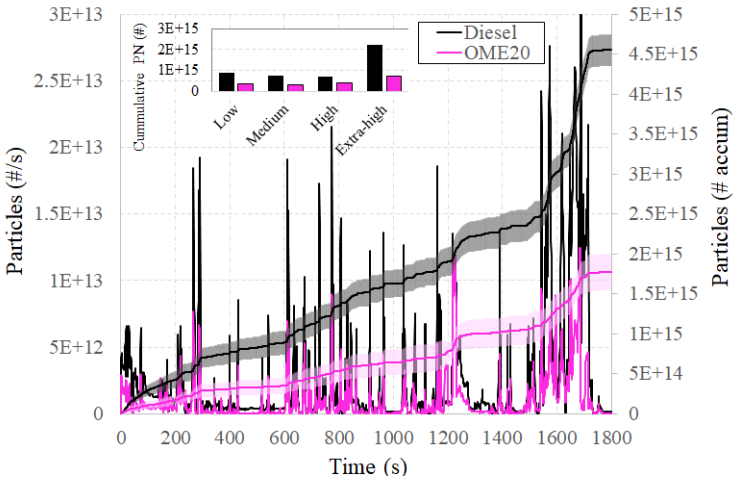

Figure 5.19: PN instantaneous (left) and accumulated (right) emissions

Figure 5.20 shows that the trend of the number of particles in the nucleation mode decreased and shifted from bimodal mode to accumulation mode and upwards and towards larger size as the driving cycle progressed. The bimodal distribution was clearly separated for the nucleation mode with solid particles smaller than 23 nm (not regulated in Euro 5 and 6 standards) and for the accumulation mode for solid particles larger than 23 nm (regulated). The particle size distribution showed a bimodal distribution at low-speed phase showing a distinctive nucleation mode with peak diameters around 9–10 nm, and an accumulation mode with peak diameters around 50–70 nm. This could be explained because when the engine is cold the amount of unburned hydrocarbons is high enough to saturate the soot particle surfaces by adsorption and heterogeneous nucleation, and subsequently favor homogeneous nucleation of small liquid particles [49]. As the cycle progresses, the in-cylinder temperature increased, and the unburned hydrocarbon emissions became relatively lower, and therefore the number of particles in nucleation mode decreased.

OME20 decreased the peak number concentrations of accumulation-mode particles at low, medium, high, and extra high-speed driving cycle phases by 54.3%, 39.7%, 71.5 and 23 %, respectively, and caused a slight shift of the particles toward smaller size compared to diesel fuel. The oxygen content prevents from soot nucleation and promotes the oxidation of the already formed soot, leading to a decrease in the number and size in soot agglomerates.

OME20 led to a reduction of PN in the nucleation mode at low-speed phase by 75%, due to the higher volatility and lower viscosity of OME20 which could improve atomization, evaporation and air mixing in the combustion chamber compared to diesel fuel. For the rest of the cycle phases, OME20 exhibited a unimodal distribution in accumulation mode particles with a maximum particle size range between 45 and

70 nm. In contrast, diesel showed a bimodal distribution in the low, medium, and high-speed phases. For the low-speed phase, diesel doubled the number of particles in the nucleation mode compared to particles in the accumulation mode.

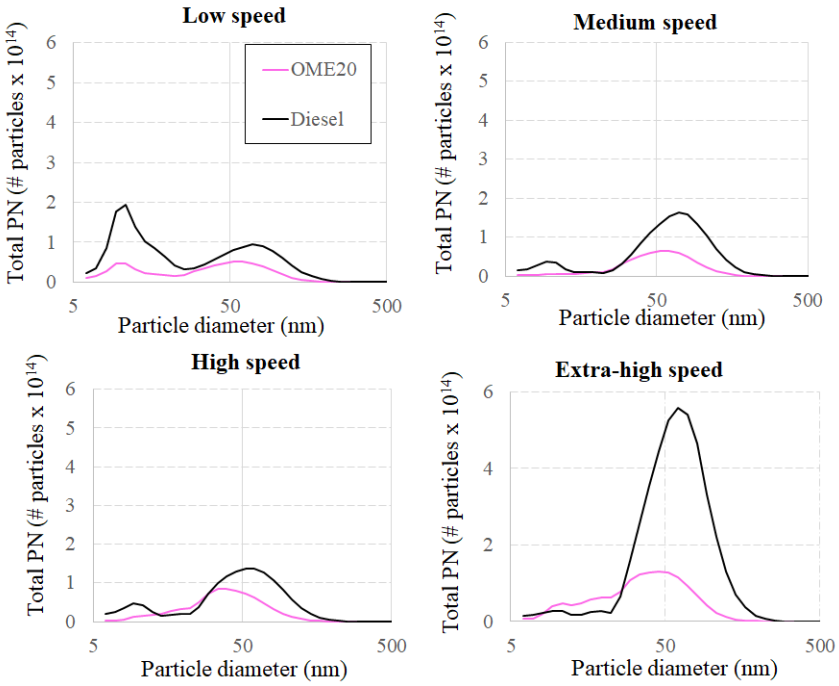

Figure 5.20: Particle size distribution per driving cycle phase of the WLTC

Significant particle reductions have been reported when diesel-OME blends are used in internal combustion engines. Despite most studies do not make any changes to the engine mapping strategy, most authors attribute these reductions mainly to fuel properties, since OME fuel is composed of C-O-C bonds, and in the chemical mechanism reaction pathway, there is no direct way leading to olefin formation (C=C), which are important soot precursors [50]. In addition, its high oxygen content plays an important role in reducing soot. Liu et al. [44] reported up to 47.6% smoke emission reduction with 30% of OME blended with diesel. In a subsequent study [51], they showed a maximum reduction in the total PN of 28% with the same OME blend. These reductions were associated with the fuel compositional effects, such as the lack of C-C bonds and the intramolecular oxygen, the high cetane number and the low viscosity and boiling temperature which improved the interior fuel atomization making the combustion of air-fuel mixture faster than diesel fuel. The experiments were performed on a 4-cylinder turbocharged intercooled common-rail diesel engine, operating under steady state. Omari et al. [52] reported a particle matter reduction around 70–90% with 35% of OME. Such reduction was attributed to the high molecular oxygen content, which improved the local oxidation conditions, the high cetane

number, as well as the high burned mass fraction, leaving less fuel to be partially oxidized in the burn-out phase. The experiments were carried out in a single cylinder engine - 0.39L, at 5 different steady state operating points, maintaining constant the center of combustion for each load point and for all EGR rates. Wu et al. [4] showed a smoke opacity reduction up to 93% by blending 25% of OME with diesel in a L12 small agricultural engine. The higher oxygen content and no C–C bonds were the main reasons argued for the achieved soot reduction.

Based on the results of this study, it can be concluded that, besides the effects associated with the fuel chemical composition, the changes in the EGR rate and in the equivalence ratio derived from the engine mapping strategy have a significant impact on the change of regulated emissions relative to diesel.

5.5 Conclusions

From the results presented in this chapter, the following conclusions can be drawn:

Regarding unregulated emissions and apoptosis

- Unregulated emissions such as PAH and carbonyls, despite being influenced by the fuel properties were markedly sensitive to the driving cycle conditions.

- High carbonyl emissions in the low-speed phase were associated with low in-cylinder temperature caused by the cold start conditions. Carbonyl emission factors exceed PAH emissions, contributing substantially to total gas phase organic emissions.

- Oxygenated fuel blends did not increase carbonyl emissions compared to oxygen-free fuels, since the combustion-related factors influenced carbonyl formation more than fuel composition.

- The majority of the PAH are emitted in the gas-phase. However, according to their physicochemical properties, high molecular weight PAH showed a higher tendency to condense and adhere to particles, thus the toxicity associated with carcinogenic PAH is equivalent in both phases.

- HVO exhibited the lowest PAH and carbonyl emissions and OFP, while diesel exhibited the highest *OFP* due to high carbonyl emissions in the low-speed phase.

- Although the net carbon emissions could be decreased with the use of zero carbon footprint biofuels and their blends with diesel, unregulated harmful compounds such as some PAH and carbonyls can remain being emitted or even

increased.

- All gas phase-derived samples induced apoptosis, which was caused partly by PAH and partly by carbonyl emissions.

Regulated emissions and performance using polyoxymethylene dimethyl ether

- OME20 led to an increase in fuel consumption proportional to the reduced heating value. However, no significant differences in the total brake thermal efficiency at the end of the driving cycle were observed. The high efficiency at the initial phases was compensated by the lower efficiency at the extra high-speed phase.

- OME20 caused a lower EGR rate (even nil during many accelerations) compared to diesel, as a consequence of the specific engine mapping strategy.

- The lower EGR rate with OME20 (engine mapping effect), the oxygen content and the higher volatility (chemical effects) compare to diesel lead to an increase of the burning rate, increasing the average in-cylinder pressure and heat release rate peaks, and consequently, shortening the combustion duration.

- NOx emissions increased with OME20 as a consequence of different reasons as follows: the increase in the local combustion temperature due to the low EGR rate, and to the high combustion velocity (engine mapping effects). In addition, the oxygen-rich zones due to the fuel-bound oxygen and the high local temperatures promote the formation of NO (chemical effects).

- Total THC and CO emissions were lower for OME20 than for diesel fuel due to a better oxidation of these pollutants as a consequence of the lower equivalence ratio (engine mapping effects). THC emissions were also influenced by the oxygen content of the blend, which improves the combustion of fuel-rich areas and increases the efficiencies of the oxidation catalyst (chemical effects).

- The use of OME20 with 11% oxygen in a Euro 6b engine, which has a specific mapping to maintain the NOx-PM trade-off, reduced PN by 61%. The combination of chemical reasons related to fuel formulation, together with engine mapping strategy, were responsible for this marked reduction in PN emissions.

Bibliography

[1] G. Karavalakis, G. Deves, G. Fontaras, S. Stournas, Z. Samaras, and E. Bakeas. The impact of soy-based biodiesel on pah, nitro-pah and oxy-pah emissions from a passenger car operated over regulated and nonregulated driving cycles. *Fuel*, 89(12):3876–3883, 2010.

[2] Fikret Inal and Selim M. Senkan. Effects of oxygenate additives on polycyclic aromatic hydrocarbons (PAHs) and soot formation. *Combustion Science and Technology*, 174(9):1–19, 2002.

[3] V. I. Babushok and W. Tsang. Kinetic modeling of heptane combustion and PAH formation. *Journal of Propulsion and Power*, 20(3):403–414, 2004.

[4] Shiliang Wu, Jiajing Bao, Ziwei Wang, Huiyan Zhang, and Rui Xiao. The regulated emissions and PAH emissions of bio-based long-chain ethers in a diesel engine. *Fuel Processing Technology*, 214, 2021.

[5] Soo Young No. Paraffinic Biofuels: HVO, BTL Diesel, and Farnesane. In *Application of Liquid Biofuels to Internal Combustion Engines*, pages 147–172. Springer, 2019.

[6] Charles J Mueller, Lyle M Pickett, Dennis L Siebers, and Glen C Martin. Effects of Oxygenates on Soot Processes in DI Diesel Engines : Experiments and Numerical Simulations. 2018.

[7] G.A. Westphal, J. Krahl, A. Munack, N. Rosenkranz, O. Schröder, J. Schaak, C. Pabst, T. Brüning, and J. Bünger. Combustion of hydrotreated vegetable oil and jatropha methyl ester in a heavy duty engine: Emissions and bacterial mutagenicity. *Environmental Science and Technology*, 47(11):6038–6046, 2013.

[8] Xinyue Cao, Xuewei Hao, Xianbao Shen, Xi Jiang, Bobo Wu, and Zhiliang Yao. Emission characteristics of polycyclic aromatic hydrocarbons and nitro-polycyclic aromatic hydrocarbons from diesel trucks based on on-road measurements. *Atmospheric Environment*, 148:190–196, 2017.

[9] B. Zielinska, J. Sagebiel, W. P. Arnott, C. F. Rogers, K. E. Kelly, D. A. Wagner, J. S. Lighty, A. F. Sarofim, and G. Palmer. Phase and Size Distribution of

Polycyclic Aromatic Hydrocarbons in Diesel and Gasoline Vehicle Emissions. *Environmental Science and Technology*, 38(9):2557–2567, 2004.

[10] McKenzie C.H. Lim, Godwin A. Ayoko, Lidia Morawska, Zoran D. Ristovski, and E. Rohan Jayaratne. Effect of fuel composition and engine operating conditions on polycyclic aromatic hydrocarbon emissions from a fleet of heavy-duty diesel buses. *Atmospheric Environment*, 39(40):7836–7848, 2005.

[11] Roger Westerholm and Li Hang. A Multivariate Statistical Analysis of Fuel-Related Polycyclic Aromatic Hydrocarbon Emissions from Heavy-Duty Diesel Vehicles. *Environmental Science and Technology*, 28(5):965–972, 1994.

[12] Xuan Zheng, Ye Wu, Shaojun Zhang, Jingnan Hu, K. Max Zhang, Zhenhua Li, Liqiang He, and Jiming Hao. Characterizing particulate polycyclic aromatic hydrocarbon emissions from diesel vehicles using a portable emissions measurement system. *Scientific Reports*, 7(1), 2017.

[13] Effects of driving behavior on real-world emissions of particulate matter, gaseous pollutants and particle-bound PAHs for diesel trucks. *Environmental Pollution*, 286(April):117292, 2021.

[14] Hsiao Hsuan Mi, Wen Jhy Lee, Chung Ban Chen, Hsi Hsien Yang, and Sheng Jong Wu. Effect of fuel aromatic content on PAH emission from a heavy-duty diesel engine. *Chemosphere*, 41(11):1783–1790, 2000.

[15] Maria L. Botero, Carolina Mendoza, Silvana Arias, Oscar D. Hincapié, John R. Agudelo, and Isabel C. Ortiz. In vitro evaluation of the cytotoxicity, mutagenicity and DNA damage induced by particle matter and gaseous emissions from a medium-duty diesel vehicle under real driving conditions using palm oil biodiesel blends. *Environmental Pollution*, 265, 2020.

[16] H.A. Dandajeh, M. Talibi, N. Ladommatos, and P. Hellier. Influence of combustion characteristics and fuel composition on exhaust pahs in a compression ignition engine. *Energies*, 12(13), 2019.

[17] L. Zou and S. Atkinson. Characterising vehicle emissions from the burning of biodiesel made from vegetable oil. *Environmental Technology (United Kingdom)*, 24(10):1253–1260, 2003.

[18] M. De Joannon, R. Ragucci, A. Cavaliere, and A. Ciajolo. Identification of oxygenated compounds in combustion systems. *Chemosphere*, 42(5-7):843–851, 2001.

[19] P.F. Nelson, A.R. Tibbett, and S.J. Day. Effects of vehicle type and fuel quality on real world toxic emissions from diesel vehicles. *Atmospheric Environment*, 42(21):5291–5303, 2008.

[20] T. Wagner. Aldehydes and ketones in engine exhaust emissions -a review. *Proceedings of the Institution of Mechanical Engineers, Part D: Journal of Automobile Engineering*, 210(2):109–122, 1996.

[21] Georgios Karavalakis, Vasiliki Boutsika, Stamoulis Stournas, and Evangelos Bakeas. Biodiesel emissions profile in modern diesel vehicles. Part 2: Effect of biodiesel origin on carbonyl, PAH, nitro-PAH and oxy-PAH emissions. *Science of The Total Environment*, 409(4):738–747, jan 2011.

[22] Keishi Takada, Futoshi Yoshimura, Yasushi Ohga, Jin Kusaka, and Yasuhiro Daisho. Experimental study on unregulated emission characteristics of turbocharged di diesel engine with common rail fuel injection system. *SAE Technical Papers*, 2003.

[23] David Donoso, David Bolonio, Rosario Ballesteros, Magín Lapuerta, and Laureano Canoira. Hydrogenated orange oil: A waste derived drop-in biojet fuel. *Renewable Energy*, 188:1049–1058, 2022.

[24] David Donoso, Rosario Ballesteros, David Bolonio, María-Jesús García-Martínez, Magín Lapuerta, and Laureano Canoira. Hydrogenated turpentine: A biobased component for jet fuel. *Energy & Fuels*, 35(2):1465–1475, 2021.

[25] Yusuke Ishizuka, Masahiro Tokumura, Atsushi Mizukoshi, Miyuki Noguchi, and Yukio Yanagisawa. Measurement of secondary products during oxidation reactions of terpenes and ozone based on the PTR-MS analysis: Effects of coexistent carbonyl compounds. *International Journal of Environmental Research and Public Health*, 7(11):3853–3870, 2010.

[26] H.-J. Liu, R.-H. Chen, and W.-C. Wang. The non-regulated emissions from a turbo-charged diesel engine under steady-state operation with hydro-processed renewable diesel (hrd). *Fuel*, 263, 2020.

[27] Paul F. Schubert, Branch J. Russell, Robert L. Freerks, Jason Devore, and E. Robert Fanick. Impact of ultra-clean Fischer-Tropsch diesel fuel on emissions in a light duty passenger car diesel engine. *SAE Technical Papers*, 2002.

[28] Bin Hao, Chonglin Song, Gang Lv, Bo Li, Xiaofang Liu, Kan Wang, and Yaowu Liu. Evaluation of the reduction in carbonyl emissions from a diesel engine using Fischer-Tropsch fuel synthesized from coal. *Fuel*, 133:115–122, 2014.

[29] Chao He, Yunshan Ge, Jianwei Tan, Kewei You, Xunkun Han, Junfang Wang, Qiuwen You, and Asad Naeem Shah. Comparison of carbonyl compounds emissions from diesel engine fueled with biodiesel and diesel. *Atmospheric Environment*, 43(24):3657–3661, 2009.

[30] Xinyue Cao, Sijie Feng, Xianbao Shen, Xin Li, Xiaolong Yao, and Zhiliang Yao. The effects of biodiesel blends on real-world carbonyl emissions from diesel trucks. *Atmospheric Environment*, 238, 2020.

[31] C. Fan, C. Song, G. Lv, G. Wang, H. Zhou, and X. Jing. Evaluation of carbonyl compound emissions from a non-road machinery diesel engine fueled with a methanol/diesel blend. *Applied Thermal Engineering*, 129:1382–1391, 2018.

[32] Xiaobing Pang, Xiaoyan Shi, Yujing Mu, Hong He, Shijin Shuai, Hu Chen, and Rulong Li. Characteristics of carbonyl compounds emission from a diesel-engine using biodiesel-ethanol-diesel as fuel. *Atmospheric Environment*, 40(36):7057–7065, 2006.

[33] Sérgio Machado Corrêa and Graciela Arbilla. Carbonyl emissions in diesel and biodiesel exhaust. *Atmospheric Environment*, 42(4):769–775, 2008.

[34] P.-M. Yang, Y.-C. Lin, K.C. Lin, S.-R. Jhang, S.-C. Chen, C.-C. Wang, and Y.-C. Lin. Comparison of carbonyl compound emissions from a diesel engine generator fueled with blends of n-butanol, biodiesel and diesel. *Energy*, 90:266–273, 2015.

[35] Chiung Yu Peng, Hsi Hsien Yang, Cheng Hang Lan, and Shu Mei Chien. Effects of the biodiesel blend fuel on aldehyde emissions from diesel engine exhaust. *Atmospheric Environment*, 42(5):906–915, 2008.

[36] Tie Li, Masaru Suzuki, and Hideyuki Ogawa. Effects of ethyl tert-butyl ether addition to diesel fuel on characteristics of combustion and exhaust emissions of diesel engines. *Fuel*, 88(10):2017–2024, 2009.

[37] Ruina Li, Zhong Wang, and Guangju Xu. Study on Carbonyl Emissions of Diesel Engine Fueled with Biodiesel. *International Journal of Chemical Engineering*, 2017, 2017.

[38] Thalita Oliveira Da Silva and Pedro Afonso De Paula Pereira. Influence of time, surface-to-volume ratio, and heating process (continuous or intermittent) on the emission rates of selected carbonyl compounds during thermal oxidation of palm and soybean oils. *Journal of Agricultural and Food Chemistry*, 56(9):3129–3135, 2008.

[39] D. Dong, M. Shao, Y. Li, S. Lu, Y. Wang, Z. Ji, and D. Tang. Carbonyl emissions from heavy-duty diesel vehicle exhaust in china and the contribution to ozone formation potential. *Journal of Environmental Sciences (China)*, 26(1):122–128, 2014.

[40] V. Bermúdez Vicente, José M. Lujan, Benjamín Pla, and Waldemar G. Linares. Comparative study of regulated and unregulated gaseous emissions during NEDC in a light-duty diesel engine fuelled with Fischer Tropsch and biodiesel fuels. *Biomass and Bioenergy*, 35(2):789–798, 2011.

[41] Jiun Horng Tsai, Sheng You Chang, and Hung Lung Chiang. Volatile organic compounds from the exhaust of light-duty diesel vehicles. *Atmospheric Environment*, 61:499–506, 2012.

[42] Anita Solhaug, Magne Refsnes, Marit Låg, Per E. Schwarze, Trine Husøy, and Jørn A. Holme. Polycyclic aromatic hydrocarbons induce both apoptotic and anti-apoptotic signals in Hepa1c1c7 cells. *Carcinogenesis*, 25(5):809–819, 2004.

[43] Silvana Arias, Verónica Estrada, Isabel C. Ortiz, Francisco J. Molina, and John R. Agudelo. Biological toxicity risk assessment of two potential neutral carbon diesel fuel substitutes. *Environmental Pollution*, 308(52):119677, 2022.

[44] Junheng Liu, Ping Sun, He Huang, Jian Meng, and Xiaohua Yao. Experimental investigation on performance, combustion and emission characteristics of a common-rail diesel engine fueled with polyoxymethylene dimethyl ethers-diesel blends. *Applied Energy*, 202:527–536, 2017.

[45] Yuwei Zhao, Yijing Xie, Xiaochen Wang, Zheyang Li, Tianlin Niu, and Shenghua Liu. Energy balance analysis, combustion characteristics, and particulate number concentration-NOx trade-off of a heavy-duty diesel engine fueled with various PODEn/diesel blends. *Energy Conversion and Management*, 225, 2020.

[46] D. T. Hountalas, G. C. Mavropoulos, and K. B. Binder. Effect of exhaust gas recirculation (EGR) temperature for various EGR rates on heavy duty DI diesel engine performance and emissions. *Energy*, 33(2):272–283, 2008.

[47] Wonah Park, Seunghyun Park, Rolf D. Reitz, and Eric Kurtz. The effect of oxygenated fuel properties on diesel spray combustion and soot formation. *Combustion and Flame*, 180:276–283, 2017.

[48] A. N. Shah, G. Yun-shan, F. H. Shah, H. U. Mughal, Z. U. Rahman, and A. Naveed. Effect of biodiesel on particulate numbers and composition emitted from turbocharged diesel engine. *International Journal of Environmental Science and Technology*, 11(2):385–394, 2014.

[49] Jerzy Merkisz and Jacek Pielecha. The process of formation of particulate matter in combustion engines. *Springer Tracts on Transportation and Traffic*, 8:19–25, 2015.

[50] Tianting Wang, Junheng Liu, Ping Sun, Qian Ji, Wanying Gao, and Chen Yang. Influence of injection parameters on combustion, gaseous emissions and particle size distribution of a CRDI diesel engine operating with PODE/diesel blends. *Fuel*, 281, 2020.

[51] Junheng Liu, Zengguang Liu, Lejian Wang, Pan Wang, Ping Sun, Hongjie Ma, and Pengcheng Wu. Effects of PODE/diesel blends on particulate matter emission and particle oxidation characteristics of a common-rail diesel engine. *Fuel Processing Technology*, 212, 2021.

[52] Ahmad Omari, Benedikt Heuser, Stefan Pischinger, and Christoph Rüdinger. Potential of long-chain oxymethylene ether and oxymethylene ether-diesel blends for ultra-low emission engines. *Applied Energy*, 239:1242–1249, 2019.

Chapter 6

Conclusions

The main motivation of this thesis was to investigate the influence of different conventional and unconventional advanced biofuels on the emissions of unregulated compounds and their impact on the biological response. This was accomplished using different analysis and characterization methodologies, some of them, used for the first time in engine emissions. A variety of fuels were selected to be reference of commercial transportation fuels.

6.1 Findings of this work

Regarding unregulated emissions

- Independently of engine test state, in steady or transient mode, and biofuel blend, most of the PAH were present in the gas-phase, with predominance of those between 3 and 4 rings. However, most human health hazardous PAH, heavier PAH (DB[a,l]P and B[a]P), were predominant in the particle phase, instead of gas phase.

- Although the alternative biofuels used in this thesis were aromatic-free, the in-cylinder combustion process, and the pyrolysis and pyrosynthesis reactions of lower molecular weight hydrocarbon compounds induced the formation of aromatic rings through condensation products, which implied even higher PAH emissions than with diesel in some cases.

- Under transient state conditions, both unregulated emissions PAH and carbonyls, despite being influenced by the fuel properties, were markedly sensitive to the driving cycle conditions, especially at cold start conditions, which exacerbate the emission trends.

- Independently of engine test state, in steady or transient mode, carbonyl emission factors exceed PAH emissions, contributing substantially to total gas phase organic emissions.

- Carbonyl emissions for pentanol were the highest among all tested fuels followed by butanol blend. This was explained by the hydroxyl-group of the linear alcohol. As a consequence, pentanol fuel blends exhibited the highest ozone formation potential. The *OFP* of renewable diesel, ULSD and their blends was similar.

Although the main concerns are related to a potential increase in regulated emissions, other toxic unregulated pollutants also increase during the vehicle fleet conversion from petroleum diesel to alternative biofuels. This is a very important subject, due to the impact that vehicle emissions have on air pollution and on health.

Regarding biological activity

- One of the mechanisms behind the genotoxicity of SOF from PM was due to the induction of oxidative DNA damage through the generation of ROS. This, since the addition of the FPG and Endo III enzymes resulted in a significant increase in the comet tail for all tested fuel blends.

- PM derived samples from the tested biofuel blends with diesel exhibited genotoxic effects, however none of them showed cytotoxicity nor ecotoxicity effects.

- The toxicological potency from the tested biofuels did not correlate to PAH equivalent toxicity. it means that the biological response is generated also by other toxic compounds which are not included in the BaP-TEQ index.

- Since the apoptosis assay is a measure of cytotoxicity, and comparing the steady and transient-state cytotoxicity results, it can be concluded that the gas phase induces cytotoxicity, while the particles tend to induce genotoxicity through oxidative damage.

- The lower aromatic content of the fuel did not imply a lower BaP-TEQ.

- The higher carbonyl emissions resulted in higher cancer risk. However, the CR for trespasser/ recreational receptor were below the threshold suggested by the U.S EPA for carcinogenic chemicals.

Regarding regulated emissions with OME20

- OME20 caused very sharp particulate matter emission reductions at the expense of some increases in NOx emissions. However, it has been demonstrated that in modern engines, the effects of the fuel chemical characteristics on the engine emissions is "multiplied" by the engine mapping strategy, and separating both effects is really challenging.

From these results, it is clear that OME fuel has the potential to achieve a cleaner combustion for diesel engines in terms of regulated and unregulated emissions. Nonetheless, to make effective this potential, it is needed to promote changes in the legislation to consider unregulated emissions with potential health effects.

6.2 Suggestions for future work

In this thesis evidence was collected on the unregulated emissions from a broad gruop of biofuels, particularly, I focused on two of the main groups of pollutants, PAHs and carbonyls, however there are other even more toxic compounds that should be considered, for example the nitrated and oxygenated PAH derivatives. PAH derivatives generally possess at least one heteroatomcontaining substituted group attached to the parent fused-ring structures. In regard to toxicity, the parent PAH may undergo photochemical reactions with NO_2, OH, and/or O_3 yielding even more toxic PAH derivatives, whic are suspect to cause overproduction of reactive oxygen species, contributing to oxidative stress and some inflammatory processes, supposedly responsible for triggering many diseases.

A natural progression from this work would be to study the biological response in selective cell lines to specific unregulated compounds. In this way it would be possible to find the correlation between the cellular response and the specific emission of pollutants. Below are some selective strains to unregulated contaminants that could be evaluated:

Strain	**Sensitive to:**
TA98	Environmental mutagens (PAH)
TA97a	Intercalating mutagens (metals)
TA104	Oxidative mutagens (carbonyls and oxy-PAHs)
YG1041	Nitro-PAH (-S9) and aromatic amines (+S9)
YG5185	PAH

Nomenclature

Abbreviations

ICE	Internal combustion engines
DME	Dimethyl ether
HVO	Hydrotreated vegetable oil
HO	Hydrogenated orange oil
HT	Hydrogenated turpentine
OME	Polyoxymethylene dimethyl ether
PAH	Polycyclic aromatic hydrocarbons
LMW	Low molecular weight
MMW	Medium molecular weight
HMW	High molecular weight
U.S.EPA	American Environmental Protection Agency
BaP	Benzo(a)pyrene
ROS	Reactive oxygen species
PM	Particulate matter
CN	Cetane number
LHV	Lower Heating Value
FAME	Fatty Acid Methyl Ester
DPF	Diesel particle filter
BSFC	Brake-specific fuel consumption
BTE	Break thermal efficiency
EGR	Exhaust gas recirculation
SOF	Soluble organic fraction
WSF	Water-soluble fraction
ULSD	Ultra-low sulfur diesel
Bu13	13% by volume of butanol blended with ULSD
HVO13	13% by volume of HVO blended with ULSD
HVO20	20% by volume of HVO blended with ULSD
Pe13	13% by volume of pentanol blended with ULSD
Pe15	15.5% by volume of pentanol blended with ULSD

Pe20	20% by volume of pentanol blended with ULSD
MTT	3-(4,5-dimethylthiazol-2-yl) -2,5-diphenyltetrazole bromide
FPG	Formamidopyrimidine DNA glycosylase
Endo III	Endonuclease III
IF	Induction frequency
PHWE	Pressurized hot water extraction
VADLLE	Vortex-assisted dispersive liquid–liquid microextraction
TEF	Toxicity risk equivalency factors
8-oxodG	8-oxo-7,8-dihydroguanine
VSP	Vehicular Specific Power
WLTC	World-wide harmonized Light duty Test Cycle
EI	Electron impact mode
MSD	Mass selective detector
DNPH	2,4-dinitrophenylhydrazine
VOCs	Volatile Organic Compounds
MIR	Maximum incremental reactivity
IUR	Inhalation unit risk
HepG2	Human Hepatocarcinoma epithelial cell line
DOC	Diesel oxidation catalyst
LNT	Lean NOx Trap
ECU	Electronic Control Unit
RLS	Road Load Simulation
THC	Total hydrocarbon emission
EEPS	Engine Exhaust Particle Sizer
NDIR	Non-dispersive infrared detector
RD	Rotating disc
TC	Thermal conditioner
FBS	Fetal bovine serum
HACA	Hydrogen-abstraction/acetylene-addition

Upper-case Roman

C_i	Individual compound emission factor (in μg/kWh or μg/km)
OFP	Ozone formation potential
$BaP-TEQ$	Equivalence toxicity to benzo(a)pyrene
EC	Exposure concentrations (in μg/m^3)
CA	Carbonyl concentration (in μg/m^3)
ET	Exposure time (hours/day)
EF	Exposure frequency (days/year)
ED	Exposure duration (years)
AT	Averaging time
CR	Cancer risk

A_{cc}	Apoptotic carcinoma cells
N_{cc}	Carcinoma cells per section
AI	Apoptotic index

Appendix A

Appendix to Chapter 3

A.1 Calibration curves

Table A.1: Analyte and deuterate areas for PAH calibration in steady state tests.

Concentration [ug/L]	10	25	50	100	300
NAP-d8	19050152.75	12977387.84	15300989.97	13920441.61	25201491.19
Ace-d10	16042972.98	11083926.86	13249578.94	11972218.78	10741571.09
NAP	142487.87	324897.28	723783.00	1119351.32	3416367.02
Acy	178502.15	470173.94	1053808.44	1640836.85	5169546.94
Ace	128585.64	321055.41	735041.74	1147063.12	3554141.41
Phen-d10	23383335.30	16041126.04	19688631.29	17671974.03	15605505.90
Phen	161897.77	392241.51	913289.18	1424211.49	4363091.13
Ant	142935.99	355389.19	858962.72	1349223.53	4222694.70
Flu	166775.98	336466.17	684338.00	1011510.88	2995965.74
Pyr	165651.38	318070.80	746882.30	1178202.35	3702442.71
Cry-d12	17076088.93	11815080.88	14591904.62	12737332.42	11357157.28
Flt	142623.98	313523.99	735547.50	1185122.70	3701325.34
B[a]A	117682.89	288324.63	678528.59	1053070.43	3373357.25
Cry	NF	290406.81	661738.44	1026645.02	3265348.02
Perylene-d12	6745655.81	4591098.68	5802489.68	5107628.95	4416547.90
B[b]F	118124.15	262023.47	615050.55	955359.08	3002980.19
B[k]F	94689.47	239194.67	555896.81	868724.93	2791526.98
B[e]P	104875.56	251088.00	584580.42	908750.38	2924483.33
B[a]P	104875.56	251088.00	584580.42	908750.38	2924483.33
DB[a,h]A	NF	10099.10	14128.92	10617.13	5871.20
IP	120617.22	278835.82	648781.42	988364.30	3179934.19
B[g,h,i]P	122274.13	296729.09	696758.16	1063829.52	3496515.96
DB[a,l]P	54776.85	123052.24	250554.85	438276.18	1411634.77

Table A.2: Area ratio (analyte/deuterate) for PAH calibration in steady state tests.

Area ratio (analyte/deuterate)					
Concentration [μg/L]	10	25	50	100	300
NAP	0.01	0.03	0.05	0.08	0.14
Acy	0.01	0.04	0.08	0.14	0.48
Ace	0.01	0.03	0.06	0.10	0.33
Phen	0.01	0.02	0.05	0.08	0.28
Ant	0.01	0.02	0.04	0.08	0.27
Flu	0.01	0.03	0.05	0.08	0.28
Pyr	0.01	0.03	0.05	0.09	0.33
Flt	0.01	0.02	0.04	0.07	0.24
B[a]A	0.01	0.02	0.05	0.08	0.30
Cry	0.00	0.02	0.05	0.08	0.29
B[b]F	0.02	0.06	0.11	0.19	0.68
B[k]F	0.01	0.05	0.10	0.17	0.63
B[e]P	0.02	0.05	0.10	0.18	0.66
B[a]P	0.02	0.05	0.10	0.18	0.66
DB[a,h]A	0.02	0.06	0.12	0.21	0.79
IP	0.02	0.06	0.11	0.19	0.72
B[g,h,i]P	0.02	0.06	0.12	0.21	0.79
DB[a,l]P	0.02	0.03	0.05	0.09	0.30

Table A.3: Calibration equation and R^2 for PAH in steady state tests.

PAH	**Calibration equation and R^2**
NAP	y = 0.0008398412x R² = 0.994
Acy	y = 0.0008398412x R² = 0.994
Ace	y = 0.0010890999x R² = 0.998
Phen	y = 0.0009196902x R² = 0.998
Ant	y = 0.0009196902x R² = 0.998
Flu	y = 0.0009258234x R² = 0.998
Pyr	y = 0.0010693098x R² = 0.998
Flt	y = 0.0007776994x R² = 0.998
B[a]A	y = 0.0009724295x R² = 0.997
Cry	y = 0.0009415981x R² = 0.997
B[b]F	y = 0.0022241496x R² = 0.997
B[k]F	y = 0.0025782014x R² = 0.996
B[e]P	y = 0.0021603445x R² = 0.996
B[a]P	y = 0.0021603445x R² = 0.996
DB[a,h]A	y = 0.0025782014x R² = 0.996
IP	y = 0.0023505913x R² = 0.996
B[g,h,i]P	y = 0.0025782014x R² = 0.996
DB[a,l]P	y = 0.0009854580x R² = 0.999

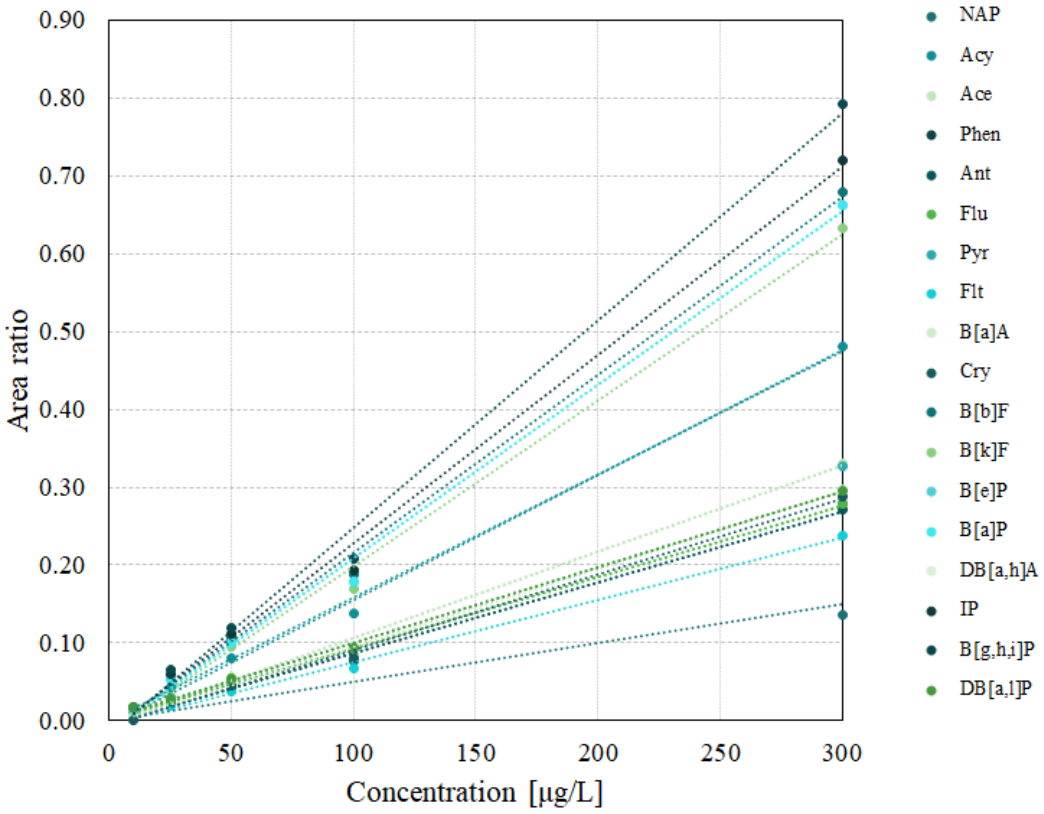

Figure A.1: Calibration curves for 18 PAH in steady state tests.

Table A.4: Analyte areas for carbonyls calibration in steady state tests.

Concentrations(μg/mL)	**40**	**20**	**10**	**5**	**1**	**0.6**
Formaldehyde	7052.5	3331.1	1399.3	842.1	206.1	134.3
Concentrations(μg/mL)	**20**	**10**	**5**	**2.5**	**0.5**	**0.3**
Acetaldehyde	3842.9	1818.8	758.2	459.5	113.2	71.5
Acrolein+Acetone	7734.1	3647.3	1528.4	915.5	232.5	146.4
Propionaldehyde	3564.8	1673.5	699.9	421.5	108.6	66.0
Crotonaldehyde	3317.4	1554.0	647.7	380.8	95.6	58.2
2-butanone	2983.3	1392.2	568.0	329.1	84.1	50.3
Butyraldehyde + Benzeldehyde	5126.8	2411.6	999.8	589.3	143.2	93.9
Valeraldehyde	3202.7	1549.3	641.7	384.8	93.2	58.9
Tolualdehyde	3395.2	1596.6	669.8	398.9	93.3	67.8
Hexaldehyde	2908.1	1358.6	584.3	335.5	79.6	51.4
Methacrolein	3242.9	1562.7	640.1	376.4	83.5	66.9

Table A.5: Calibration equation and R^2 for carbonyls in steady state tests.

Carbonyl	**Calibration equation and R^2**
Formaldehyde	y = 172.69x 0.996
Acetaldehyde	y = 188.23x 0.996
Acrolein+Acetone	y = 378.57x 0.996
Propionaldehyde	y = 174.31x 0.996
Crotonaldehyde	y = 162.05x 0.996
2-butanone	y = 145.43x 0.996
Butyraldehyde + Benzeldehyde	y = 250.61x 0.996
Valeraldehyde	y = 157.6x 0.997
Tolualdehyde	y = 166.07x 0.996
Hexaldehyde	y = 142.15x 0.997
Methacrolein	y = 159.31x 0.997

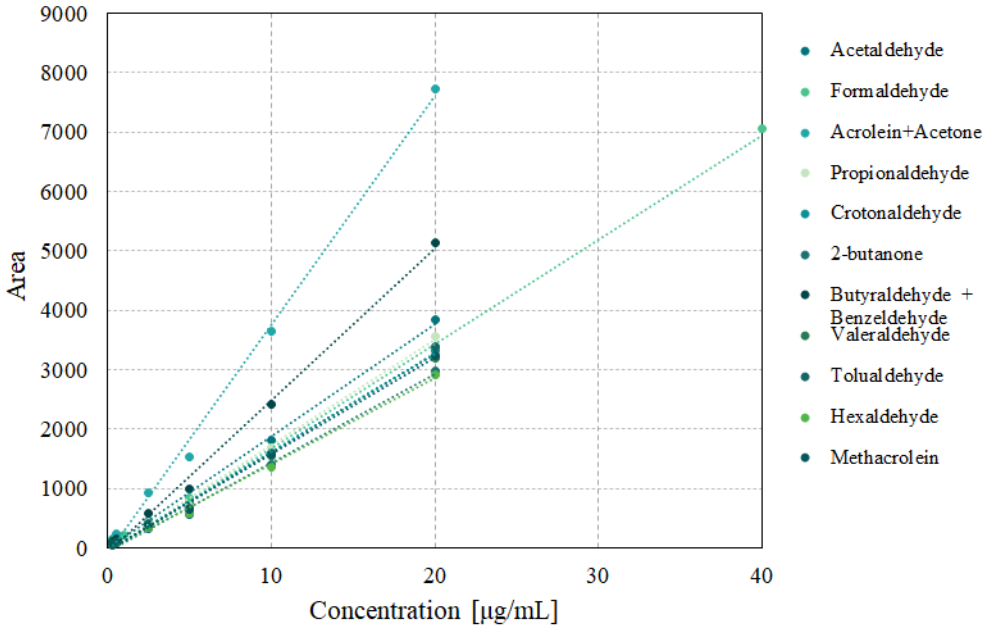

Figure A.2: Calibration curves for 13 carbonyls

Table A.6: Analyte areas for PAH calibration in transient state tests.

Concentration [ug/L]	**25**	**50**	**100**	**500**
NAP	6004481	14216239	20104993	71327820
Acy	282356	691512	1020027	4692763
Ace	430758	961020	1661084	6853430
Flu	1646099	3442296	4943274	26632873
Phen	4547997	12241078	17749248	64459726
Ant	9854131	19854734	24336919	65419643
Flt	1121853	3040462	4407291	21297632
Pyr	994069	2419533	3627543	16274342
B[a]A	2880923	6565823	11294837	43663106
Cry	3877225	8425291	13758741	45982180
B[b]F	3087337	6673957	11368906	37311473
B[k]F	2718622	5719784	9525324	31196928
B[a]P	2853895	6032219	10175433	37376090
DB[a,h]A	795034	1720805	2729675	11464149
B[g,h,i]P	1354529	2739967	4604278	20132565
IP	3564195	7260184	12127805	46169199

Table A.7: Calibration equation and R^2 for PAH in transient state tests.

PAH	**Calibration equation and R^2**
NAP	y= 146453x R²= 0.995
Acy	y=9463.3x R²= 0.998
Ace	y=13878x R²= 0.999
Flu	y=53298x R²= 0.997
Phen	y=131993x R²= 0.992
Ant	y=138271x R²= 0.997
Flt	y=42830x R²= 0.989
Pyr	y=32858x R²= 1.000
B[a]A	y=88784x R²= 0.999
Cry	y=94575x R²= 0.999
B[b]F	y=76783x R²= 1.000
B[k]F	y=64247x R²= 1.000
B[a]P	y=76308x R²= 0.999
DB[a,h]A	y=23225x R²= 0.999
B[g,h,i]P	y=40656x R²= 1.000
IP	y=94060x R²= 0.999

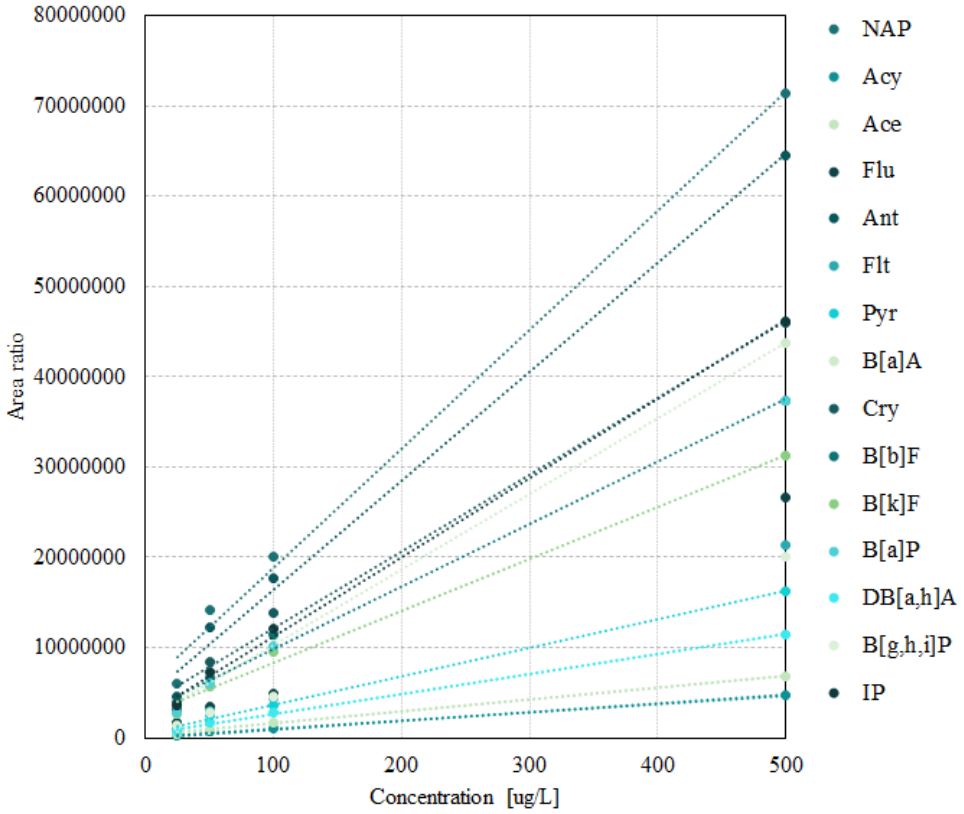

Figure A.3: Calibration curves for 16 PAH in transient state tests.

Table A.8: Analyte areas for carbonyls calibration in steady state tests.

Concentrations(μg/mL)	**40**	**20**	**10**	**5.2**	**1.2**
Formaldehyde	18819853.0	6910194.0	3566509	1810019	446470
Concentrations(ug/mL)	**20**	**10**	**5**	**2.6**	**0.6**
Acetaldehyde	5884853.0	2657568.0	1378071	701742	172229
Acroleina	5139783.0	2373652.0	1161997	618842	148745
Acetone	4201723.0	1860613.0	1017884	489944	124652
Propionaldehyde	4557777.0	2049304.0	1061733	538592	131710
Crotonaldehyde	3867383.0	1753354.0	902038	456789	110106
2-Butanone	4672682.0	2141213.0	1117327	562702	134415
Butiraldehyde + benzaldehyde	6478219.0	2918878.0	1493582	761700	185041
Valeraldehyde	2616973.0	1195800.0	623113	316180	70640
p-Tolualdehyde	3013189.0	1380950.0	719831	363710	83873
Hexaldehyde	2148109.0	991939.0	515788	262045	61694
Methacrolein	2548780.0	1175908.0	612201	305980	72526

Table A.9: Calibration equation and R^2 for carbonyls in transient state tests.

Carbonyl	**Calibration equation and R^2**
Formaldehyde	y=440037x R²= 0.981
Acetaldehyde	y=287700x R²= 0.997
Acroleina	y=251899x R²= 0.998
Acetone	y=204989x R²= 0.996
Propionaldehyde	y=222575x R²= 0.997
Crotonaldehyde	y=189140x R²= 0.998
2-Butanone	y=229264x R²= 0.998
Butiraldehyde + benzaldehyde	y=316306x R²= 0.997
Valeraldehyde	y=128312x R²= 0.998
p-Tolualdehyde	y=147840x R²= 0.998
Hexaldehyde	y=105576x R²= 0.998
Methacrolein	y=125225x R²= 0.998

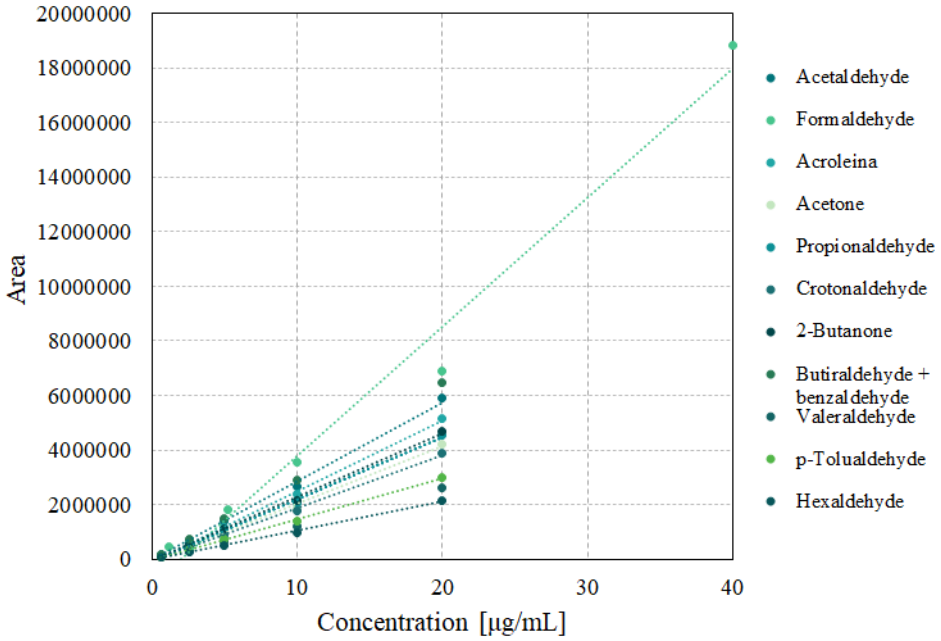

Figure A.4: Calibration curves for 13 carbonyls for transient state tests.

A.2 Experimental conditions during the exposure of *D. pulex*

Table A.10: Experimental conditions during the exposure of *D. pulex* to the samples.

Parameters	**Condition**
Test duration	48 h
Temperature	21 ± 2°C
Light intensity	538 – 1076 lux
Test concentration	Five concentrations and two controls
Observed effect	Immobility or death
Replicas by concentration	4
Acceptability criterion of the test	90% survival in negative control
Specimens by concentration	20
Dilution water	Moderately hard reconstituted water
Photoperiod	16 light hours
Solution volume	25 mL per replica
Age of the specimens	24 hours
Specimens per test chamber	5

Table A.11: Physicochemical variables controlled in the samples and controls.

Controls	**Dissolved oxygen**				**pH**		**Temp**		**Conductivity**	
	mg/L		%		pH units		°C		μS/cm	
	Initial	Final	Initial	Final	Initial	Final	Initial	Final	Initial	Final
Negative control	5.78	6.89	74.4	91.1	7.35	7.68	21.8	22.8	295	309
ULSD	6.31	6.44	86.9	85.7	7.38	7.78	21.3	22.8	297	313
Negative control	5.78	6.89	74.4	91.1	7.35	7.68	21.8	22.8	295	309
Bu13	6.31	6.42	84.3	86.1	7.65	7.87	20.4	22.9	291	314
Negative control	6.35	5.28	89.3	72	7.33	7.42	21.8	23	301	316
HVO13	6.8	5.27	89.7	71	7.95	7.58	22.5	22.9	302	318
Negative control	5.4	4.7	73.6	66.1	7.38	7.8	22.4	23	283	285
HVO20	5.7	4.52	76.5	60.5	7.31	7.75	21.6	29.9	274	304

Appendix B

Appendix to Chapter 4

B.1 Steady State: Engine performance and regulated emissions

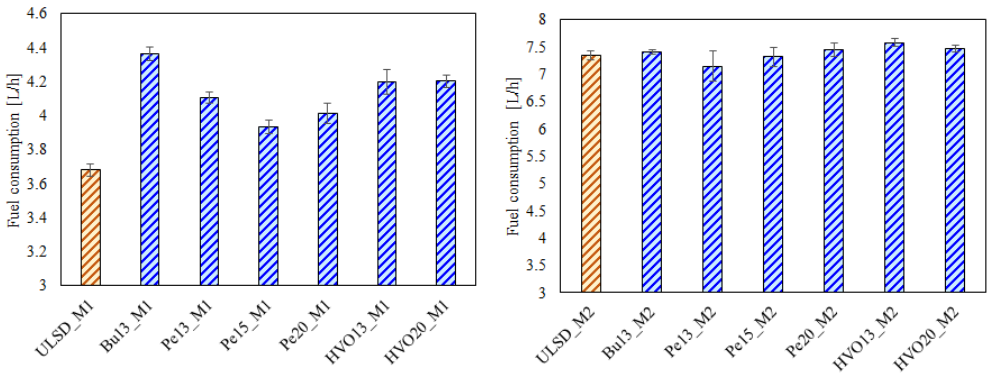

(a) Fuel consumption for M1

(b) Fuel consumption for M2

Figure B.1: Fuel consumption [L/h] for the tested fuels.

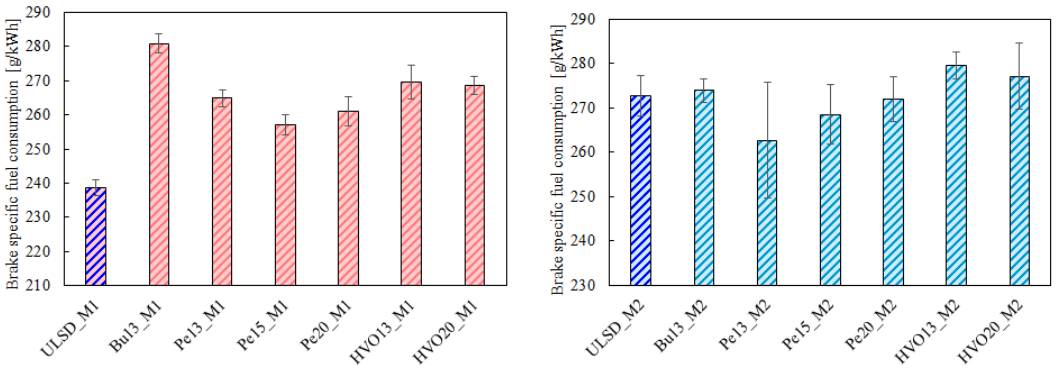

(a) Brake specific fuel consumption for M1

(b) Brake specific fuel consumption for M2

Figure B.2: Brake specific fuel consumption (g/kWh) for the tested fuels.

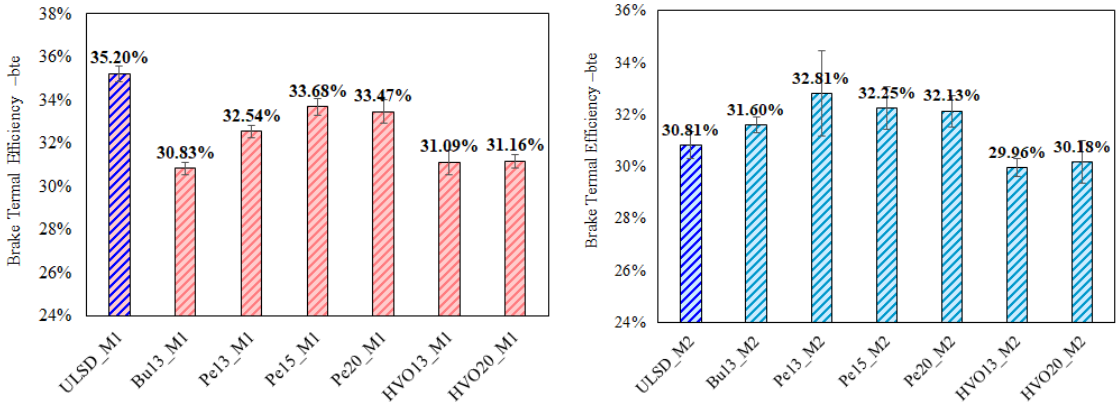

(a) Brake thermal efficiency for M1

(b) Brake thermal efficiency for M2

Figure B.3: Brake thermal efficiency for the tested fuels.

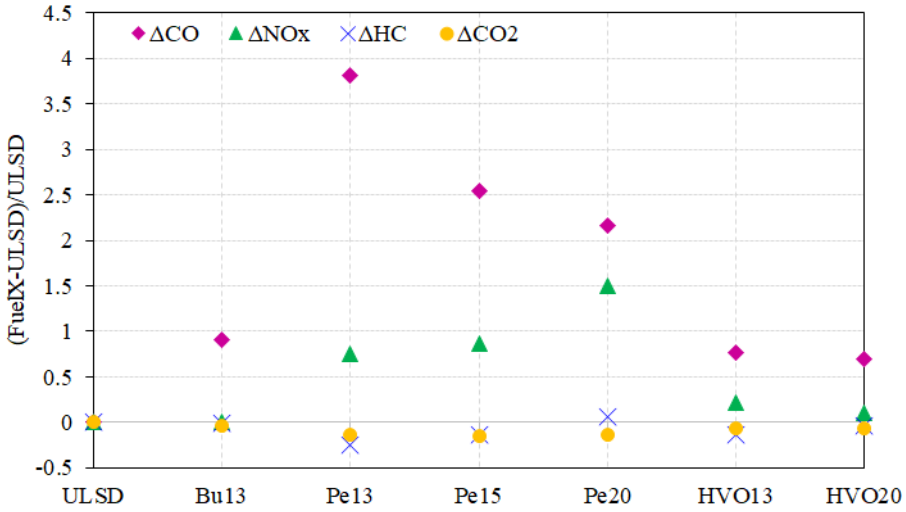

Figure B.4: Change in regulated emissions compared to ULSD